



This is to certify that the

dissertation entitled

Wetting, Spreading and Interphase Formation in a Liquid Composite Molding Environment

presented by

Brent Kevin Larson

has been accepted towards fulfillment of the requirements for

Ph.D. degree in Chemical Engineering

Lawrence T. Dyal
Major professor

Date 10/29/93

LIBRARY Michigan State University

PLACE IN RETURN BOX to remove this checkout from your record. TO AVOID FINES return on or before date due.

DATE DUE	DATE DUE	DATE DUE

MSU is An Affirmative Action/Equal Opportunity Institution

WETTING, SPREADING AND INTERPHASE FORMATION IN A LIQUID COMPOSITE MOLDING ENVIRONMENT

By

BRENT KEVIN LARSON

A DISSERTATION

Submitted to
Michigan State University
in partial fulfillment of the requirements
for the degree of

DOCTOR OF PHILOSOPHY

Department of Chemical Engineering

1993

ABSTRACT

WETTING, SPREADING AND INTERPHASE FORMATION IN A LIQUID COMPOSITE MOLDING ENVIRONMENT

By BRENT KEVIN LARSON

Liquid Composite Molding (LCM) encompasses the processes Resin Transfer Molding (RTM) and Structural Reaction Injection Molding (SRIM) in which a liquid resin impregnates a fiber preform to produce a composite having high strength, high modulus and large area with complex shapes. The effects of the interfacial free energy driving force on the interactions between sized glass fibers and liquid matrix and the resulting fiber-matrix adhesion and composite mechanical properties have been quantified. The surface free energy of both the sized glass fibers and the reacting liquid resin are important to wetting and/or spreading in the liquid composite molding environment. Wetting of the fibers by the matrix is a prerequisite to the development of strong adhesion across the fiber-matrix interface. Favorable interfacial thermodynamics (including fiber and matrix surface free energy and sizing solubility in the matrix) results in fiber-matrix interphase formation through which the level of fiber-matrix adhesion may be controlled and consequently composite mechanical properties may be engineered to meet design criterion.

The surface free energies of a vinyl ester resin and a series of sized glass fibers having a wide range of surface properties and solubilities in the matrix were measured. The fiber-matrix interactions were quantified with micro-Wilhelmy and wicking experiments, and microdielectric analysis facilitated measurement of the diffusion coefficients describing fiber-matrix interactions. Fiber-matrix adhesion and composite shear and flexural strengths were determined.

Research objectives included development of an experimental protocol for measurement of the key wetting parameters of the fiber and matrix, and quantification of wetting effects on composite mechanical properties manufactured by liquid composite molding. The research has culminated in the formulation of a time and temperature dependent model of the liquid composite molding process which incorporates both interfacial free energy effects and the sizing solubility in the matrix.

TO LOIS, FOR HER LOVE AND ENCOURAGEMENT,

AND ANNA, FOR PROVIDING JOY AND LAUGHTER.

ACKNOWLEDGMENT

The Lord Jesus Christ has had a profound impact on my life and has provided me with the strength to overcome seemingly insurmountable obstacles.

The research for this dissertation was accomplished at the Composite Materials and Structures Center at Michigan State University. My special thanks to Professor L.T. Drzal for providing guidance and encouragement. Thanks also to my committee members for their contributions to this research: Professor K. Jayaraman, Professor E. Grulke and Professor J. Stille.

My appreciation for helpful discussions of research problems goes to Shri Iyer, Venkatesh Rao, Craig Chmielewski, Nancy Losure, Ed Drown and Greg Fisher. Technical assistance has been provided by Mike Rich and Brian Rook. Many others have given of their time to improve my research, for which I am thankful.

I am also appreciative of financial support from the Automotive Composites Consortium and the National Science Foundation State/Industry/University Cooperative Research Center on Low Cost High Speed Polymer Composite Processing a Michigan State University. Materials were graciously provided by PPG Company and Dow Chemical Company.

TABLE OF CONTENTS

LI	ST OF TABLES							•	viii
LI	ST OF FIGURES								ix
1.	INTRODUCTION								1
2.	BACKGROUND								8
	THEORY							•	10
3.	EXPERIMENTAL METH	IODS							13
	DYNAMIC SCANNIN								13
	DYNAMIC MECHAN								14
									14
	MICRO-WILHELMY								15
	WICKING EXPERIM								17
	AXIAL WICK								19
	PENETRATIO								20
	TRANSVERSE								21
	HIGH-SPEED RESIN								22
	EQUIPMENT								22
	COMPOSITE 1								22
	FIBER-MATRIX ADI	•							23
	VOID FRACTION A								25
	MECHANICAL TEST								25
	MECHANICAL 1EST					• • • •	• • •	• •	23
4.	MATRIX CHARACTERI	ZATION							27
	INTRODUCTION								27
	FREE RADICAL CH								27
	THEORETICAL EXT	ENT OF REA	CTION	AT G	ELATI	ON .			28
	REACTION KINETIC	S							30
	AUTOCATAL								30
	INHIBITOR D								31
	EXPERIMENTAL EX								32
	RESIN VISCOSITY A								34
	SIZING EFFECTS O								35
	SIDEACE EDEE EN				• • •		- •		36

5 .	FIBER-MATRIX INTERACTIONS	8
	INTRODUCTION 3	8
	GLASS FIBER MANUFACTURE	9
	SIZING SYSTEMS 3	9
	SIZED GLASS FIBERS	1
	EXPERIMENTAL PROCEDURE	3
	RESULTS AND DISCUSSION	3
	FIBER SURFACE FREE ENERGY 4	.3
	SINGLE FIBER CONTACT ANGLE 4	5
	WICKING EXPERIMENTS	6
	Axial Wicking	6
		8
		9
		1
	· • • - • · · · · · · · · · · · · · ·	2
	CONCECUTO	_
6	DIELECTRIC ANALYSIS OF INTERPHASE FORMATION 5	4
٥.		4
		55
	***************************************	5
		6
		6
		9
		2
		3
		;3
		4
		55
		, <u> </u>
	CONCLUSIONS	v
7	COMPOSITE MATERIAL MECHANICAL PROPERTIES 7	1
		11
		12
E/		12
		13
		' 3 14
		14
		15
		_
		15
M		16
		16
		76
RI		17
		77
	COMPOSITE PLACIF APPEARANCE	79

VOID VOLUME FRACTIONS	80
FIBER-MATRIX ADHESION	81
INTERPHASE TENSILE PROPERTIES	83
COMPOSITE SHEAR STRENGTH	
LONGITUDINAL COMPOSITE FLEXURAL STRENGTH	87
SHEAR FRACTURE SURFACES	89
FLEXURE FRACTURE SURFACES	96
CONCLUSIONS	102
8. LIQUID COMPOSITE MOLDING MODEL	104
INTRODUCTION	104
BACKGROUND	106
EXPERIMENTAL PROCEDURE	109
COMPOSITE PROCESSING CYCLES	110
RESULTS AND DISCUSSION	110
FIBER SURFACE FREE ENERGY	111
FIBER-MATRIX ADHESION	111
COMPOSITE SHEAR STRENGTH	113
LONGITUDINAL COMPOSITE FLEXURAL STRENGTH .	114
LIQUID COMPOSITE MOLDING MODEL	115
CONCLUSIONS	119
9. CONCLUSIONS	121
REFERENCES	123

LIST OF TABLES

1.1	Reaction Injection Molding Material Requirements. (Macosko, 1989)
4.1	Viscosity as a Function of Sizing Concentration for Derakane 411-C50 with Soluble Polyester Sizing (#4) and Semi-Soluble Polyvinyl Acetate Sizing (#3).
5.1	Composition of Polyurethane, Polyvinyl Acetate, Polyester and Epoxy Glass Fiber Sizing Formulations
5.2	Comparison Between Single Fiber and Axial Wicking Contact Angles and Experimental and Predicted Penetration Distances for Derakane 411-C50 Wicking into Fiber Bundles.
5.3	Axial and Transverse Wicking Hydraulic Constants from Hexadecane Wicking into Fiber Bundles with 45% and 50% Fiber Volume Fractions, Respectively.
5.4	Comparison Between Axial and Transverse Wicking Results: Contact Angles and One Second Penetration Distances for Derakane 411-C50 Wicking into Fiber Bundles with 45% and 50% Fiber Volume Fraction, Respectively 49
5.5	Volume Fraction Voids for Composites Processed with Vacuum Assist (V.A.) and Heat Pretreat (H.P.)
6.1	Effective Diffusion Coefficients for Derakane 411-C50 Swelling Glass Fiber Sizing Systems (D _R) and Sizing Systems Dissolving into Derakane (D _S) at 25°C.
7.1	Volume Fraction Voids for Composites Processed with Vacuum Assist (V.A.) and Heat Pretreat (H.P.)
7.2	Tensile Properties of Derakane 411-C50 and Mixtures of Derakane and 25 Weight Percent Polyvinyl Acetate (#3) and Polyester Sizing (#4) 84
8.1	The Effect of the Mold Temperature on the Time for Interphase Formation $(t_{I.F.})$. Which is Equal to the Gelation Time (t_g) , Interfacial Shear Strength (IFSS), Short Beam Shear Strength (SBSS), and Flexural Strength (FS)

LIST OF FIGURES

1	Schematic Diagram of Resin Transfer Molding Equipment	3
2	Schematic Diagram of a Pendant Drop with Pertinent Dimensions	15
3	Schematic Diagram of Micro-Wilhelmy Technique for Measuring Contact Angles on Single Fibers.	16
4	Schematic Diagram of Axial Wicking Experiment	18
5	Schematic Diagram of Transverse Wicking Cell	21
6	Schematic Diagram of the Interfacial Testing System (ITS)	24
7	Schematic Diagram Showing the Structure of the Derakane Vinyl Ester and Styrene.	28
8	Comparison Between Reaction Model and Experimental Data for Derakane 411-C50.	31
9	Relationship Between Maximum Extent of Reaction of Derakane 411-C50 and Temperature.	nd 32
10	Comparison Between Initial Reaction Kinetics Model and Experimental Data Derakane 411-C50.	for 33
11	Derakane Surface Free Energy Measured by Pendant Drop Technique for Reacting and Non-Reacting Systems.	37
12	Surface Free Energy Comparison of PPG Sized Glass Fibers Calculated from Polar/Dispersive Analysis	n 44
13	Interfacial Shear Strength Comparison Between Derakane/Glass Fiber Compositor Vacuum Assist and Heat Pretreat Cycles Measured by Interfacial Testing System.	
14	Schematic diagram of one-dimensional unsteady-state diffusion of resin into siz film on microdielectric sensor face	ing 57
15	Schematic diagram of one-dimensional unsteady-state diffusion of sizing film fr microdielectric sensor face into resin semi-infinite media	om 59
16	Calibration curve relating dried polyester sizing concentration in resin to ior conductivity measured by a low conductivity microdielectric sensor.	nic 60

17	ionic conductivity measured by a low conductivity microdielectric sensor.	61
18	Schematic diagram of a microdielectric sensor and its circuitry. Used with a permission of Micromet Instruments.	he 63
19	Typical conductivity-time profile for a soluble sizing showing sizing swelling a dissolution into the resin.	ınd 66
20	Typical conductivity-time profile for an insoluble sizing showing sizing swell and no sizing dissolution into the resin.	ing 67
21	Experimental data and the one-dimensional unsteady-state diffusion model describing resin swelling of the sizing film.	68
22	Experimental data and the semi-infinite media diffusion model describing dissolution of the sizing film into resin.	69
23	Surface Free Energy Comparison of PPG Sized Glass Fibers Calculated from Polar/Dispersive Analysis	n 78
24	Interfacial Shear Strength Comparison Between Derakane/Unidirectional Gla Fiber Composites for Vacuum Assist and Heat Pretreat Processing Cycles Measured by Interfacial Testing System	ss 82
25	Short Beam Shear Strength Comparison Between Derakane/Unidirectional Gl Fiber Composites with 50% Fiber Volume Fraction for Vacuum Assist and H Pretreat Processing Cycles.	
26	Longitudinal Flexural Strength Comparison for Derakane/Unidirectional Gla Fibers with 50% Fiber Volume Fraction for Vacuum Assist and Heat Pretre Processing Cycles.	
27	Shear Fracture Surface of Mold Release Sized Fiber (#1) Composite.	91
28	Shear Fracture Surface of Insoluble Polyurethane Sized Fiber (#2) Composite.	91
29	Shear Fracture Surface of Semi-Soluble Polyvinyl Acetate Sized Fiber (#3) Composite.	93
30	Shear Fracture Surface of Soluble Polyester Sized Fiber (#4) Composite.	93
31	Shear Fracture Surface of Soluble Epoxy Sized Fiber (#5) Composite.	95

32	Shear Fracture Surface of Water Sized Fiber(#6) Composite	95
33	Tensile Fracture Surface of Insoluble Polyurethane Sized Fiber (#2) Composite.	98
34	Tensile Fracture Surface of Semi-Soluble Polyvinyl Acetate Sized Fiber (#3 Composite.) 98
35	Tensile Fracture Surface of Soluble Polyester Sized Fiber (#4) Composite.	100
36	Tensile Fracture Surface of Soluble Epoxy Sized Fiber (#5) Composite.	100
37	Tensile Fracture Surface of Water Sized Fiber (#6) Composite	101
38	Moldability Diagram for the Filling Step of the Liquid Composite Molding Process. (Gonzalez-Romero and Macosko)	106
39	Moldability Diagram for the Curing Step of the Liquid Composite Molding Process. (Gonzalez-Romero and Macosko)	108
40	Interfacial Shear Strength of Derakane/Glass Fiber (with Soluble Polyester Siz Composites Processed with Vacuum Assist vs. Mold Temperature	ing) 112
41	Short Beam Shear Strength of Derakane/Glass Fiber (with Soluble Polyeste Sizing) Composites with 50% V _f Processed with Vacuum Assist vs. Mold Temperature.	r 114
42	Flexural Strength of Derakane/Glass Fiber (with Soluble Polyester Sizing) Composites with 50% Volume Fraction Processed with Vacuum Assist vs. M. Temperature.	Iold 115
43	Moldability Diagram for the Curing Step of the Liquid Composite Molding Process Incorporating the Effects of the Sizing Solubility and Surface Free Energy.	117

1. INTRODUCTION

Liquid composite molding (LCM) describes processes for composite production in which a liquid resin is injected into a mold containing reinforcement. Resin transfer molding (RTM) is the oldest liquid composite molding process, and is a slow process for producing large structural composites. Advances in resin technology such as lower resin viscosities and faster reaction rates have shortened molding cycle times and led to the process referred to as high speed resin transfer molding (HSRTM). Structural reaction injection molding (SRIM) takes advantage of the fast reaction chemistry of polyurethanes to make simple shapes with low fiber volumes. Recent research in polyurethane reaction chemistry involves lengthening the gelation time to allow production of more complicated shapes and/or composites with higher fiber volume fractions. Future advances in liquid composite molding will require the ability to understand and optimize the interactions that take place between reacting liquid resin and fiber in these processes which have short times for interaction.

Resin transfer molding is the process to manufacture high strength, high modulus composites with two high quality surfaces in a processing cycle short compared with autoclave processing times. Complex part shapes may be produced with good surface detail and accuracy, with a minimum amount of trimming required. Resin transfer molding involves the infusion of liquid resin into a dry fiber preform enclosed in a mold.

Fiber preforms are shaped arrays of reinforcing fibers which have dimensional stability under the forces associated with resin impregnation, often through the use of a thermoplastic binder. They may be made from chopped fibers to produce a random or oriented mat, or continuous fibers may be woven in patterns varying from coarse to fine to produce braid, weave or cloth fabric. Since the best composite mechanical properties in one direction are achieved when continuous fibers are not woven but aligned in a single direction, the placement of a preform into a mold before resin injection allows exact fiber placement and variable fiber volume fraction within different regions of a composite. The local composite strength requirements dictate local control of fiber volume fraction and orientation. Regions of the composite requiring high strength may be composed of a high volume fraction of fibers, and regions where less strength is demanded may require little or no fiber reinforcement. At the conclusion of the resin transfer molding process, solidification of the resin permanently locates the fibers in place. Solidification is the result of polymerization reactions initiated by thermal activation or mixing activation, and the product is a large complex structural composite material at reduced fabrication cost compared to other processing methods.

The resin transfer molding process may be described in terms of six steps: 1) placing the fiber preform into and closing the mold, 2) metering the reactants to provide correct stoichiometry, 3) mixing the reactants to produce a homogeneous resin mixture, 4) impregnating the resin into the heated mold and throughout the fiber preform, 5) curing the resin to the desired extent of reaction, and 6) removing the composite from the mold. Some processes include a postcure to increase the extent of reaction. See Figure 1 for a schematic diagram of a simple resin transfer molding process.

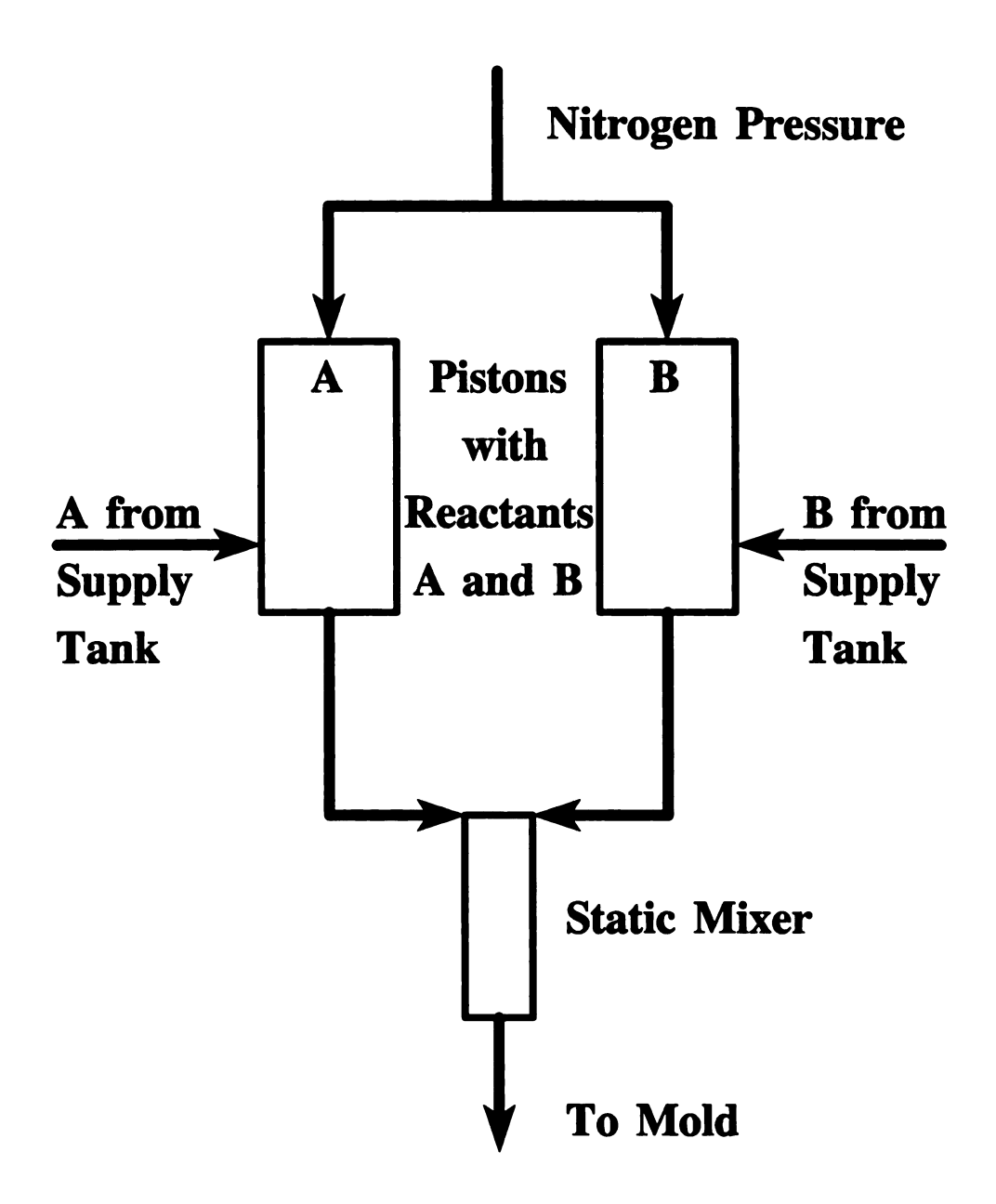


Figure 1. Schematic Diagram of Resin Transfer Molding Equipment.

Resin transfer molding is similar to other liquid molding processes such as reaction injection molding in that a low viscosity thermoset resin is injected into a mold, but a fiber preform is placed in the mold prior to injection in resin transfer molding. Reaction injection molding uses an impingement mixhead, whereas a static mixer is used in most resin transfer molding. The time scale for gelation in resin transfer molding may be more than two orders of magnitude greater than that in reaction injection molding. For example, resin transfer molding polyurethane systems have gel times on the order of 5 seconds, whereas resin transfer molding epoxy systems have gel times exceeding 30 minutes. Requirements for reaction injection molding resins have been succinctly listed by Macosco¹ in Table 1.1. These requirements provide good guidelines for LCM resins, and are the result of consideration of each unit operation in the reaction injection molding process.

The mechanical properties which may be achieved in a resin transfer molding composite material far exceed those of a reaction injection molding material because of the inclusion of high strength, high modulus fibers. Reinforcements such as chopped glass, hammer milled glass, flake glass, or mica have been incorporated in reaction injection molding resins to improve its mechanical properties while retaining the short processing times allowed by polyurethane chemistry². The reinforcement is dispersed in the polyol with the other processing steps the same as in reaction injection molding. This process is referred to as reinforced reaction injection molding (RRIM), and only low fiber loadings are possible (less than 25% reinforcement). A much greater mechanical property improvement is realized by the incorporation of continuous fibers in structural

Table 1.1. Reaction Injection Molding Material Requirements. (Macosko, 1989)

Supply * stable ≥ 1 week

* pumpable

Condition * initial temperature < 60°C

< 150°C (high temperature machine)

Meter * two components

* ± 0.5% stoichiometry

Mix * viscosity < 1 Pa· sec

* compatibility

* adiabatic gel time > 0.1 sec

Fill * adiabatic gel time > fill time > 1 sec

* viscosity > 10 - 100 m Pa· sec to prevent bubbles

Cure * mold wall temperature < 100°C

< 200°C (high temperature mold)

* mold wall temperature < (degradation temperature - adiabatic

temperature rise)
* control by-products

* compensate for shrinkage

Demold * mold wall temperature < melting or phase mix temperature

* mold wall temperature > glass transition, precipitation

* demold time < 3 min (sufficient green strength)

< 45 sec (high production)

* easy mold release

Finish * little flash

* minimize post cure

* paintable

reaction injection molding (SRIM). Compared with resin transfer molding, low fiber volume fractions and simple shapes are necessary to retain short processing times.

The mechanical properties of resin transfer molded composites approach those of preimpregnated, autoclaved composites which have maximum strength to weight ratios, developed through three step processing. The preimpregnation step which produces a "prepreg tape" assures intimate fiber-resin contact. The hand lay-up of prepreg tapes allows fiber orientation to be controlled in the production of laminates. Vacuum is maintained on the laminates as pressure and temperature are used to consolidate the laminates into a composite in an autoclave. The fiber-matrix contact time, the time the *liquid* matrix resin is in contact with the fiber, is long in the autoclave process. The gel time of the resin determines the fiber-matrix contact time. This processing is expensive because it is labor and time intensive.

Resin transfer molding is much less expensive than prepreg/autoclave processing because of labor and time savings due to the automation of the preform production which produces the desired fiber orientation in the composite. The impregnation and consolidation steps are accomplished in the relatively quick mold filling step. Thus resin transfer molding offers the advantages of being quicker and less expensive compared with prepreg/autoclave processing to produce composites with mechanical properties approaching those of prepreg/autocalve processing. However the fiber-matrix contact time is much less than in the autoclave process and the shorter time for fiber-matrix interactions is one reason for the mechanical properties of resin transfer molded composites processed in short cycle times to be less than the mechanical properties yielded by the autoclave process.

Intimate contact between fiber and matrix is a prerequisite to good fiber-matrix adhesion, which is mandatory for optimization of composite mechanical properties³. Current resin transfer molding systems suffer from problems such as poor fiber wet-out, resin flow induced fiber motion, inadequate fiber-matrix adhesion, and processing cycles which are not optimized. Poor fiber wet-out results in high void fractions which may seriously compromise the strength of a composite. Poor fiber-matrix adhesion results in low stress transfer across the fiber-matrix interface, which leaves the fiber reinforcement underutilized and the resulting composites having less than the designed-for mechanical properties. Less than optimized processing cycles yield extended cycle times and lower productivity.

Researchers have just begun to investigate the fiber wetting kinetics which are important in LCM. Important variables in the mold filling process, such as viscosity and matrix liquid surface free energy, must be determined as functions of temperature and extent of reaction, because the gel time is near the fill time in an optimized LCM process.

This research is directed at identifying the main factors responsible for fiber wetting in a LCM environment in order to develop a comprehensive model of the LCM process which describes the process limits for production of a composite as a function of time, mold temperature, initial resin temperature, resin viscosity, resin reaction kinetics, resin surface free energy, and fiber surface free energy.

2. BACKGROUND

Sharpe was one of the earliest to research the important influence of wetting on adhesion between polymeric materials. He determined that wetting is a prerequisite to good adhesion through two simple experiments⁴. Liquid epoxy resin was poured onto solid polyethylene and cured, but poor adhesion resulted because the contact angle between the liquid and the solid was high, indicating poor wetting. When molten polyethylene was poured onto solid epoxy resin the contact angle was near zero indicating wetting, and good adhesion resulted. This research also showed that wetting is independent of viscosity when sufficient time for wetting is allowed. The viscosity of liquid epoxy is near 1 Pa*s compared with 10³ Pa*s for molten polyethylene, yet at equilibrium the polyethylene wet the solid epoxy, and the liquid epoxy did not wet the solid polyethylene.

The important influence of wetting may be studied through the observation of the contact angle between a liquid and a solid using optical microscopy. However, data are difficult to collect on small diameter reinforcing fibers. Wilhelmy⁵ discovered a gravimetric method of obtaining the contact angle which was less time consuming and reduced error. He discovered that the force (F) exerted on a solid surface of perimeter P as it is brought into contact with a liquid may be related to the contact angle (θ) through the following equation:

$$F = \gamma_{LV} P \cos \theta - \rho_L g y A_S$$

where ρ_L is the liquid density, g is the gravitational constant, y is the immersion depth, and A_S is the cross-sectional area of the plate. The buoyancy force, the second term in the equation, is easily calculated and usually negligible when working with small immersion depths.

The micro-Wilhelmy technique was developed for evaluating the surface free energy of glass monofilaments at the Textile Research Institute in Princeton, New Jersey⁶. Early researchers using this technique include Chadburd and Mozzo⁷, and Neumann and Tanner⁸. Many researchers have used this technique to investigate the surface energetics of a wide range of fibers, including glass, Kevlar, carbon, polypropylene, and polyethylene^{9, 10, 11, 12, 13, 14, 15, 16}. Hammer and Drzal explained why improved fiber-matrix adhesion results from oxidative fiber surface treatment, through documentation of the effects of carbon fiber surface treatment or wettability with this method. They showed that treatment of carbon fibers increases the surface oxygen concentration, which causes an increase in the polar component of the fiber surface free energy¹⁷. The technique of Kaelble was used to determine the polar and dispersive components of the surface free energy of the fibers.

Both static and dynamic observations of the fiber-liquid contact angle have been made. Velocities were chosen from 0.12 to 0.3 mm/min, which are very slow compared to resin velocities in high speed RTM processes which may exceed 1000 mm/min. An analysis by Cain, et al.¹⁸, on silane treated glass plates immersed in water, discusses the immersion rate effect, with rates varied from 0.05 to 0.7 mm/min. The behavior of this

system was divided into three regions separated by sharp transitions. At low rates the contact angle increased linearly as the rate increased, but at intermediate rates the contact angle was constant. At higher rates the contact angles again increased linearly with increasing rate, but with a lower slope than before. These results were interpreted to indicate that a diffusion process was taking place in which the surface free energy of the silane surface was modified by water penetration. As the immersion rate increased, the time that the water was in contact with the glass was shortened so that the surface modification did not occur and a constant contact angle was measured. Finally, it was noted that at high rates, water inertial flow effects caused the contact angle to increase as the rate of immersion continues to increase. Hysteresis is described as being attributable to surface roughness, surface modification (adsorption), heterogeneity, and deformation.

THEORY

The three phase equilibrium boundary between a solid, liquid and vapor is described by the thermodynamic relationship known as Young's equation¹⁹:

$$\gamma_{SV} - \gamma_{SL} = \gamma_{LV}(\cos\theta) \tag{2}$$

where three of the terms are surface free energies (often referred to as surface tensions) of the solid-liquid (γ_{SL}), solid-vapor (γ_{SV}), and liquid-vapor (γ_{LV}) interfaces. The angle measured in the liquid, which the liquid makes with the solid is called the contact angle (θ). The contact angle is used as a measure of the degree of attraction of the liquid for the substrate. If the contact angle is 0° then the liquid is said to "spread" on the substrate, and the Young equation must be modified because equilibrium no longer exists.

$$\gamma_{SV} - \gamma_{SL} \ge \gamma_{LV} \tag{3}$$

If the contact angle is less than 90°, the liquid is said to "wet" the substrate, and if it is greater than or equal to 90° the liquid-solid interaction is termed to be "non-wetting".

Thermodynamic "spreading" or "wetting" as described above is the *necessary* condition for acceptable processability as well as attainment of acceptable mechanical properties in any composite system. It assists in displacement of the gas phase from the fiber surface by the matrix²⁰. In order to ensure good wetting the liquid phase should have a surface free energy lower than the solid surface free energy.

The thermodynamic work of adhesion (W_a) is a measure of the interaction between two phases, the total attraction per unit area. It is the reversible work required to generate the solid-vapor and liquid-vapor interfaces and eliminate the solid-liquid interface:

$$W_a = \gamma_{LV} + \gamma_{SV} - \gamma_{SL} \tag{4}$$

Using Young's equation (1), equation 3 may be written in terms which are readily determined experimentally:

$$W_a = \gamma_{LV}(1 + \cos\theta) \tag{5}$$

At the fiber-matrix interface a high work of adhesion is desired to not only ensure maximum adhesion but also to optimize processability²¹.

Fowkes²² hypothesized that the total surface free energy could be described as the sum of dispersive and higher order forces. Kaelble²³ built upon Fowkes' postulate by devising a scheme to allow determination of the polar and dispersive components of the

surface free energy of a solid (γ_S^P) and γ_S^d using the known components of liquids (γ_L^P) and γ_L^d . This technique involves measuring the contact angle between a set of liquids of known ratios of polar to dispersive surface free energy components. A proposed equation describes the work of adhesion in terms of the components of the surface free energies of the liquid and solid:

$$W_{c}/2 = (\gamma_{S}^{p} \gamma_{L}^{p})^{1/2} + (\gamma_{S}^{d} \gamma_{L}^{d})^{1/2}$$
 (6)

The equation may be rearranged to yield a linear equation with the slope and intercept equal to the polar and dispersive components of the solid surface tension, respectively, when the first term is plotted against the square root of the ratio of the polar to dispersive liquid surface tension components:

$$W_a / (2\gamma_L^{D^{1/2}}) = \gamma_S^{D^{1/2}} + \gamma_S^{P^{1/2}} (\gamma_L^P / \gamma_L^D)^{1/2}$$
 (7)

3. EXPERIMENTAL METHODS

DIFFERENTIAL SCANNING CALORIMETRY

A DuPont Thermal Analysis 9900 system with model 910 differential scanning calorimeter (DSC) was used to monitor the reaction kinetics of the resin in both dynamic and static temperature modes. The dynamic experiments were used to determine the total heat of reaction for the resin system, and static experiments provided information on the isothermal reaction kinetics of the resin system.

Derakane 411-C50 is the vinyl ester resin system under consideration, and it is composed of 50 wt% styrene and 50 wt% vinyl ester resin. A small concentration of inhibitor is included to deter premature polymerization. A "masterbatch" of resin was produced for use throughout the DSC experiments by adding accelerator, 0.10 wt% of N,N-dimethylanaline (Aldrich), to one liter of Derakane. DSC specimens were prepared by adding 1.0 wt% of benzoyl peroxide powder (Aldrich) initiator to 30 g of masterbatch resin. The initiator was hand stirred for 9 minutes until it was completely dissolved in the resin. Samples of 12 ± 1 mg were hermetically sealed in DSC pans to prevent styrene evaporation. A nitrogen purge of the DSC cell, 50 cm³/min, provided short equilibration times, and for isothermal conditions the DSC cell was raised to the experiment temperature before the sample was placed in the cell.

DYNAMIC MECHANICAL SPECTROMETER

A Rheometrics Mechanical Spectrometer 800 was used to monitor the storage and loss moduli as the curing resin viscosity increased. The experiment was performed concurrently with dynamic scanning calorimetry to determine the extent of reaction at the gel point. Resin from a masterbatch was initiated and a sample was given the same thermal history in each of the experiments at the same time. A parallel plate geometry was used in the mechanical spectrometer with a plate diameter of 50 mm, strain rate of 1 rad/second and strain amplitude of 30%. The parallel plates were preheated to experiment temperature before the resin was introduced. (The same technique was used with the dynamic scanning calorimeter.) Experiments were performed at 30, 40 and 50°C and were concluded when the storage modulus increased to the magnitude of the loss modulus.

PENDANT DROP TECHNIQUE

The resin surface free energy was measured using the pendant drop technique. The pendant drop technique is dependent upon the relationship between the shape of a drop hanging from a tip and the liquid-vapor surface free energy. A digitized image of the drop profile will provide input to a computer program which compares the curve to the theoretical profile generated by the dimensionless Bashforth and Adams equation²⁴:

$$\frac{b}{R} + \frac{\sin \phi}{x/b} = \beta(\frac{z}{b}) + 2 \tag{8}$$

where the equation is in terms of a drop profile shape factor (β , equal to $\Delta \rho g a^2/\gamma_{LV}$), capillary constant (a, equal to the square root of $2\gamma/\Delta \rho g$), radius of curvature at drop bottom (b), radius of curvature at the point x,z (R), angle from droplet profile to x-axis

 (ϕ) , density difference between liquid and gas $(\Delta \rho)$, gravitational constant (g), and liquid-vapor surface free energy (γ_{LV}) . See Figure 2 for a schematic diagram of a pendant drop showing the experimentally measured variables in the Bashforth and Adams equation. The drop profile shape factor is compared with computed profiles to yield the liquid-vapor surface free energy.

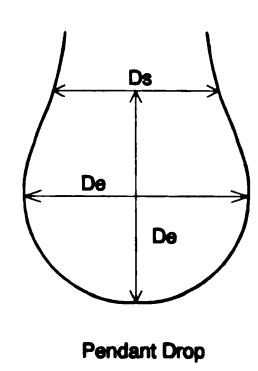


Figure 2. Schematic Diagram of a Pendant Drop with Pertinent Dimensions.

MICRO-WILHELMY

The Micro-Wilhelmy technique is an indirect method of contact angle measurement between single fibers and liquids. The technique relies on gravimetric measurement of the force exerted on a single fiber by a liquid and the diameter of the fiber to obtain the contact angle. An automated Micro-Wilhelmy system developed at Michigan State University was used to make the measurements. The system includes a Cahn electrobalance and a microstepping motor for providing vertical motion at 25 microns per second. Dynamic and equilibrium measurements are easily made in advancing and receding mode with the automated system. The fiber diameters were measured using an Olympus Corporation Micro 300 Video Caliper in conjunction with an optical microscope after the Micro-Wilhelmy measurements were made.

Sample preparation for the Micro-Wilhelmy technique for single fiber contact angle measurement involved mounting the fibers on hooks using cyanoacrylate adhesive

immediately before testing. Care was taken to not contaminate the fiber surface to be contacted by liquid.

Figure 3 shows a schematic diagram of the Micro-Wilhelmy equipment which was enclosed in an environmental chamber flushed with dry air maintained at zero relative humidity and 23°C. The mounted single fiber was suspended from the electrobalance above the probe liquid. Immediately before commencement of the test, the surface of the liquid was refreshed by adding a few drops of uncontaminated liquid to the liquid container. After the electrobalance was zeroed with the mass of the fiber and hook, the fiber was lowered

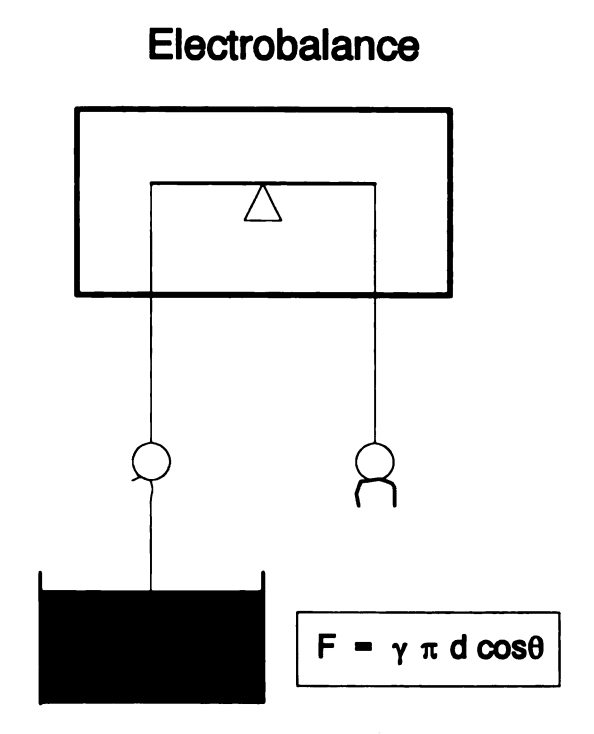


Figure 3. Schematic Diagram of Micro-Wilhelmy Technique for Measuring Contact Angles on Single Fibers.

until it contacted the liquid. Then the automated control was initiated, and the fiber was immersed in the liquid at a rate of 25 microns/second. Dynamic measurements were taken as the fiber was immersed to obtain the advancing dynamic contact angle, and then the microstepping motor stopped for a prespecified equilibration time. After equilibrium measurements were made to obtain the advancing equilibrium contact angle, the cycle was repeated with additional dynamic measurements. This cycle was repeated 10 times, then the receding measurements were made as the fiber was raised out of the liquid.

Contact angles are calculated from the force measurements using equation 1 and the fiber diameter measurements.

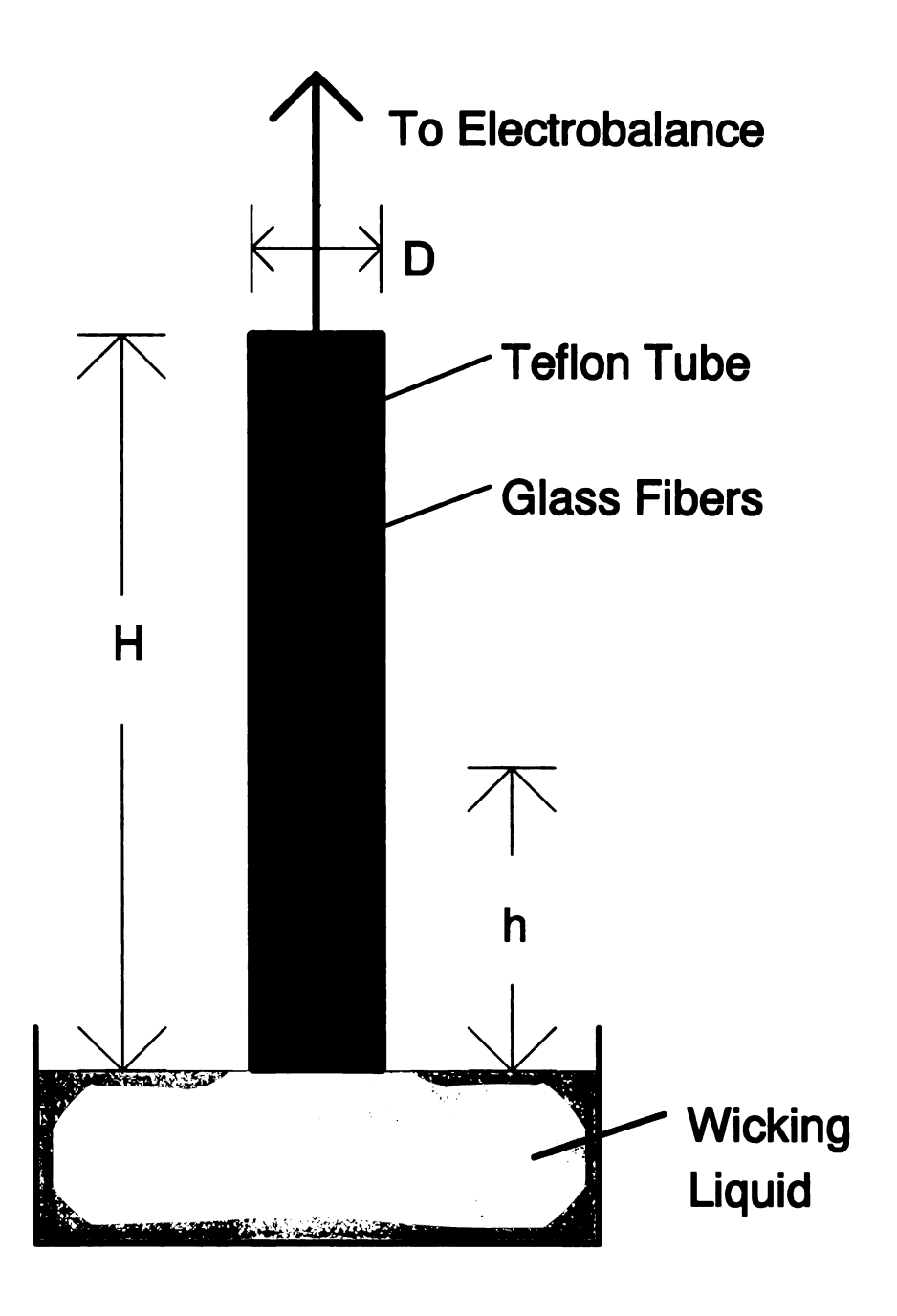
All glassware used in the experiments was cleaned with Chromerge (VWR Scientific) and stored in an oven at 100°C. Prior to experimentation, glassware was moved to the controlled environment enclosing the Micro-Wilhelmy apparatus and cooled to 23°C. Research grade liquids were obtained to ensure liquid purity and published surface tensions.

Four probe liquids were used which provide a wide range of the ratio of polar to dispersive components of surface free energy: reverse osmosis deionized water, ethylene glycol, formamide and methylene iodide. Literature values for the surface tensions of the liquids were used²⁵.

WICKING EXPERIMENTS

Wicking experiments offer an alternative to the Micro-Wilhelmy technique as a method of measuring the contact angle between fibers and liquids. This technique has the advantage that the geometry is very similar to the physical situation encountered in liquid composite molding. Specifically, the fiber tow geometry is important to this test, whereas in the Micro-Wilhelmy test the fiber tow geometry has no bearing on the results.

Wicking studies yield information on the interfacial free energy change as a liquid is wicked by capillary force into a packed fiber bed. The contact angle between the fiber and liquid may be calculated from the interfacial free energy change. Two wicking experimental configurations were used in this research. The resin flow was in the fiber direction (axial flow) in the initial experiments, and transverse resin flow was also studied with flow perpendicular to the fiber direction. In these studies the porosity of



Schematic Diagram of a Wicking Experiment

Figure 4. Schematic Diagram of Axial Wicking Experiment.

the packed fiber bed was very similar to that typically encountered in liquid composite molding, 55% and 50% for the axial and transverse cases, respectively.

AXIAL WICKING

This experimental procedure is based on the research of Chwastiak²⁶. Capillary forces are responsible for the flow of liquids between closely spaced surfaces and are dependent upon the interfacial free energy change as the liquid covers the solid surface. Capillary forces must overcome viscous (ϕ_v) , gravitational (ϕ_g) , and inertial (ϕ_i) forces:

$$\Delta \gamma = \frac{1}{C_f} (\phi_v + \phi_g + \phi_i) \tag{9}$$

The capillary flow may be monitored in a teflon tube packed with fibers suspended from an electro-balance and placed in contact with a liquid, as shown in Figure 4. The change in mass as a function of time may be correlated, through the Kozeny-Carman equation, with the viscous component of the change in interfacial free energy:

$$\phi_{\nu} = \chi \Delta p = \frac{512\eta H}{V_{\tau}} \left(\frac{1}{\epsilon}\right) \left(\frac{1-\epsilon}{kd_{\ell}\epsilon\rho_{l}}\right)^{2} \left(m\frac{dm}{dt}\right)$$
 (10)

$$\phi_g = mg \tag{11}$$

$$\phi_i = \frac{4H\alpha (2\alpha - 1)m^2}{\eta V_{\alpha} \rho_i t^2}$$
 (12)

where ϵ is the porosity of the fiber bundle, H is the height of liquid rise at t, m is the weight of liquid in the fiber bundle at t, ρ_f is fiber density, α is the slope of wicking rate data on a log-log plot, K is a hydraulic constant, V_T is the volume inside of the tube, W_f is fiber weight in bundle, ρ_l is liquid density, and d_f is fiber diameter.

Analysis of the wicking data (m vs. t) allows calculation of the axial wicking contact angle (θ_{AW}) between each type of fiber and resin. The change in interfacial free energy between the wetting liquid and the fiber surface and the liquid-vapor surface free energy (γ_{LV}) determine the contact angle:

$$\theta_{AW} = \cos^{-1}(\Delta \gamma / \gamma_{IV}) \tag{13}$$

PENETRATION DISTANCE

The capillary equation provides a description of the pressure driving force (Δp) for flow in a single cylindrical channel based on the contact angle data:

$$\Delta p = 4\gamma_{LV}\cos\theta/D_e \tag{14}$$

where D_e may be taken as an equivalent hydraulic channel diameter. The penetration distance (L) of liquid flowing into a capillary tube for a time (t) is described by the Poiseuille equation combined with a mass balance:

$$L = \frac{D_e}{4} \left(\frac{t\Delta p}{2\eta}\right)^{1/2} \tag{15}$$

where η is liquid viscosity yielding an average capillary flow velocity.

TRANSVERSE WICKING

The specimen geometry was different for the transverse wicking case compared with the axial flow case. A rectangular holder was designed to constrain the fibers, keeping the porosity of the fiber bed constant. Figure 5 shows a schematic diagram of the fiber holder, which was produced by bending a 1 mm thick aluminum sheet three times and adhering the ends of the sheet at the fourth corner. Holes were made in the bottom of the holder to allow resin to flow in the transverse fiber direction. The holder is designed to constrain a bundle of fibers 51 mm x 13 mm x 27 mm in volume. The aluminum fiber holder was coated with Mono Coat mold release (Chem Trend) to lower the surface free energy so that the holder would not provide any wicking surface for the resin. Thus the wicking was only due to the fibers. The transverse wicking experimental procedure was different from the axial wicking experiments because the transverse wicking specimen was too heavy to be suspended from the electrobalance. A

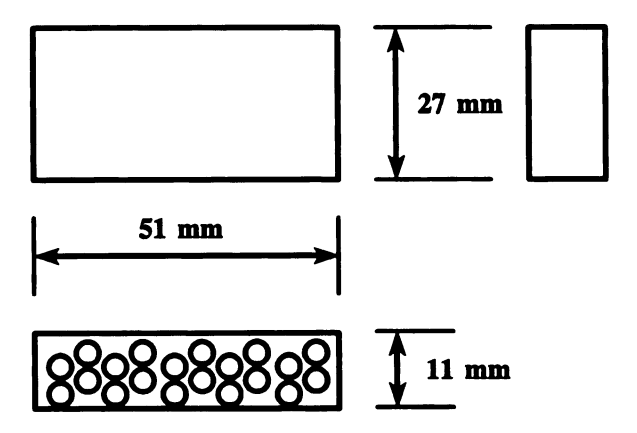


Figure 5. Schematic Diagram of Transverse Wicking Cell.

Sartorius balance was used to monitor the mass change as a function of time as the resin wicked into the fibers. The data analysis was the same in both types of wicking experiments.

HIGH SPEED RESIN TRANSFER MOLDING

EQUIPMENT

A preform winder was constructed to manufacture unidirectional fiber preforms. The apparatus consists of a motor to provide rotation of the preform frame and a linear motion motor to place the fiber tow appropriately on the rotating preform frame. A counter monitored the number of winds of fiber tow which had been placed on the preform frame. This was the means of monitoring the mass of fibers in the preform as the fiber mass per length was measured and determined to be constant for each of the fiber types.

A three part mold was constructed which was instrumented with nine thermocouples for monitoring temperature and two pressure gauges to monitor inlet and outlet pressure. The preform frame is held in place in the mold to deter fiber washing. A composite is produced with variable fiber volume fraction and orientation depending upon the fiber preform.

A Semco 550 Sealant Gun with disposable liquid holding tank was used to inject resin into the mold. Nitrogen was chosen as the pressure translation gas because the oxygen in air could act as an inhibitor in the resin system.

COMPOSITE PLAQUE PROCESSING

Two composite processing cycles were developed for producing unidirectional 152 mm x 152 mm x 3 mm advanced composite plaques with 50% E-glass fiber volume

fraction. The vacuum assisted high-speed resin transfer molding processing cycle consists of a room temperature portion with the mold, preform, and resin at 23°C. The mold (with preform in place, fibers oriented parallel to the mold filling direction) was vacuum evacuated for 10 minutes prior to resin injection to draw volatiles out of the fiber sizing system. An injection pressure of 20 psi was used to fill the evacuated mold, and a packing pressure of 100 psi was required to obtain high quality surfaces on both sides of the composite plaque. After 12 hours of room temperature cure, the composites were postcured at 80°C for 2 hours.

Preheating of the preform was used as an alternative to vacuum assisted processing to remove volatiles from the sizing system. The heat pretreat process involved placing the preform in an oven at 80°C for 20 minutes before positioning the preform into the mold. The remaining processing steps were the same as for the vacuum assisted processing, with 20 psi resin injection, 100 psi packing pressure, 12 hour room temperature cure, and 2 hour cure at 80°C. The heat pretreat processing cycle produced composites of comparable appearance to the vacuum assisted processing cycle, nearly void-free and with high quality surfaces. Composites produced without vacuum assist or heat pretreat contained small voids distributed throughout the composite due to volatiles evolving from the sizing system.

FIBER-MATRIX ADHESION

The fiber-matrix adhesion was quantified using the Interfacial Testing System (ITS), a micro-indentation technique, to determine the effect of the sizings and their interaction with the matrix on fiber-matrix adhesion. ITS specimens were prepared from each type of composite by cutting 1 cm x 1 cm pieces from the composite. The sample

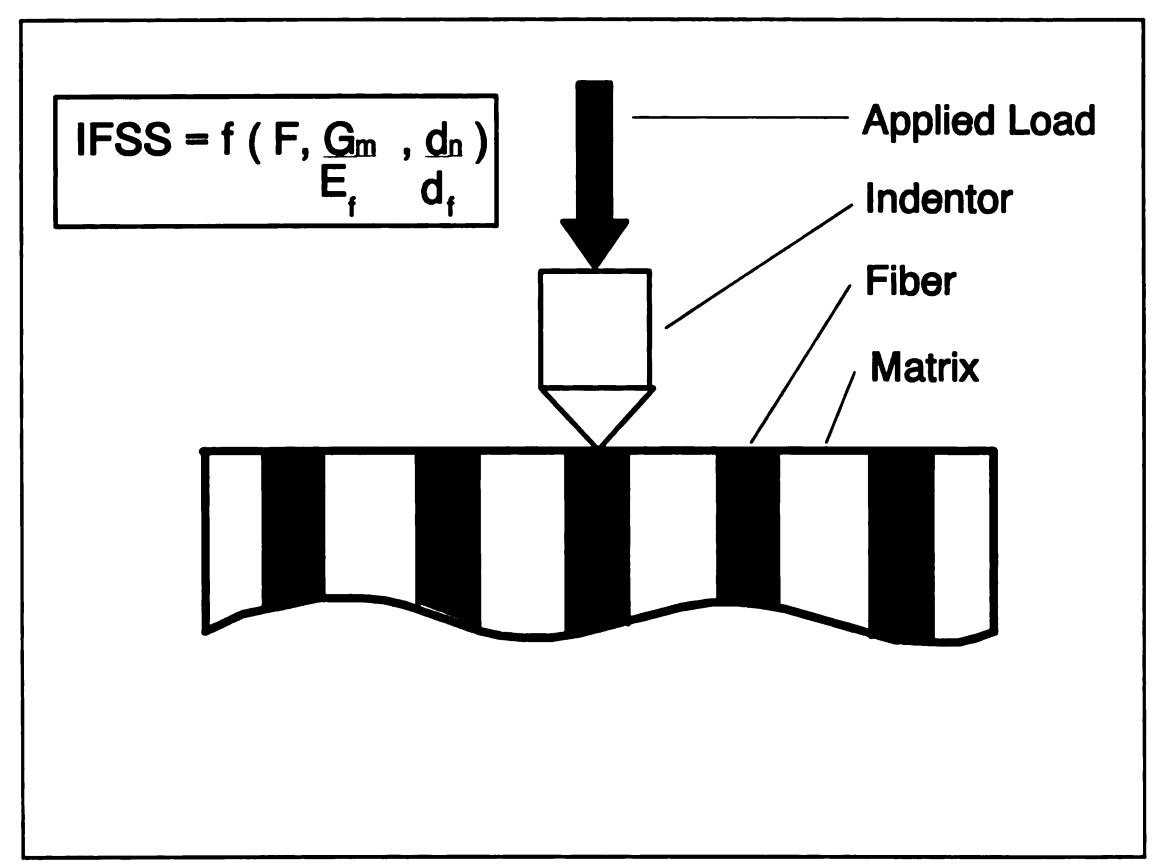


Figure 6. Schematic Diagram of the Interfacial Testing System (ITS).

surfaces which were perpendicular to the fiber alignment were polished to a mirror surface with 0.05 μ m diamond particles in an aqueous polishing media using a three hour polishing cycle. ITS testing protocol involved application of force to a fiber end through a 10 μ m diameter diamond-tipped indenter to induce fiber-matrix debonding, as shown in Figure 6. The testing involved applying one gram of force to the fiber and then checking the fiber for debonding. If no debonding was present, the force was increased in one gram increments and checked until 25% of the fiber perimeter was debonded from the matrix. As failure was approached the step size of the force increment was reduced to 0.5 gram. An equation based on the finite element analysis of the specimen geometry allows the interfacial shear strength in psi (IFSS) to be computed based on the fiber

tensile modulus in psi (E_f) , fiber diameter in microns (d_f) , matrix shear modulus in psi (G_m) , the distance between the tested fiber and the fiber closest to it in microns (d_n) , and the force required to produce fiber-matrix debonding along 25% of the fiber perimeter in grams (F).

IFSS =
$$F [0.875696\sqrt{G_m/E_f} - 0.018626\ln(d_n/d_f) - 0.026496]$$
 (16)

Selecting the fibers to be tested was an important part of obtaining reproducible results. The tested fibers and the fibers nearest to them had to be without scratch, chip, or crack, and any fiber which cracked during testing was disallowed. The axial fiber direction must be perpendicular to the polished composite surface, as evidenced by having a circular cross-section. The distance between the tested fiber and the fiber closest to it must exceed 2 μ m, and the distance between the tested fiber and at least three fibers must be within half the tested fiber's diameter.

VOID FRACTION ANALYSIS

Void content determination was accomplished using digitized images of the polished composite surface containing fiber ends. An image analysis system was used to obtain the volume fraction of voids for each of the composites²⁷. Ten 0.1 mm x 0.1 mm areas from each composite were analyzed. Since this is an optical technique, voids present in the composite had to be at least one micron in size to be discerned by the image analysis system.

MECHANICAL TESTING

Composite mechanical properties were tested at 23°C on a United Testing System

in accordance with ASTM standards for short beam shear (ASTM D2344) and 3-point bend testing (ASTM D790). Flexural specimens measured 25 mm x 75 mm x 3.2 mm and short beam shear specimens were 25 mm x 6.4 mm x 3.2 mm. Tensile testing was accomplished in accordance with ASTM D638 using a United Testing System with laser extensometer and a test rate of 1 mm/min. Type IV specimens were used with 25 mm gage length and 0.7 mm thickness.

4. MATRIX CHARACTERIZATION

INTRODUCTION

Dow's Derakane 411-C50 vinyl ester resin system was chosen as a representative matrix for this research because it is formulated for resin transfer molding and its gel time is easily varied. Derakane has exceptionally low viscosity because of the inclusion of 50 weight percent styrene which participates in the free radical chain polymerization reaction with the vinyl ester. The initiator and accelerator concentrations afford control over the gel time when good temperature control is maintained. The gel time may be controlled from 5 to 60 minutes at room temperature through varying the initiator and accelerator concentrations. The molecular structure of the Derakane vinyl ester is shown in Figure 7, along with the structure of the comonomer, styrene.

FREE RADICAL CHAIN POLYMERIZATION

Free radical chain polymerization provides a method of obtaining high molecular weight and/or crosslinked polymer in a relatively short time period compared with step polymerization. The radical species has a very short half-life, and reacts immediately with a nearby monomer or oligomer. Typical monomers for radical chain polymerization contain carbon-carbon double bonds (vinyl monomer) or carbon-oxygen double bonds (aldehydes and ketones)²⁸.

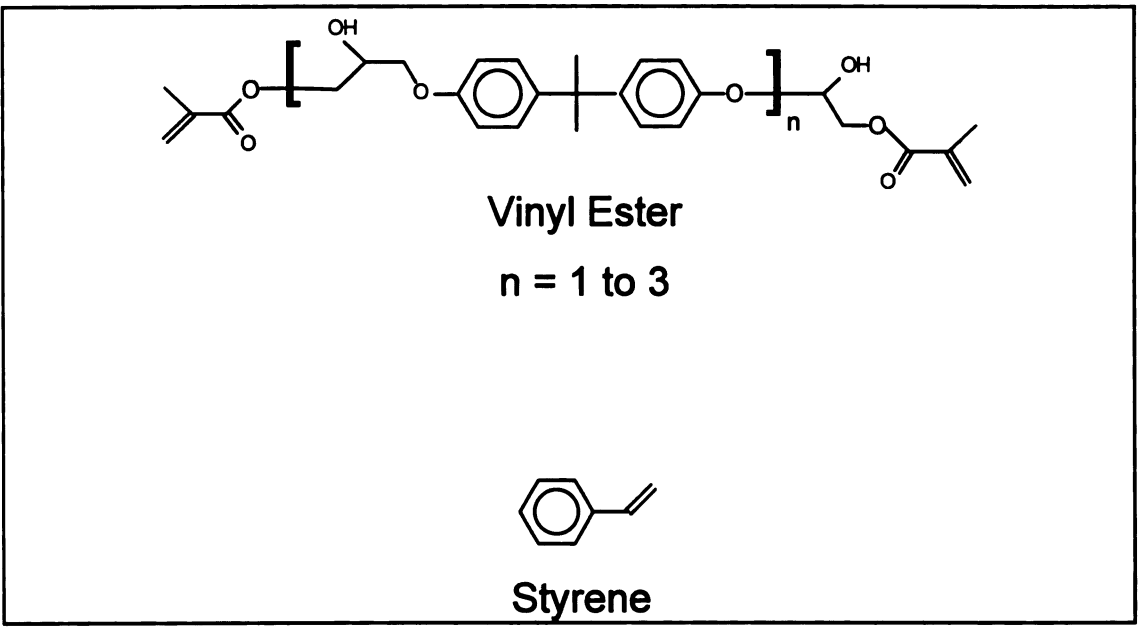


Figure 7. Schematic Diagram Showing the Structure of the Derakane Vinyl Ester and Styrene.

THEORETICAL EXTENT OF REACTION AT GEL POINT

The prediction of the extent of reaction at gel point must take into account the reaction mechanism. The case of a free radical chain polymerization involving copolymerization of a monomer with a double bond (monomer A) and a diene (monomer BB) has been investigated²⁹. The double bonds are treated as having equal reactivities. The gel point occurs when the number of crosslinks per chain is 0.5, and the critical extent of reaction at the gel point (p_c) may be expressed in terms of the double bond concentrations and the weight-average degree of polymerization (X_w) as

$$p_c = \frac{[A] + [BB]/2}{X_w [BB]/2}$$
 (17)

The weight-average degree of polymerization may be taken as that of the polymerization of monomer A alone with the same initiator concentration used in the copolymerization.

The kinetic chain length (ν) in a free radical chain polymerization may be expressed in terms of monomer and initiator concentrations ([M] and [I]), an initiator efficiency factor (f), and kinetic coefficients for propagation, dissociation, and termination $(k_p, k_d \text{ and } k_t)$.

$$v = \frac{k_p [M]}{2(f k_d k_t [I])^{1/2}}$$
 (18)

The benzoyl peroxide efficiency factor and kinetic coefficients for benzoyl peroxide and styrene are available from Odian³⁰. The temperature of interest for polymerization was 40° C, and the values for that temperature are as follows: f = 0.6, $k_p = 90.6$ l/mol.sec., $k_d = 1.37E-7$ /sec, and $k_t = 4.99E7$ l/mol.sec. Thus ν is 1003 for this system. The termination mechanism determines the relationship between ν and X_w . If disproportionation is the termination mechanism, then ν and X_w are equal. If coupling predominates, then X_w is twice ν . For the polymerization of styrene coupling predominates, so X_w is 2006 for this system, and considering that the weight fractions of styrene and vinyl ester are equal at 50%, the concentrations of vinyl ester and styrene are 0.6274 mol/l and 4.80 mol/l, respectively. The double bond concentration from the vinyl ester is 1.25 mol/l, double the concentration of the vinyl ester, whereas the double bond concentration from the styrene is equal to the styrene concentration. Equation (17) shows that p_c is 0.24% for this system.

The gel point occurs at a low extent of conversion in radical chain polymerization. This has an effect on the liquid composite molding process, because the mold must be filled before 0.24% extent of reaction has been reached. Mold filling in less than the gel time is accomplished by using an inhibitor to delay the commencement of polymerization.

Once the inhibitor has been depleted the polymerization reaction proceeds at a rapid rate, generating high molecular weight polymer from the onset of the polymerization.

REACTION KINETICS

Based on DSC data from isothermal experiments ranging in temperature from 30 to 100°C two kinetic models were developed; an autocatalytic model which describes the entire reaction, shown in Figure 8, and an inhibitor depletion model to describe the initial stages of the reaction.

AUTOCATALYTIC MODEL

The autocatalytic form of the kinetic model for the entire reaction is necessary because of the fast initial reaction rate. The model describes the reaction rate as:

$$\frac{dX}{dt} = k(\alpha)^m (1 - \alpha)^n \tag{19}$$

where X is the extent of reaction, t is time in minutes, k is an Arrhenius form kinetic coefficient with units of inverse minutes, α is X/X_{max} , where X_{max} is the maximum extent of conversion for the specified temperature, and m and n are kinetic exponents which were checked for temperature dependence. Vitrification occurs at temperatures below 100° C and hinders the reaction from proceeding to 100% conversion. This effect is incorporated into the model using X_{max} , which has the linear temperature dependence displayed in Figure 9.

Based on isothermal DSC experiments ranging in temperature from 30 to 100° C the following values have been determined: n=1.22, m=2.64-0.00616T where T is temperature in Kelvin, k=2.352exp(-3233/T), and $X_{max}=-0.7475+0.004692T$ where X_{max} may not exceed unity.

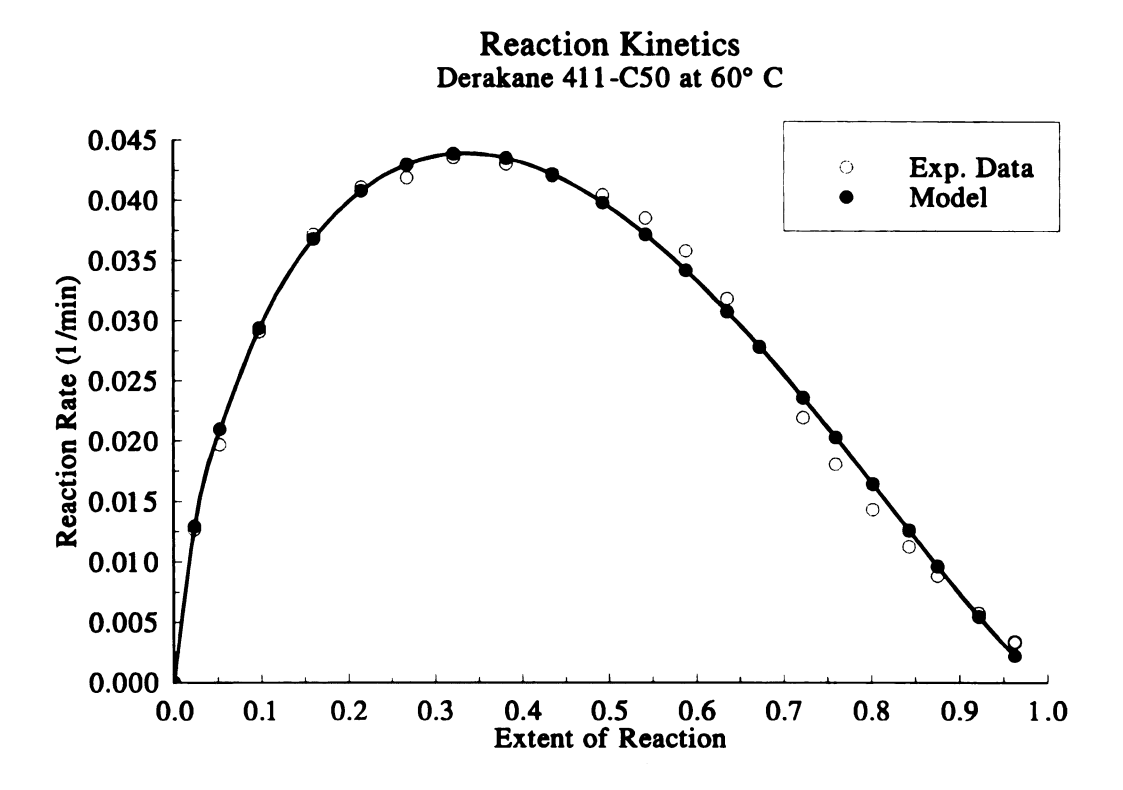


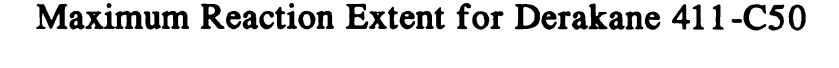
Figure 8. Comparison Between Reaction Model and Experimental Data for Derakane 411-C50.

INHIBITOR DEPLETION MODEL

The inhibitor depletion model is required to describe the initial stages of the reaction because the gel point occurs at approximately 0.25% conversion. The autocatalytic kinetic model is acceptable for describing the entire reaction, but lacks the desired accuracy near the gel point. The inhibitor depletion model has the form:

$$\frac{dX}{dt} = \frac{k_i(1-X)}{t_z-t} \tag{20}$$

The kinetic coefficient, k_i , and the inhibition time, t_z , have the typical Arrhenius form. The coefficients for this model were determined using data from 30 to 70°C: $k_i = 10^{-10}$



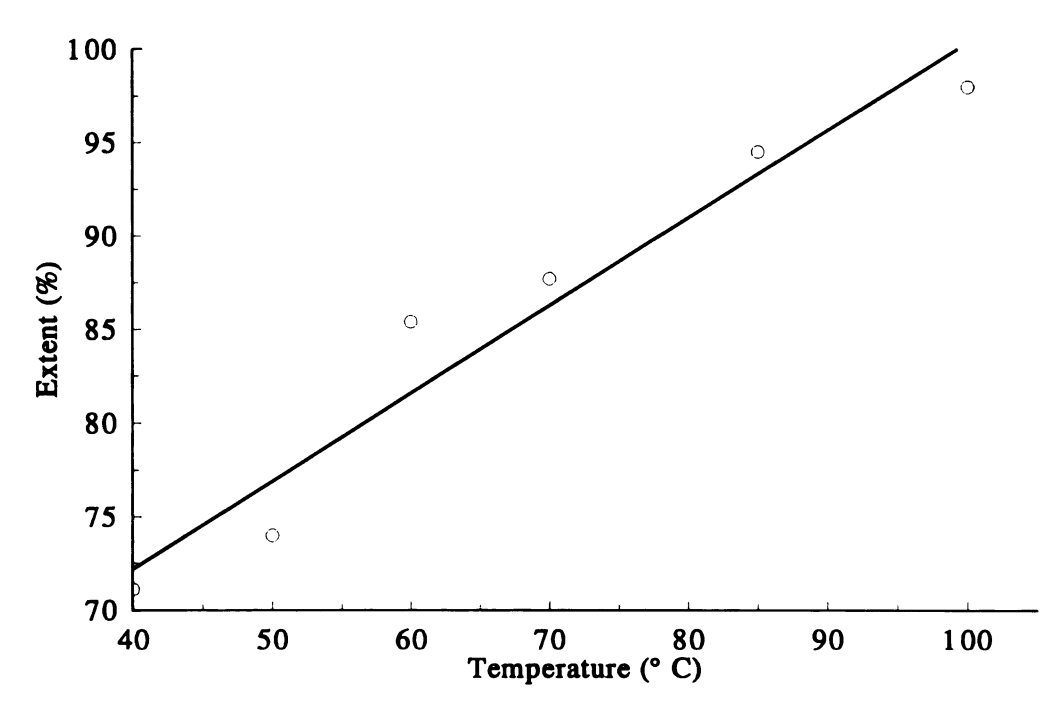


Figure 9. Relationship Between Maximum Extent of Reaction of Derakane 411-C50 and Temperature.

5.69E11 exp(-10360/T), and $t_z = 1.70E-11exp(8555/T)$. Figure 10 compares the experimental data with results predicted by the inhibitor depletion model.

EXPERIMENTAL EXTENT OF REACTION AT GELATION

Isothermal viscosity measurements were made with a Brookfield viscometer and a Rheometrics Mechanical Spectrometer 800 (RMS). The gel point was determined to be $0.25 \pm 0.27\%$ from RMS measurements by monitoring the storage and loss moduli of the curing resin system while a DSC experiment was monitoring the reaction exotherm concurrently at the same temperature. The resin used in the concurrent experiments was from the same sample which was mixed at the same time. The gel point is defined as

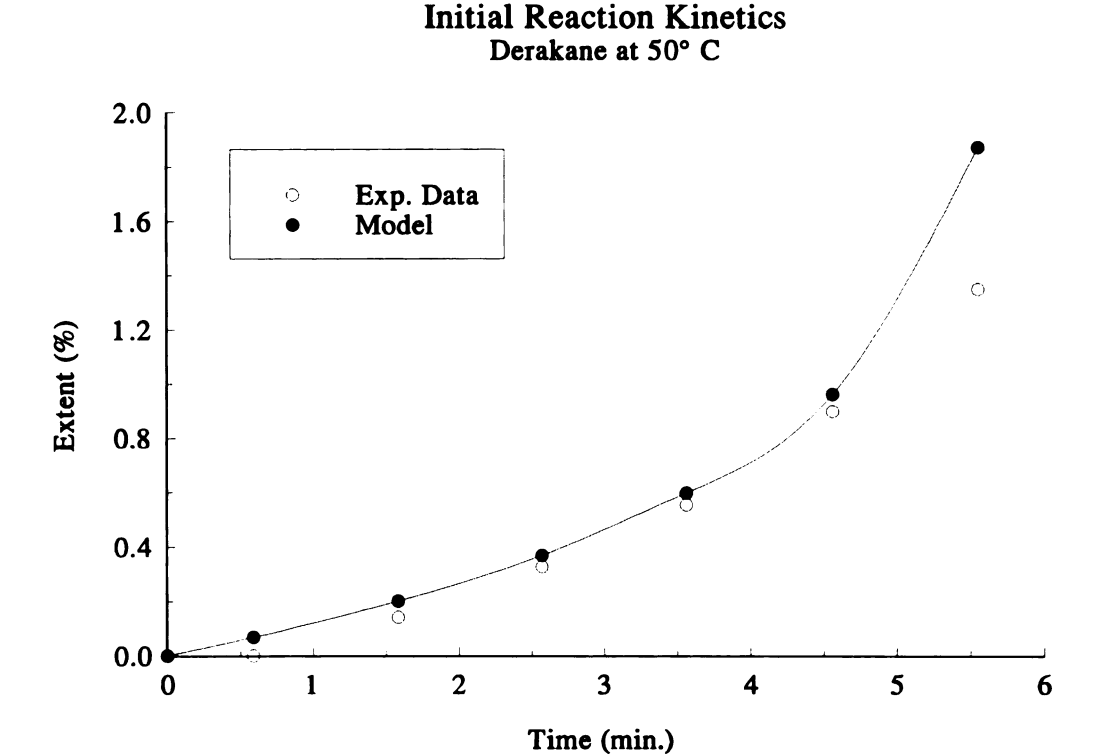


Figure 10. Comparison Between Initial Reaction Kinetics Model and Experimental Data for Derakane 411-C50.

the point at which the storage and loss moduli intersect as the storage modulus increases due to increasing molecular weight of the polymer. The resin reaches thermal equilibrium quickly in the RMS because only a small sample of resin was placed between the parallel plates having a large area for heat transfer. Experiments were conducted at 30, 40 and 50°C, but the DSC has poor sensitivity at the lower temperature, and the accuracy of the RMS measurements is poor at the higher temperature because of the low viscosity of the reacting Derakane at 50°C. Thus the value of conversion at the gel point was obtained from data at 40°C.

RESIN VISCOSITY AND RHEOKINETICS

The viscosity of the Derakane 411-C50 at 23°C is 156 cP, below the accurate range of the RMS. Therefore the Brookfield viscometer was used to measure the viscosity of Derakane without catalyst as a function of temperature. The resin was placed into a preheated cell where a thermocouple was placed into the middle of the resin to measure the temperature. Again the resin reached thermal equilibrium quickly because of the small sample size and spindle motion.

The viscosity dependence on extent of reaction was determined by monitoring the viscosity with the Brookfield viscometer while measuring the reaction exotherm from the polymerization reaction concurrently in the DSC. The resin used in the concurrent experiments was from the same sample which was mixed at the same time.

The viscosity modelling was accomplished by combining two models, one for describing temperature dependence and one for describing the effect of extent of reaction. The combined model assumes that the fluid is Newtonian, which is a good assumption for low molecular weight liquids. The temperature dependence of the monomer viscosity (η_m) is described by an Arrhenius-type equation:

$$\eta_m = A_n e^{E_n/T} \tag{21}$$

where $A_{\eta} = 1.171E-5$ cP and $E_{\eta} = 4854$ K. The relation between resin viscosity (η) and extent of reaction involves an empirically derived exponential model:

$$\frac{\eta}{\eta_m} = (1 - g)^{a_1 g + b_1} \tag{22}$$

where $g = X/X_g$, and $X_g =$ the extent of reaction at the gel point (1.5%), and a_n and b_n are constants having values of -3.32 and 0.656 respectively.

SIZING EFFECTS ON RESIN VISCOSITY

The viscosity of the soluble sizing solutions were measured with a Brookfield rheometer. The viscosity of the solutions were significantly increased as the concentration of the sizings increased, as shown in Table 4.1. All measurements were performed at 24° C, measured with a thermocouple placed into the liquid prior to measurement. Derakane 411-C50 has a viscosity of 168 cP. The viscosity effect of the insoluble polyurethane sizing could not be measured by the Brookfield rheometer because of the two phases present. The swollen polymer would wrap around the spindle and cause erroneous viscosity measurements. The semi-soluble polyvinyl acetate sizing (#3) has a strong effect on the solution viscosity. A linear increase in viscosity with sizing content was noted (90 \pm 5 cP per wt% sizing). The soluble polyester sizing (#4) also causes a linear increase in the solution viscosity (28 \pm 1 cP per wt% sizing).

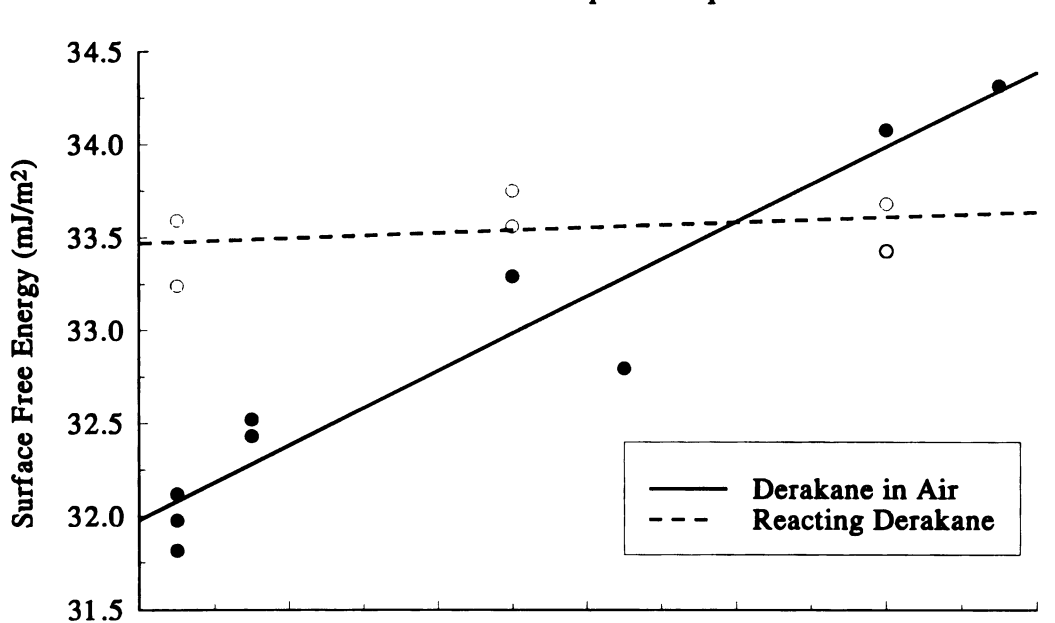
Table 4.1. Viscosity as a Function of Sizing Concentration for Derakane 411-C50 with Soluble Polyester Sizing (#4) and Semi-Soluble Polyvinyl Acetate Sizing (#3).

Concentration (%)	η #4 (cP)	η #3 (cP)
0	168	168
0.5	177	202
1.0	191	246
2.0	212	345
4.0	278	

SURFACE FREE ENERGY

Pendant drop analysis of Derakane 411-C50 was conducted for the uncatalyzed system in air and air saturated with styrene and also for the catalyzed system in air saturated with styrene. The first experiment quantified the effect of styrene evaporation on the surface tension. The second experiment was a control experiment, and the third quantified the change in surface tension with the extent of the reaction. Derakane in liquid form with no curing agent has an initial surface free energy of $32.0 \pm 0.2 \text{ mJ/m}^2$ when in contact with air at 22°C , relative humidity 40%. The surface free energy increases as a function of time at the rate of $0.15 \pm 0.05 \text{ mJ/m}^2/\text{min}$ in this environment due to evaporation of styrene, as shown in a sample of the data in Figure 11. Wetting of surfaces of comparable surface free energy will be less favorable at longer air exposure times because of the increasing resin surface free energy.

In order to determine the effect of chemical reaction on surface tension without styrene evaporation, a small chamber was filled with air saturated with styrene. Pendant drops of uncatalyzed Derakane were formed in the chamber and monitored for 30 minutes. No change in the liquid surface tension could be detected. Benzoyl peroxide powder catalyst was added to Derakane and the mixture was stirred for nine minutes to dissolve the catalyst into the resin. Again pendant drops were formed in the chamber saturated with styrene, and again no change in the surface tension could be detected, as shown in Figure 11. The resin gelled 33.7 ± 1.6 minutes after stirring was complete. Note that the initial surface free energy of the catalyzed resin was 33.5 mJ/m^2 , compared to 32.0 mJ/m^2 for the uncatalyzed resin. The difference is due to the styrene evaporation



Derakane 411-C50 Surface Free Energy Pendant Drop Technique

Figure 11. Derakane Surface Free Energy Measured by Pendant Drop Technique for Reacting and Non-Reacting Systems.

6

Time (min.)

8

10

12

4

2

which occurred during the nine minutes while the catalyst was being dissolved into the resin. The magnitude of surface free energy increase due to stirring the resin is near the increase in a pendant drop exposed to air for nine minutes. This result shows that the Derakane surface free energy is independent of chemical reaction to the gel point if compositional equilibrium can be maintained during mold filling. In vacuum assisted liquid composite molding, the tendency for styrene to evaporate from the resin is accelerated, and the surface free energy of the resin will increase at a much faster rate than that shown in Figure 11.

5. FIBER-MATRIX INTERACTIONS

INTRODUCTION

Glass fibers are available which are recommended for use in a broad range of applications, and for many composite manufacturing processes with a variety of different matrices. In order to understand the characteristics which distinguish these diverse sized glass fibers it is necessary to consider the glass fiber manufacturing process, additional processing glass fibers undergo, and composite manufacturing demands on the fibers.

A goal of this research is to quantify the characteristics of a glass fiber sizing which is optimized for liquid composite molding. Another goal of this research is to develop a quality control tool to identify the key parameters of a sized glass fiber which are important in liquid composite molding.

A series of patented sized glass fibers were studied having a large range of surface free energy and solubility in the matrix resin. The sized glass fiber surface free energy was determined using a polar/dispersive analysis of single fiber contact angle data. Single fiber contact angle measurements were made between the fibers and the matrix resin. Alternatively, wicking measurements were made on fiber bundles in the axial and transverse fiber direction to determine the contact angles. A high speed resin transfer molding process was used to produce 50% volume fraction fiber unidirectional composites from each of the fiber types using two processing cycles: vacuum assist and

preform preheat. The fiber-matrix adhesion and void content of the composites were evaluated to determine the effects of the fiber surface free energy and sizing solubility.

GLASS FIBER MANUFACTURE

Glass fibers are spun from molten glass which is passed through a die to produce thousands of fibers having diameters typically ranging from 10 to 20 micrometers in diameter. Immediately after the fibers have exited the die a "sizing" or "finish" of complex composition is applied to the fibers. The sizing fulfills many purposes, among which is the prevention of fiber surface damage during processing. Glass fibers are flaw sensitive, and the surface of the glass is easily scratched, even by another glass fiber, resulting in reduced strength glass fibers. The further processing of the fibers will result in abrasion unless the fiber surface is protected by sizing. Composite materials produced from extensively flawed fibers have significantly less strength compared to composites produced from fibers which have been adequately protected.

SIZING SYSTEMS

The "sizing" is an emulsion, a complex water-based mixture with polymer particles dispersed in it. The major component of the mixture is water, but this will be evaporated in subsequent processing, so the composition of the "sizing" is typically referred to in terms of the weight of the solids in the mixture which will remain on the surface after drying of the glass fibers. Sizings are typically proprietary formulations containing film-formers, coupling agents, anti-static agents, lubricants and/or other components³¹. Often surfactants are necessary to maintain the emulsion, although they may have deleterious effects on composite mechanical properties.

The sizing does much more than protect the fibers through lubricant action. It contains a "film-former", the largest component of the dried sizing, which provides compatibility between the sized fiber surface and the matrix used in composite production. This compatibility provides favorable interactions between the fiber and the matrix, evidenced by a small contact angle between them at the matrix flow front. A high degree of compatibility is necessary for good fiber-matrix adhesion.

Most "sizings" contain less than one percent coupling agent to improve fiber-matrix adhesion. The coupling agent is capable of chemical bonding between the glass surface and the matrix, although a probable mechanism for sizing-matrix adhesion is the formation of an interpenetrating network between the sizing and the matrix. This is in contrast to the adhesion at the glass-sizing interface, where the coupling agent chemisorbs to the glass fiber surface³². Coupling agents are especially important in maintaining fiber-matrix adhesion in humid conditions. Water has a corrosive effect on the interfacial shear strength in glass fiber reinforced polymer matrix composites without coupling agents. The addition of a silane coupling agent to the fiber surface results in a fiber-matrix interphase which is resilient in humid environments, because of hydrolyzable bond formation between the silane and the fiber surface which is reversible. The bonds may be broken and reformed to relieve stress in the fiber-matrix interphase³³.

Anti-static agents and lubricants are processing aids which combat specific problems to improve the ability to manufacture composite materials without hindering the action of the other components in the sizing system. Static buildup causes a problem with handling the fiber tow in processing operations such as weaving or braiding. Placement of a charged tow is inconsistent and therefore elimination of static charge is

desirable. A lubricant helps to keep the fiber tow from becoming frayed due to fiber damage. If insufficient lubricant is included in a sizing system, the fiber tow may break as a result of the accumulation of fiber damage. This is undesirable because of the additional expense associated with the process interruption which it causes.

Other components of sizing systems include emulsifying agents (surfactants) and strand hardening agents. The emulsifying agents are sometimes necessary to maintain the aqueous polymer dispersion. The strand hardening agents are especially useful when the fiber tow will be chopped in later processing. The additional stiffness afforded by the strand hardening agent makes the fiber tow easier to chop. Sometimes the aqueous emulsion pH needs to be reduced to speed a hydroxylation reaction and acetic acid is typically used. Other agents may be included for special purposes, but the typical constituents used in commercial sizings have been identified.

SIZED GLASS FIBERS

E-glass fibers produced with six different sizings were selected because the glass fiber sizings provide a wide range of surface free energy and solubility in the matrix. These commercial-type fibers provided by PPG Company have sizings which contain film-formers, silane coupling agents, lubricants and other constituents typical of commercial sizings. The compositions of the sizings are listed in Table 5.1. The sized glass fiber types are referred to by the film-formers present in the sizing systems: water (#6) - has no organic material on the fiber surface; soluble epoxy (#5) - contains an epoxy soluble in the vinyl ester matrix; soluble polyester (#4) - contains a polyester soluble in the vinyl ester matrix; semi-soluble polyvinyl acetate (#3) - contains a polyvinyl acetate (PVA) slightly soluble in the vinyl ester matrix; insoluble polyurethane

Table 5.1. Composition of Polyurethane, Polyvinyl Acetate, Polyester and Epoxy Glass Fiber Sizing Formulations.

Common Fiber Name	Insoluble Polyurethane (#2)	Semi-soluble Polyvinyl Acetate (#3)	Soluble Polyester* (#4)	Soluble Epoxy (#5)
Component	Pat.# 3,803,069 Example 1	Pat.# 4,027,071 Example 1	Pat.# 4,752,527 Example 2	Pat.# 3,997,306 Example 1
Solvent	water	water	water	water
Coupling Agent	gamma aminopropyl- triethoxy silane	gamma ethylene diamine propyl trimethoxy silane methacrylic acid complex of chromic chloride	gamma-methacryloxy- propyltrimethoxy silane	 methacryloxyalkyl- trialkoxysilane aminosilane coupling agent
Film Former	curable, blocked polyurethane resin emulsion	polyvinyl acetate	unsaturated bisphenolic glycol-maleic polyester	epoxy resin
Lubricant		1. cationic fatty acid amide 2. tetraethylene pentamine	polyethyleneimine polyamide	 tertiary amine salt polyethylene glycol
pH Control		acetic acid	acetic acid	
Emulsifying Agent				oxyalkylene glycol oxyalkylated vegetable oil alkylphenoxypoly-alkylene oxyalkanol
* Liber time #A electronists a cot		the common the common of the c	the contraction on participation of	Carlo Caronio mintomomi ammonium na topo am antichetia accest and an amichina methodological

* Fiber type #4 also contains a cationic organic quaternary ammonium salt for an antistatic agent and an aqueous methylated melamine-formaldehyde resin for a strand hardening agent.

(#2) - contains a polyurethane completely insoluble in the vinyl ester matrix; and a non-wettable, soluble sizing system (#1). This fiber (#1) was not supplied by PPG and was produced by coating the soluble polyester sized fiber (#4) with Mono Coat mold release agent (Chem Trend) and heating at 120°C for two hours to evaporate the solvent.

EXPERIMENTAL PROCEDURE

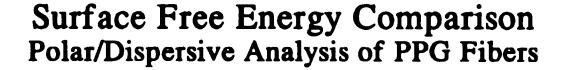
The experimental procedure for the Micro-Wilhelmy measurement of single fiber contact angles and wicking in the axial and transverse fiber directions has been discussed in chapter 3. Composite plaque processing, the interfacial testing system for measuring fiber-matrix adhesion, and the void content analysis technique have also been outlined in chapter 3. The matrix resin used in the research is Dow's Derakane 411-C50 which has been thoroughly investigated in chapter 4.

RESULTS AND DISCUSSION

FIBER SURFACE FREE ENERGY

Fiber surface free energies were determined from micro-Wilhelmy measurements on the six glass fiber types with four probe liquids of known polar and dispersive components³⁴ (water, ethylene glycol, formamide and methylene iodide). Figure 12 shows the results of polar/dispersive analysis of equilibrium contact angle data. The error bars show the error associated with the total surface free energy. The sized glass fibers provide a range of total surface free energies from 28 to 59 mJ/m².

The total surface free energy of the sized glass fibers is an indicator of thermodynamic wetting. The resin (surface free energy of 32.2 mJ/m²) would be expected to initially "wet" water-sized glass fibers the best (smallest contact angle) because they have the highest total surface free energy (58.7 mJ/m²). The water-sized



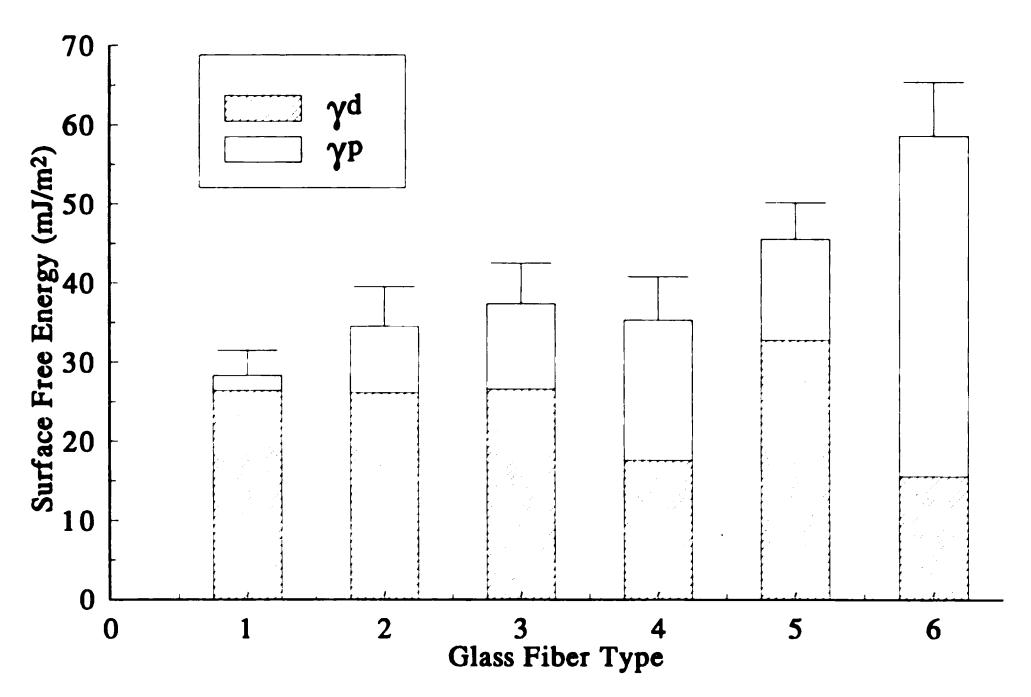


Figure 12. Surface Free Energy Comparison of PPG Sized Glass Fibers Calculated from Polar/Dispersive Analysis.

fiber has a hydroxylated surface from the application of water to the fiber immediately after it was manufactured. The hydroxylated surface is very polar and consequently this fiber has by far the highest polar component of surface free energy among the fibers $(43.1 \pm 4.3 \text{ mJ/m}^2)$, and the highest total surface free energy $(58.7 \pm 6.8 \text{ mJ/m}^2)$. The other fibers would be expected to have larger contact angles and hence poorer "wetting". The mold release sized fibers (#1) have a low polar component of surface free energy $(1.8 \pm 0.7 \text{ mJ/m}^2)$, and the lowest total surface free energy. The dispersive component of surface free energy is constant for most of the fibers. Fibers #2, #3 and #4, polyurethane, polyvinyl acetate, and polyester sized fibers have very similar total surface

free energies (approximately 35 ± 5 mJ/m²). The low value of dispersive surface free energy for fiber #4 (17.6 \pm 2.8 mJ/m²) may be an artifact that is not only indicative of surface effects because of the solubility of this sizing in the dispersive probe liquids. If the highly dispersive probe liquids dissolved the sizing during the contact angle measurements then the dispersive component of surface free energy would be lowered. The expected dispersive component should be similar to that of fibers #1, #2 and #3 (26 mJ/m²) which would increase the total surface free energy for fiber #4 to approximately 44 mJ/m^2 . The soluble epoxy sizing (#5) has the highest total surface free energy of any of the fibers with commercial type sizings, and is expected to give the most favorable wetting conditions.

SINGLE FIBER CONTACT ANGLE

Micro-Wilhelmy experiments were also performed to determine the single fiber contact angle (θ_s) between the fibers and resin. The single fiber was immersed in the resin at a rate of $25\mu\text{m}/\text{second}$ to obtain the dynamic advancing contact angle. These results are included in Table 5.2, and indicate that favorable wetting will occur with fibers #2 to #6 because they have small contact angles. Note that the errors associated with small contact angles are larger than expected because of the nature of the cosine function. The penetration distance (L_s), the distance the resin flows in one second due to capillary forces, was calculated from these data using the capillary equation physical constants from the wicking experiments. The capillary equation may also be used to calculate the wicking rate.

Table 5.2. Comparison Between Single Fiber and Axial Wicking Contact Angles and Experimental and Predicted Penetration Distances for Derakane 411-C50 Wicking into Fiber Bundles.

<u>Gl</u>	ass Fiber Sizing	<u>θ_s (°)</u>	L_{s} (μm)	θ_{AW} (°)	L_{AW} (μm)
1.	Mold Release	33 ± 3	550 ± 30	>90	0
2.	Insoluble Polyurethane	12 ± 7	590 ± 30	69 ± 5	360 ± 40
3.	Semi-Soluble PVA	10 ± 8	880 ± 20	82 ± 1	320 ± 20
4.	Soluble Polyester	18 ± 5	650 ± 30	86 ± 1	160 ± 20
5.	Soluble Epoxy	18 ± 6	875 ± 15	69 ± 5	530 ± 60
6.	Water	8 ± 10	765 ± 15	29 ± 26	730 ± 160

WICKING EXPERIMENTS

Axial Wicking

The hydraulic constant (K) relates the average equivalent diameter of a pore in a fiber bundle to the volume and the surface area of the pore. The hydraulic constant was determined for the five fiber types (#2 - #6) using hexadecane as the wicking liquid. Hexadecane's low surface tension (27.6 mJ/m²) provided a zero contact angle with these fibers, allowing calculation of the hydraulic constants (Table 5.3) from the wicking rate data. Note that the hydraulic constant was not calculated for the mold release sized fibers (#1) because the resin would not "wet" the fibers, showing that the bundle contact angle is greater than 90°.

The water-sized fiber bundles have a smaller hydraulic constant because of lower surface area (more cylindrical geometry) compared with sized fibers, which have increased surface area due to the unevenly distributed sizing. Taking these surface area differences into consideration through the hydraulic constant allows comparison of rate data of resin wicking into fiber bundles.

Table 5.3. Axial and Transverse Wicking Hydraulic Constants from Hexadecane Wicking into Fiber Bundles with 45% and 50% Fiber Volume Fractions, Respectively.

Glass Fiber Sizing		$\underline{\mathbf{K}}_{\mathbf{AW}_{-}}$	$\underline{\mathbf{K}}_{TW_{-}}$	
2.	Insoluble Polyurethane	3.49	0.0392	
3.	Semi-Soluble PVA	4.33	0.0385	
4.	Soluble Polyester	5.31	-	
5 .	Soluble Epoxy	4.80	0.0554	
6.	Water	2.61	0.0775	

In order to relate the wicking effects to mold filling rates in a direction parallel to the fibers, the penetration distances (L) for a time of one second were calculated from the single and bundle contact angle data and are included in Table 5.2. The contact angle data are in reasonable agreement for the water-sized fibers, but for the other fibers the single fiber contact angle is always smaller than the bundle contact angle. Examination of sized fiber bundles shows that the sizing morphology is not uniform. Sizing bridges between fibers, fills entire areas and creates closed-end pores. The fiber sizing controls the fiber tow geometry and inhibits resin penetration, causing the bundle contact angle to be greater than the single fiber contact angle. The bundle contact angle is a volume-averaged value over all the pores, and the large pores are weighted more heavily than the small pores. Their much larger volume causes the bundle contact angle to be larger than the single fiber contact angle. The bundle contact angle for the soluble polyester sized fibers is exceptionally large (86 ± 1°), and is surely increased by an increase in resin viscosity from the dissolution of fiber sizing during the experiment. The relatively high molecular weight of the fiber sizing, compared with the resin, has a strong effect on the resin viscosity even in small amounts. Note that the bundle penetration distances are different in fibers #2 and #5 although their bundle contact angles are the same due to the larger fiber diameter of the soluble epoxy sized fibers.

Transverse Wicking

The results from the axial and transverse wicking experiments are included in Table 5.4 below: contact angles and one second penetration distances. The results agree qualitatively, and the axial penetration (and wicking rate) is approximately an order of magnitude greater than the transverse wicking. These results are in agreement with previous studies which have shown that the wicking rate in the transverse direction is an order of magnitude less than the rate in the axial direction³⁵. The contact angle from the transverse wicking may be elevated by dissolution of the semi-soluble polyvinyl acetate sizing (#2). Subsequent experimentation has shown that this fiber sizing (#2) has a large diffusion coefficient in the matrix compared with the soluble polyester sizing (#4)³⁶. The results from transverse wicking data show that the water sized fibers (#6) are not significantly different from the soluble epoxy fibers (#5). This suggests that the transverse wicking experiment is less sensitive to the presence of a sizing on the glass fiber surface compared to the axial wicking experiment.

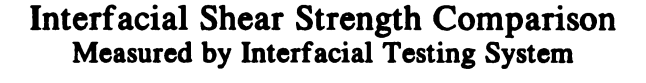
Table 5.4. Comparison Between Axial and Transverse Wicking Results: Contact Angles and One Second Penetration Distances for Derakane 411-C50 Wicking into Fiber Bundles with 45% and 50% Fiber Volume Fraction, Respectively.

Gl	ass Fiber Sizing	θ_{AW} (°)	L_{AW} (μm)	<u>θ_{rw} (°)</u>	L_{TW} (μ m)
1.	Mold Release	>90	0	- .	-
2.	Insoluble Polyurethane	69 ± 5	360 ± 40	45 ± 41	70 ± 38
3.	Semi-Soluble PVA	82 ± 1	320 ± 20	77 ± 10	33 ± 14
4.	Soluble Polyester	86 ± 1	160 ± 20	-	-
5.	Soluble Epoxy	69 ± 5	530 ± 60	39 ± 37	80 ± 31
6.	Water	29 ± 26	730 ± 160	35 ± 31	86 ± 39

FIBER-MATRIX ADHESION

The fiber-matrix adhesion data obtained from ITS measurements on unidirectional composite specimens fabricated with each of the six fibers and the vinyl ester resin are shown in Figure 13. The adhesion results are similar for the vacuum assist and preform preheat processing cycles. There is a strong correlation between the fiber-matrix adhesion and the fiber total surface free energy. Fiber-matrix adhesion tends to be higher for the fibers with higher fiber total surface free energy. The formation of an interphase between the soluble sized fibers (#4 and #5) and the resin can be important in increasing adhesion in these systems. Chemical bond formation between the matrix and the soluble sizings as well as dissolution of the sizings by the resin further the development of an interphase with the soluble sized fibers (#4 and #5).

The water-sized fibers (#6) would be expected to have the highest fiber-matrix adhesion based on a thermodynamic argument alone, but the low value measured has been attributed to an artifact in the sample preparation process. The fiber-matrix interface was not protected by a silane coupling agent and was most probably damaged



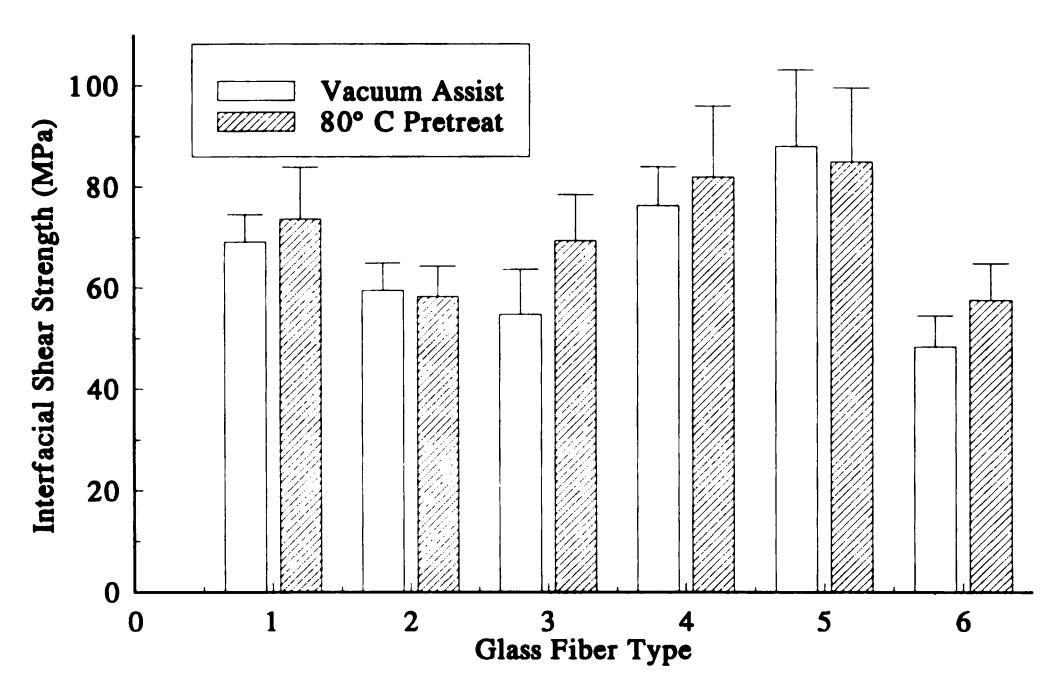


Figure 13. Interfacial Shear Strength Comparison Between Derakane/Glass Fiber Composites for Vacuum Assist and Heat Pretreat Cycles Measured by Interfacial Testing System.

by exposure to water in the polishing procedure. Since maximum shear stress is encountered within a few microns of the surface the adhesion was much lower than the value expected for a fiber with this high level of total surface free energy.

The mold release sized fibers (#1) have higher interfacial shear strength than expected (70 MPa), because the soluble sizing underneath the mold release was dissolved by the resin, carrying the low surface energy material away from the fiber interphase and allowing fiber-matrix adhesion similar to the soluble polyester sized fibers (#4) to be attained. This was verified by coating water sized fibers (#6) with the mold release

coating and processing them with preheating into a composite of 50% fiber volume fraction. The resulting fiber-matrix adhesion determined by ITS was 29.4 \pm 9.0 MPa, which is attributable to the low surface energy produced on the glass surface by the application of the mold release.

The minimum interfacial shear strength values were measured with the polyurethane and polyvinyl acetate sized fibers (#2 and #3). The low surface free energy associated with the fiber surfaces limited the level of interaction between the sizings and the matrix. The insoluble polyurethane sizing (#2) does not form an interphase, consequently the stress transfer from matrix to fiber is low.

VOID CONTENT

Void volume fractions were analyzed in the composites produced with each fiber type and both processing cycles. Table 5.5 shows that the void contents are exceptionally low for these fill rates and processing conditions. The composite properties are not expected to be effected by such low void fractions. The first set of three composites, produced with mold release, polyurethane and polyvinyl acetate sized fibers (#1, #2 and #3), has a slightly higher void fraction than the second three composites, produced with polyester, epoxy and water sized fibers (#4, #5 and #6). However, the difference between these two data sets is minimal. It is concluded that the relatively low resin flow rate and high packing pressure used in fabricating the composite specimens superseded surface conditions which would be expected to cause void formation. The composites produced with the mold release sized fibers (#1) were expected to contain a much higher void fraction because the contact angle between the matrix and the fibers

was greater than 90°, whereas the contact angles between the matrix and the other fibers was much less.

Table 5.5. Volume Fraction Voids for Composites Processed with Vacuum Assist (V.A.) and Heat Pretreat (H.P.).

Glass Fiber Sizing	$\underline{\mathbf{V}}_{\mathbf{v}}$ V.A. (%)	V_v H.P. (%)
1. Mold Release	0.102 ± 0.065	0.045 ± 0.054
2. Insoluble Polyurethane	0.28 ± 0.04	0.39 ± 0.11
3. Semi-Soluble PVA	0.61 ± 0.27	0.37 ± 0.14
4. Soluble Polyester	0.013 ± 0.019	0.005 ± 0.010
5. Soluble Epoxy	0.108 ± 0.031	0.31 ± 0.15
6. Water	0.031 ± 0.014	0.002 ± 0.004

CONCLUSIONS

Single fiber contact angle measurements are not sufficient by themselves to predict the velocity of resin flow into a sized fiber bundle due to capillary forces. Wicking experiments are more appropriate because they take into consideration the fiber tow geometry and morphological effects of the fiber finish. A 50% reduction in wicking rate was measured for sized fibers bundles compared with water sized fibers (#6) and the reduction was attributed to fiber finish morphology.

The surface free energy of sized glass fibers provides predictive information about the level of fiber-matrix interaction which occurs in liquid composite molding. A favorable thermodynamic driving force is necessary for obtaining a well developed interphase, which will result in good fiber-matrix adhesion. The fibers with greater surface free energies had much higher levels of adhesion.

Rheological factors such as resin flow rate and packing pressure have superseded the surface influences which were expected to cause voids in the liquid composite molded composites produced with a variety of sized glass fibers having a wide range of surface free energies.

6. MICRODIELECTRIC ANALYSIS OF INTERPHASE FORMATION

INTRODUCTION

When glass fibers reinforce a polymeric matrix in a composite material, the strength of the composite depends on the adhesion between the fiber and the matrix. To achieve improved fiber-matrix bonding the fibers are coated with a sizing system. Commercial sizing systems are engineered to serve many functions including enhancing fiber-matrix adhesion, making handling easier by binding the fibers into a cable tow, improving resin wet-out, and protecting the fiber during processing³⁷. Sizing systems are emulsions containing proprietary complex compositions. The primary component is a film former, a polymer which will cover the glass surface to protect it and to provide favorable physical and/or chemical interactions with the resin matrix. Another component is the coupling agent which is typically a silane. It provides chemical bonding between the glass fiber surface and the matrix. Often lubricants and anti-static agents are also used in the sizing system to enhance processability³⁸.

Optimization of composite processing requires an understanding of the processes which occur as the matrix resin interacts with the fiber surface. The interactions which occur in glass fiber reinforced polymeric composites are complex because of the commercial sizings applied to the glass fiber surface. The evaluation of the swelling and

dissolution rates for glass fiber sizings in matrix resin for these processes is an important step in quantifying the time dependencies of the interactions between the sizing and the resin. The dissolution of the sizing into the matrix in a reacting system is a necessary condition for optimum composite properties. In a liquid composite molding process matrix reactivity and/or fill times could limit the time available for dissolution of the sizing into the matrix. Optimum processing cycles need to be based on allowing a proper amount of time for sizing-matrix interaction. Measurement of this interaction time is a prerequisite for determining the processing window for liquid composite molding processes.

The diffusion coefficients for the resin through three sizing system films were determined by measuring, with a microdielectric sensor, the change in the dielectric properties of the sizing system after placing the sizing and matrix in contact. The changes in dielectric properties of the swollen sizing films were monitored as the sizings diffused into the resin, providing data which facilitated the evaluation of diffusion coefficients describing this process.

THEORY

DIELECTRIC

When the molecules in a liquid are subjected to an electromagnetic field, the dipoles align with the field and ions move toward the field poles. The dipoles and ions in a solid, however, are slower to respond because they are constrained by the structure of the solid. The dielectric properties of a sizing film change as the film is penetrated and is swollen by liquid resin because the ions and dipoles in the solid become less constrained as the resin swells the film. The permittivity is a measure of the degree of

alignment of dipoles, and the loss factor is a measure of the energy expended to align dipoles and move ions. Ionic conductivity is the result of current flow and is a measure of the ion concentration and mobility through the material³⁹.

Measuring the change in the dielectric response of the sizing over time is an indirect measure of the resin or sizing concentration at the surface of the microdielectric sensor. From monitoring these concentrations the rate of diffusion of the resin into the sizing film and the rate of diffusion of the sizing film into the resin may be calculated.

FICKIAN DIFFUSION

The Fickian diffusion model provides a mathematical description of the mass transfer of a material due to a concentration gradient. The mass transfer is proportional to the concentration gradient through the diffusion coefficient, D. The differential equation describing unsteady-state one dimensional Fickian diffusion in a plane sheet where concentration, C, is described in relation to time, t, and distance, x, is⁴⁰:

$$\frac{dC}{dt} = D\frac{d^2C}{dx^2} \tag{23}$$

This equation is applied to the penetration of resin into sizing films. When an uncrosslinked polymeric solid is contacted with a good solvent two processes occur: the solid absorbs solvent and is swollen, then the swollen solid is dissolved into the solvent.

SIZING FILM SWELLING

The following equations may be used to relate the conductivity of a material to time, a length scale, and the diffusion coefficient for a liquid penetrating into a sizing film. Initial conditions for the sample geometry described in Figure 14 include a uniform resin concentration C_0 in the sizing film and the surface resin concentration maintained

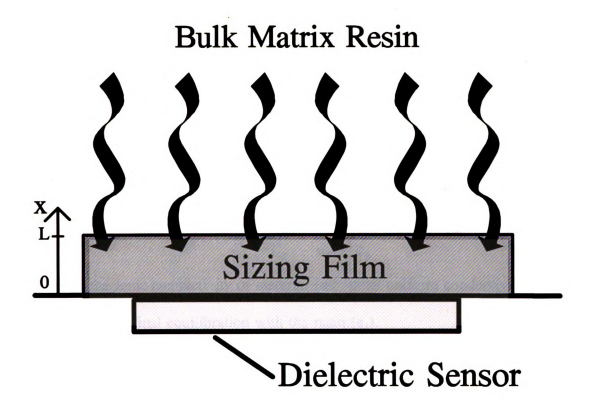


Figure 14. Schematic diagram of one-dimensional unsteady-state diffusion of resin into sizing film on microdielectric sensor face.

constant at C_1 . The solution to equation 1 follows and is the basis for the calculation of the diffusion coefficient, D_R , for the resin penetrating into the sizing system film⁴¹:

$$\frac{C_R - C_0}{C_1 - C_0} = 1 - \frac{4}{\pi} \sum \frac{(-1)^n}{2n+1} \exp(\frac{-D_R (2n+1)^2 \pi^2 t}{4L^2}) \cos(\frac{(2n+1)\pi x}{2L})$$
 (24)

In terms of concentration of resin a distance x into the sizing film from the sensor face (C_R) , initial uniform concentration of resin in the sizing film (C_0) , surface resin concentration in equilibrium with bulk resin (C_1) , Diffusion coefficient of resin into the

sizing film (D_R) , time from contact of sizing coated sensor with resin (t), distance from the sensor face into the sizing film (x), and sizing film thickness (L).

A linear correlation between the resin concentration and the conductivity is assumed, and a linear relationship between dielectric properties and concentration has been demonstrated with other materials being absorbed into films for some polymer systems^{42, 43, 44}:

$$\frac{C_R - C_0}{C_1 - C_0} = \frac{\sigma - \sigma_0}{\sigma_1 - \sigma_0}$$
 (25)

In terms of the ionic conductivity of material (σ) , initial uniform conductivity (σ_0) , and conductivity after final equilibration with the resin (σ_1) .

The sizing film conductivity measured by the microdielectric sensor is an average measurement over a volume of film which covers the area of the sensor face and extends from the sensor/film interface 18 microns into the film. The sensed region volume was determined by monitoring the conductivity as successive 6 micron thick films of sizing were added to the sensor face in the manner described in the experimental procedure. The conductivity varies linearly with the film thickness over the sensing range, 18 microns. Proper weighting of the dielectric signal as a function of distance into the film was accomplished by setting x equal to 9 microns in equation 2. The sizing film thicknesses were calculated from the mass and area of the sizing film and the density of the film former. The diffusion coefficient was calculated using the Levenberg-Marquardt algorithm to perform non-linear least squares analysis on the conductivity as a function of time data.

SIZING FILM DISSOLUTION

The second event to occur after an uncrosslinked polymeric solid is contacted with a good solvent for that solid is dissolution of the solid. For the sizing film diffusing into

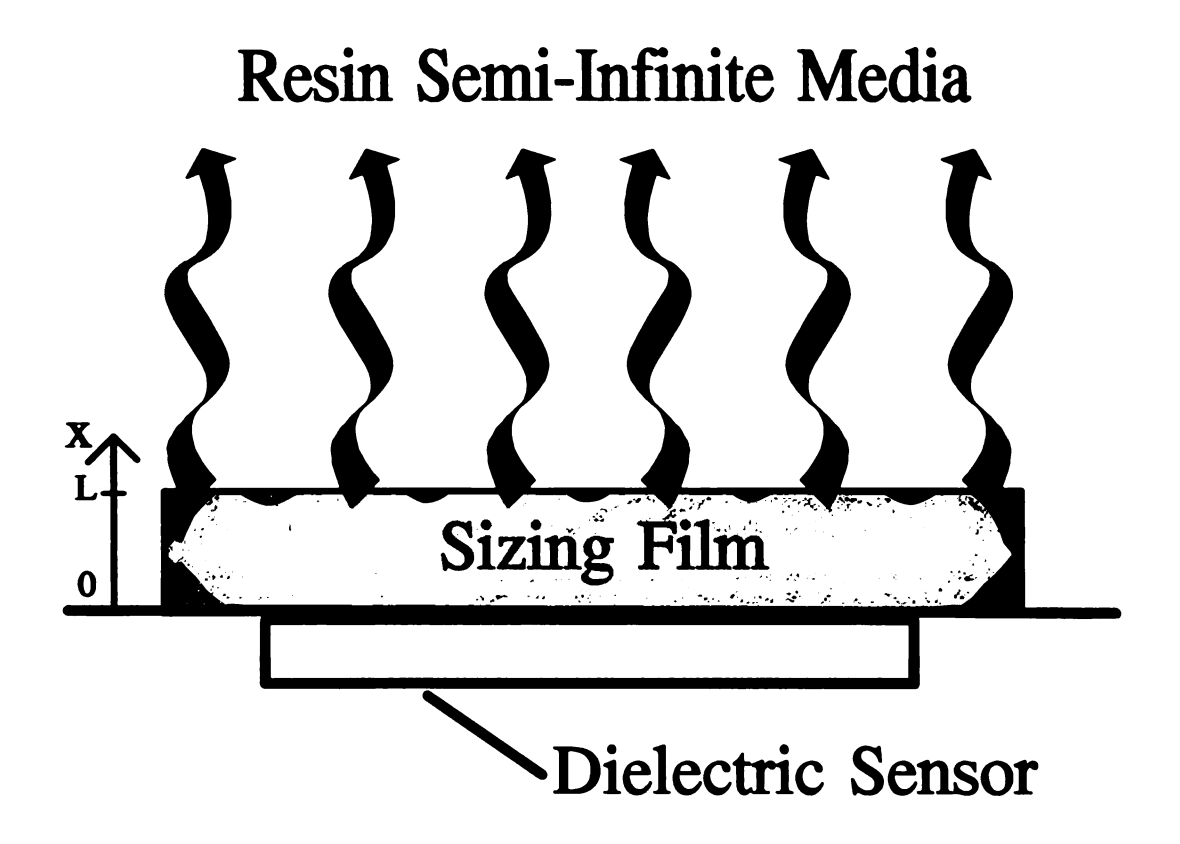


Figure 15. Schematic diagram of one-dimensional unsteady-state diffusion of sizing film from microdielectric sensor face into resin semi-infinite media.

the resin, a plane source model for one dimensional unsteady-state Fickian diffusion with the assumption of a semi-infinite resin volume is a good approximation to the physical situation shown schematically in Figure 15. Initial conditions include the instantaneous presence of a planar source and initial sizing concentration in the bulk resin of zero. The equation that describes the concentration as a function of distance from the sensor face and time is⁴⁵:

$$C_S = \frac{M}{(\pi D_S t)^{1/2}} \exp(\frac{-x^2}{4D_S t})$$
 (26)

In terms of concentration of sizing film a distance x into the resin from the planar source (C_s) , mass of the sizing film (M), diffusion coefficient for the sizing film into the resin (D_s) , time from contact of sizing coated sensor with resin (t), and distance from the sensor face into the sizing film (x).

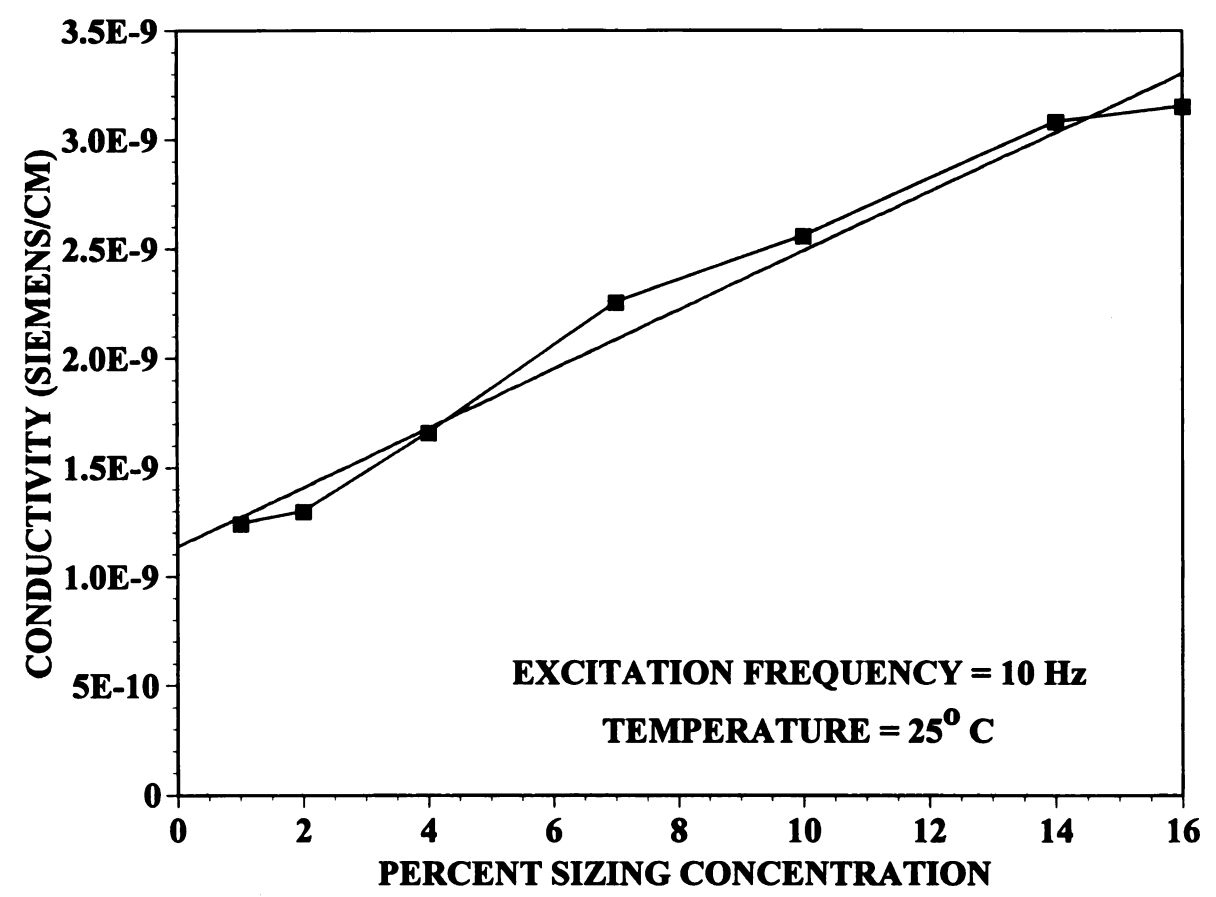


Figure 16. Calibration curve relating dried polyester sizing concentration in resin to ionic conductivity measured by a low conductivity microdielectric sensor.

A linear correlation between the sizing concentration and the conductivity has been demonstrated for the soluble sizings. Figure 16 and Figure 17 show the calibration curves for polyester and polyvinyl acetate sizings which were generated by measuring

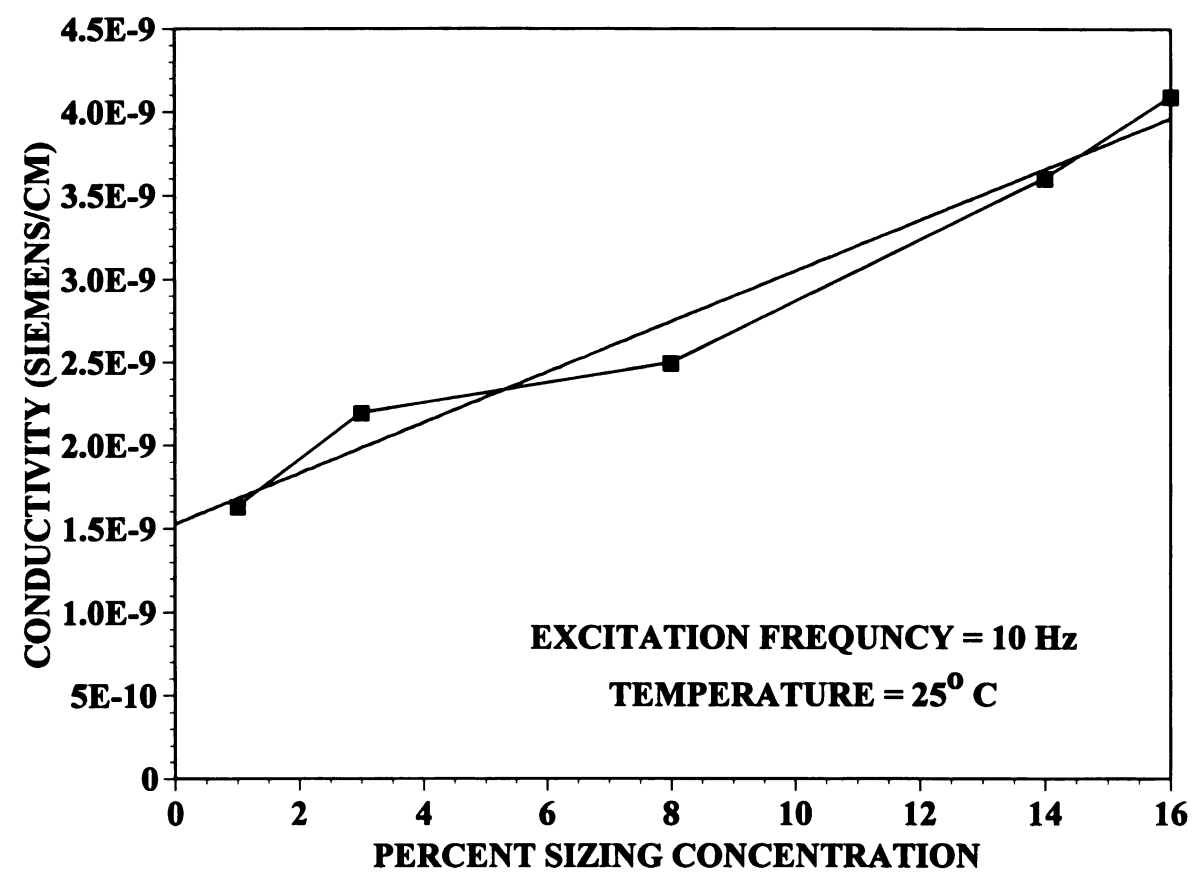


Figure 17. Calibration curve relating dried polyvinyl acetate sizing concentration in resin to ionic conductivity measured by a low conductivity microdielectric sensor.

the dielectric properties of solutions of known sizing concentration. The conductivity is linearly dependent on the sizing concentration over the range of sizing concentrations pertinent to this research. Since the volume of resin is many orders of magnitude larger than the volume of sizing system film the semi-infinite media assumption is valid. The conductivity provides an average measurement of the sizing concentration 18 microns into the film from the sensor/film interface, so x is 9 microns in equation 4 to account for the averaging. However, the exponential portion of the equation is approximately unity because relatively long times are under consideration. From the slope of a plot of

conductivity versus t^{-1/2}, determined by least squares linear regression, the diffusion coefficient may be calculated. Rearranging equation 4 gives the diffusion coefficient:

$$D_S = \frac{1}{\pi} (\frac{2M \Delta \sigma}{S})^2 \tag{27}$$

Where $\Delta \sigma$ = change in conductivity

S = slope of the plot of σ vs. $t^{-1/2}$

M = mass per unit area of sizing film

MATERIALS

The vinyl ester resin system used was Derakane 411-C50 made by Dow Chemical Company. A reactive diluent, styrene, is used to lower the viscosity of the resin system to make it suitable for applications requiring extremely fast wet-out, including liquid composite molding, centrifugal casting, and other applications. The resin system is one half styrene and one half vinyl ester by weight.

The sizing systems used in this research are similar to proprietary commercial sizing systems. The liquid sizing systems are aqueous emulsions, and the primary component of the sizing systems are the film former. PPG provided non-commercial, model liquid sizing systems with film formers of varying solubilities in Derakane: soluble polyester (based on patent number 4,752,527), semi-soluble polyvinyl acetate (based on patent number 4,027,071) and insoluble polyurethane (based on patent number 3,803,069).

EXPERIMENTAL SET UP

A Eumetric System III Microdielectrometer and disposable low conductivity sensor from Micromet Instruments, Inc. were used for making the dielectric measurements and data acquisition. Data was acquired at a rate of 1 measurement every 10 seconds for the first 10 minutes

conductivity, loss factor, permittivity and temperature were measured using a 10 Hz input signal. The low conductivity microdielectric sensor, shown schematically in Figure 18, measures an average of the dielectric properties of a material within 18 microns of the sensor face, with the weighting of the average being equal for material regardless of its distance from the sensor face.

and then once every 2 minutes for the

next 170 minutes.

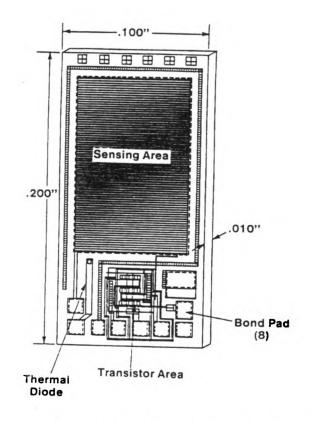


Figure 18. Schematic diagram of a microdielectric sensor and its circuitry. Used with the permission of Micromet Instruments.

EXPERIMENTAL PROCEDURE

The preparation of the sizing film sample on the sensor is similar to the commercial process used in the manufacture of glass fibers. First a drop of a liquid sizing system of known mass was applied to a Micromet low-conductivity disposable

microdielectric sensor face. The sensor was then heated to 110° C for 12 hours, which resulted in the formation of an approximately 40μ m thick film. The sensor was slowly allowed to cool to room temperature before testing. The sensor was next calibrated to establish the dielectric response of the sizing film prior to resin contact. Data acquisition began immediately when the sensor was placed into 50 ml of uncatalyzed resin at 25°C. At least six trials were performed with each of the sizing system films.

SOLUBILITY OBSERVATIONS

The liquid sizing systems, consisting of an emulsion of filmformer and other components in aqueous mixture, were dried by placing a small amount of liquid sizing system on a glass plate and raising its temperature to 110°C for 12 hours. The water was driven off causing the emulsion to coalesce and form a sizing film, and because the film forming polymer was above its glass transition temperature it flowed to produce a relatively uniform film thickness. This preparation of the dried sizing films followed the guidelines of the patent literature for the processing of these sized glass fibers.

This sizing film was scraped off the glass plate and 0.5, 1.0 and 2.0% by weight dried sizings were added to 20 ml of resin to determine the solubility of each dried sizing system in the resin system. Two distinct processes were observed: the sizing film was first swollen by the resin, followed by dissolution of the film at much greater times. Within the first seconds after the sizing films were added to the resin, the appearance of the sizing films changed from opaque to semi-transparent at the edges. The semi-transparent region grew inward from the edges toward the middle of the pieces of sizing film after approximately 10 minutes. This is evidence for the swelling of the sizing film

by the matrix. The matrix contains styrene and vinyl ester. The molecular weight of styrene (104) is much less than that of the vinyl ester (797), leading to the conclusion that styrene is predominantly responsible for the swelling of the sizing film. After a period of hours the polyester and polyvinyl acetate sizings were completely dissolved in the matrix, but the polyurethane sizing would not dissolve in the matrix even at the lowest concentration, 0.5% by weight, even after one month.

RESULTS AND DISCUSSION

Several assumptions were made in these experiments. The first was that the styrene dominated the swelling of the sizing film. This assumption was verified by performing the same experiment with pure styrene instead of Derakane as the liquid solvent. The time for complete swelling with styrene was less than that required with Derakane, as expected, considering that the styrene concentration was twice that in the experiments with Derakane (Derakane is 50 wt% styrene).

Figure 19 shows a typical plot of the conductivity vs. time data for a polyester sizing system film in Derakane resin. The conductivity vs. time plots for the polyvinyl acetate sizing system films are very similar to Figure 19, because both the polyvinyl acetate and polyester sizing systems are soluble in the resin. The sharp increase in the conductivity in the first few minutes of the experiment is attributed to swelling of the sizing film by styrene. As the sizing film is swollen, the mobility of the sizing molecules is increased, which results in an increase in the measured conductivity. The more gradual decline observed over the next several hours detects the dissolution of the sizing film as the more polar molecules in the sizing diffuse away from the microdielectric sensor and are replaced with less polar molecules from the resin.

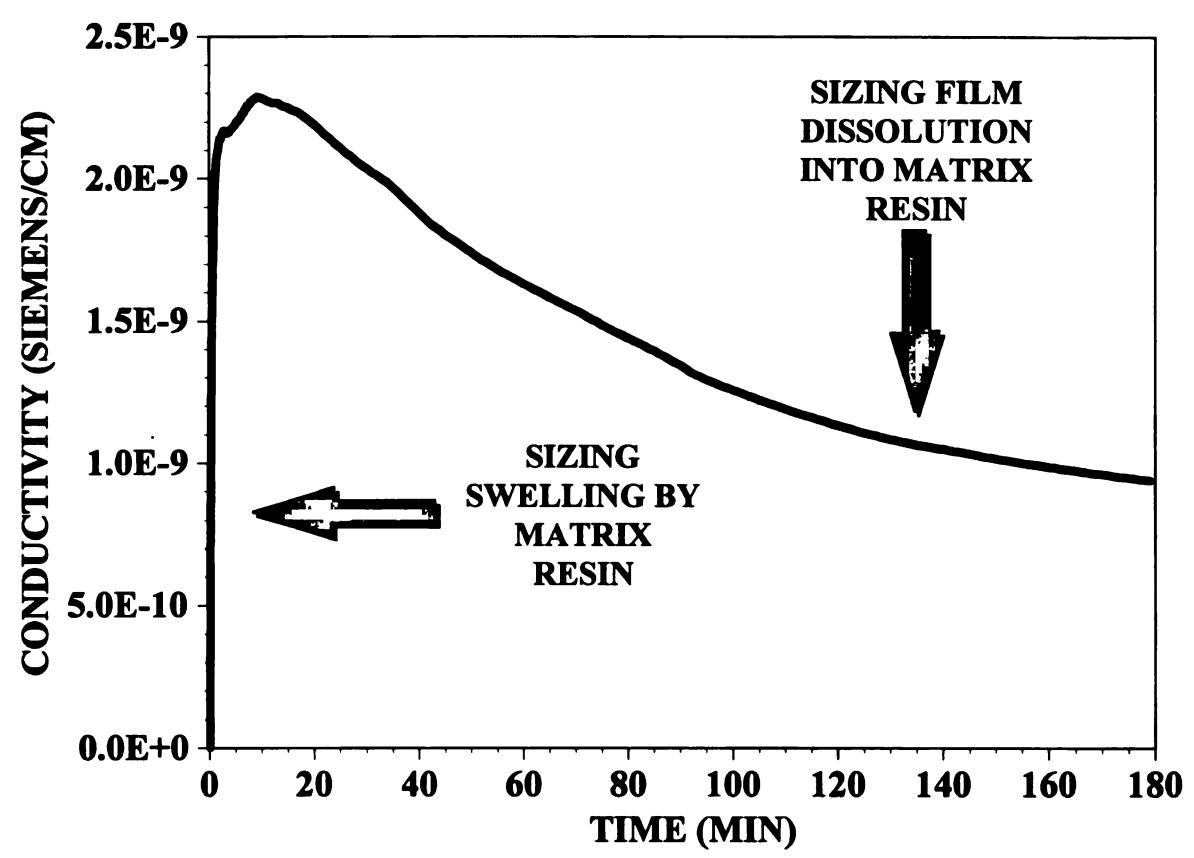


Figure 19. Typical conductivity-time profile for a soluble sizing showing sizing swelling and dissolution into the resin.

The experiments with the insoluble polyurethane sizing system show penetration of the sizing film by the resin at short contact time, similar to that of the polyvinyl acetate sizing system. The polyurethane sizing film is not soluble in the resin, and does not exhibit the gradual decline in conductivity which occurs with the soluble sizing systems as they are dissolved by the resin, as shown in Figure 20.

The diffusion coefficients were calculated, and Figure 21 shows good agreement between the experimental data and the model (equation 2) that describes the swelling of the polyester sizing film. Initially there is a slight time lag in the conductivity as the resin penetrates the outer portion of the film, beyond the sensing range of the

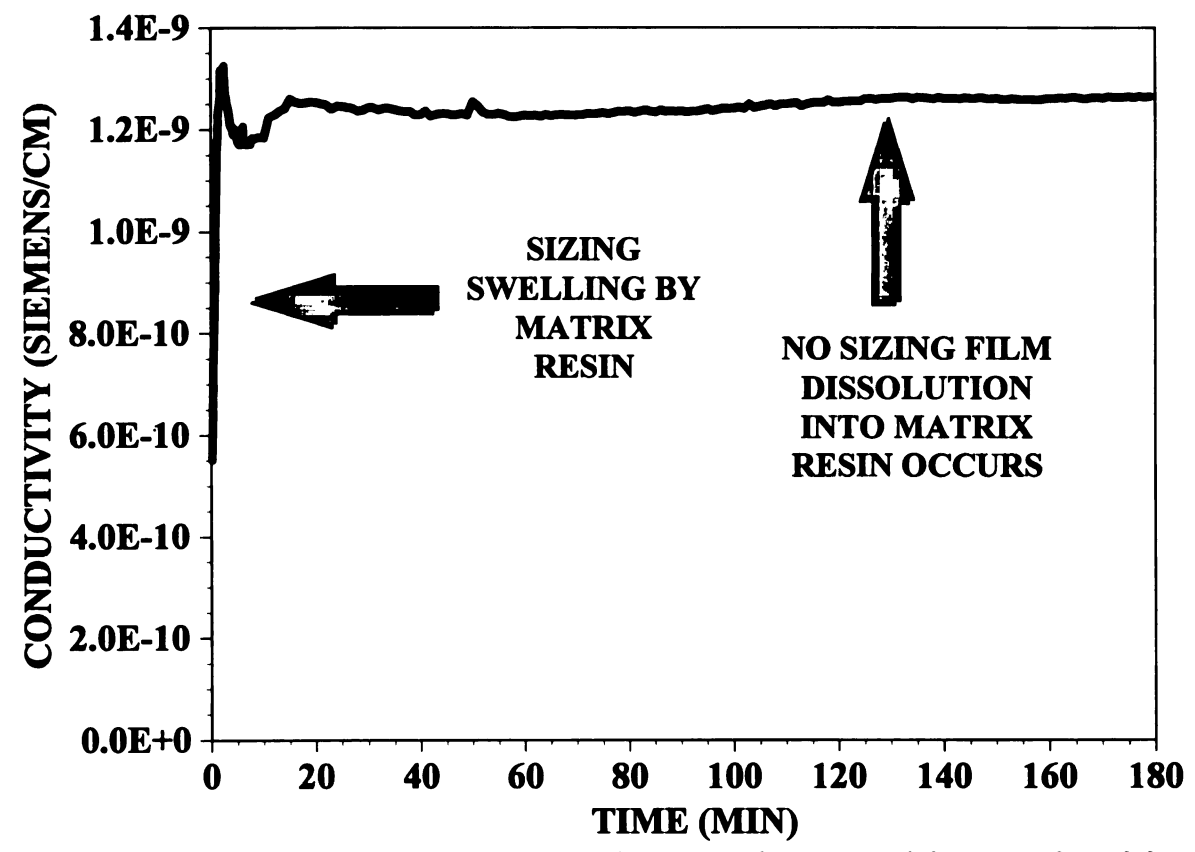


Figure 20. Typical conductivity-time profile for an insoluble sizing showing sizing swelling and no sizing dissolution into the resin.

microdielectric sensor. After this short time lag a low resin concentration is detected as it reaches the portion of the film within 18 microns from the sensor/film interface. The continual increase in the resin concentration is monitored until the film becomes saturated with the resin. The resin concentration increases exponentially to the saturation value.

The diffusion coefficient describing the dissolution of the sizing film into the resin was determined using equation 5. Figure 21 compares the experimental data for a polyvinyl ester sizing film and the model (equation 4) for a sizing film dissolving into resin. The model provides a good description of the exponential decay of the average sizing concentration as the sizing film dissolves into the resin.

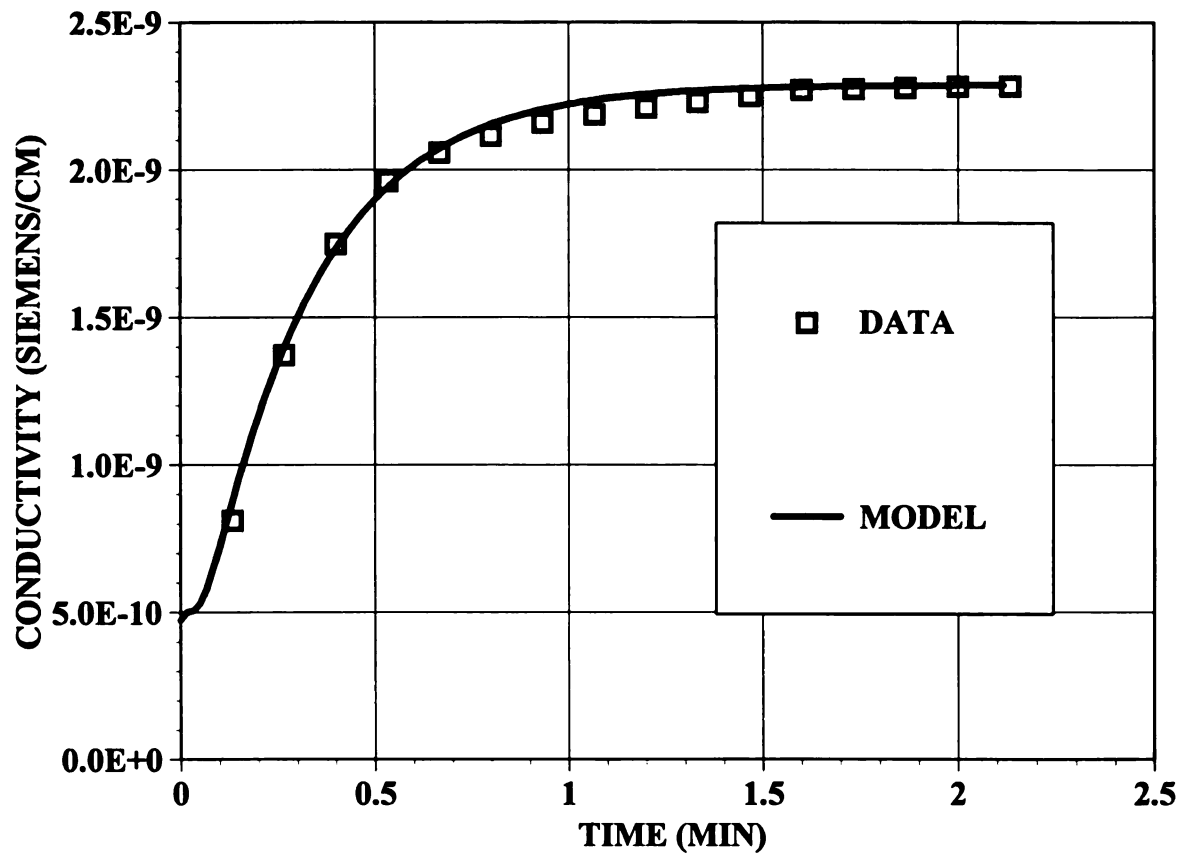


Figure 21. Experimental data and the one-dimensional unsteady-state diffusion model describing resin swelling of the sizing film.

The computed effective diffusion coefficients for resin penetrating the sizing film and for the film dissolving into the resin are included in Table 6.1. The diffusion coefficients are the average of six experiments, and the standard deviation is reported.

Table 6.1. Effective Diffusion Coefficients for Derakane 411-C50 Swelling Glass Fiber Sizing Systems ($D_{\rm R}$) and Sizing Systems Dissolving into Derakane ($D_{\rm S}$) at 25°C.

Glass Fiber Sizing	Swelling D_R (cm ² /sec)	$\begin{array}{c} \textbf{Dissolution} \\ \textbf{D_s} \ (\textbf{cm}^2/\textbf{sec}) \end{array}$
Insoluble Polyurethane	$3.4 \pm 2.5 \times 10^{-7}$	
Semi-Soluble PVA	$3.2 \pm 1.7 \times 10^{-7}$	1.6 ±2.2 x 10 ⁻¹⁰
Soluble Polyester	$2.6 \pm 0.8 \times 10^{-7}$	$2.5 \pm 0.9 \times 10^{-11}$

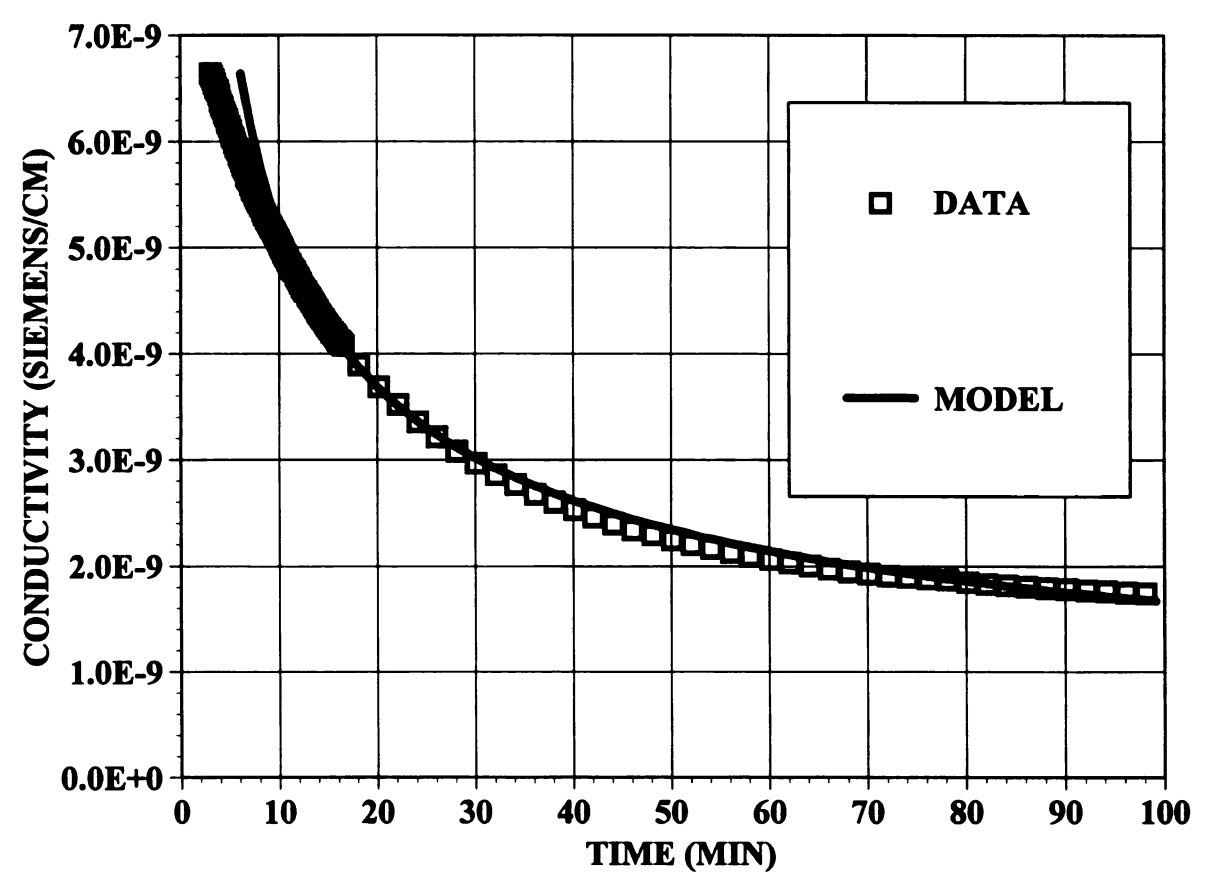


Figure 22. Experimental data and the semi-infinite media diffusion model describing dissolution of the sizing film into resin.

CONCLUSIONS

Microdielectrometry is a potentially valuable tool for determining the diffusion coefficients of a liquid matrix penetrating a thin solid film of sizing and of the dissolution of the sizing into the matrix. The diffusion coefficients at 25°C for Derakane 411-C50 vinyl ester resin system swelling insoluble polyurethane, semi-soluble polyvinyl acetate, and soluble polyester sizing systems are $3.4 \pm 2.5 \times 10^{-7}$, $3.2 \pm 1.7 \times 10^{-7}$, and $2.6 \pm 0.8 \times 10^{-7}$ cm²/s, respectively. The swelling of the sizing films is dominated by the styrene component present in the resin system. These results show that the styrene penetration of these sizing systems is only slightly dependent on the solubility of the sizing systems in the resin.

The diffusion coefficients for the dissolution of the semi-soluble polyvinyl acetate and soluble polyester sizing systems in Derakane are $1.6 \pm 2.2 \times 10^{-10}$, and $2.5 \pm 0.9 \times 10^{-11}$ cm²/s, respectively. It is expected that similar trends would be encountered locally in a liquid composite molding environment between sized glass fibers and a vinyl ester resin.

7. COMPOSITE MECHANICAL PROPERTIES

INTRODUCTION

Liquid Composite Molding (LCM) is a process for producing large area advanced composites having high strength and high modulus while maintaining high speed and low cost compared to other advanced composite processing techniques. Extensive research has been directed at the mold filling step of the process with a focus on using Darcy's law and the Carman-Kozeny equation to describe resin flow into the fiber preform^{46, 47, 48, 49, 50, 51, 52, 53}. Many researchers have also described the curing of the resin once the mold is filled^{1, 54, 55, 56}, but little research has been carried out on the interactions between sized glass fibers and the reacting liquid matrix⁵⁷. These interactions are of utmost importance in developing fiber-matrix adhesion which results in optimum composite mechanical properties.

Favorable interfacial thermodynamics between the glass fiber sizing and reacting liquid matrix are important in optimizing the liquid composite molding of advanced composites. A minimization of the total interfacial free energy for the system provides the driving force for the formation of solid-liquid interfaces, ideally allowing the gas phase to be displaced from the fiber preform in the mold by resin without leaving voids. Intimate fiber-matrix contact requires wetting of the sized fibers by the matrix, and is a prerequisite to the development of adhesion across the fiber-matrix interface⁵⁸. Favorable interfacial thermodynamics are also necessary for fiber-matrix interphase formation,

which requires the timely dissolution of the fiber sizing into the matrix to create an interphase region with gradually changing physical and chemical properties. The changes in surface free energy and viscosity that the reacting matrix undergoes as well as its interaction with the fiber sizing during impregnation can affect the "wetting" of the preform in different ways at different stages of mold filling, consequently affecting the mechanical properties of the composite⁵⁹. Once these processes are understood it will be possible to formulate a model of the liquid composite molding process which incorporates the solubility of the sizing in the resin and the surface properties of both the sized fiber and the reactive matrix resin.

This investigation of interphase formation in liquid composite molding has incorporated using a series of sized glass fibers with commercial-type sizings having a wide range of surface free energies and solubilities in the vinyl ester matrix. Two composite processing cycles were developed for producing composites of low void fraction and good surface quality. The effects of the different sizings on interphase formation were quantified by measuring the fiber-matrix adhesion in the composites and the composites' shear and flexural properties. Finally, the shear and flexural failure modes were documented in photomicrographs of the fracture surfaces using scanning electron microscopy.

EXPERIMENTAL PROCEDURE

MICRO-WILHELMY

Contact angle measurements were made using the micro-Wilhelmy technique, a gravimetric method of measuring the contact angle between a single fiber and a liquid

discussed in chapter 3. The force (F) exerted on a fiber of perimeter P by a liquid is related to the single fiber contact angle (θ) through the following equation:

$$F = \gamma_{IV} P \cos\theta \tag{28}$$

An electrobalance measures the force applied to a fiber by a liquid, and a microstepping motor allows measurements to be made in equilibrium or dynamic mode, advancing or receding⁶⁰.

COMPOSITE PROCESSING CYCLES

Two composite processing cycles were developed for producing unidirectional 152 mm x 152 mm x 3 mm advanced composite plaques with 50% E-glass fiber volume fraction. Preform fabrication was accomplished by winding a fiber tow unidirectionally on a fiber frame parallel to the mold filling direction. The vacuum assisted high-speed resin transfer molding processing cycle consists of a room temperature portion with the mold, preform, and resin at 23°C. The mold (with preform in place) was vacuum evacuated for 10 minutes prior to resin injection to draw volatiles out of the fiber sizing system. An injection pressure of 20 psi was used to fill the mold, and a packing pressure of 100 psi was required to obtain high quality surfaces on both sides of the composite plaque. After 12 hours of room temperature cure, the composites were postcured at 80°C for 2 hours.

Preheating of the preform was used as an alternative to vacuum assisted processing to remove volatiles from the sizing system. The heat pretreat process involved placing the preform in an oven at 80°C for 20 minutes before positioning the preform into the mold. The remaining processing steps were the same as for the vacuum

assisted processing, with 20 psi resin injection, 100 psi packing pressure, 12 hour room temperature cure, and 2 hour cure at 80°C. The heat pretreat processing cycle produced composites of comparable appearance to the vacuum assisted processing cycle, nearly void-free and with high quality surfaces. Composites produced without vacuum assist or heat pretreat contained small voids distributed throughout the composite due to volatiles evolving from the sizing system.

VOID FRACTION ANALYSIS

Void content determination was accomplished using digitized images of the polished composite surface containing fiber ends. An image analysis system was used to obtain the volume fraction of voids for each of the composites⁶¹. Ten 0.1 mm x 0.1 mm areas from each composite were analyzed. Since this is an optical technique, voids present in the composite had to be at least one micron in size to be discerned by the image analysis system.

FIBER-MATRIX ADHESION

Fiber-matrix adhesion was quantified for each composite using the Interfacial Testing System (ITS), a micro-indentation technique⁶². ITS specimens were prepared from each type of composite by cutting 10 mm x 10 mm pieces from the composites. The sample surfaces perpendicular to the fiber alignment direction were polished to a mirror surface with 0.05 μ m aluminum oxide particles in an aqueous polishing media using a three hour polishing cycle. ITS testing protocol involves application of force to a fiber end through a 10 μ m diameter diamond-tipped indenter to induce fiber-matrix debonding. Force is applied to the fiber until 25% of the fiber perimeter has debonded from the matrix. An equation based on finite element analysis allows the fiber-matrix

interfacial shear strength to be computed based on the fiber Young's modulus and diameter, matrix shear modulus, the distance between the tested fiber and the fiber closest to it, and the force required to produce fiber-matrix debonding along 25% of the fiber perimeter.

MECHANICAL TESTING

The mechanical properties of a region of fiber-matrix interphase were estimated by studying the properties of a mixture of fiber sizing and resin. Polyvinyl acetate and polyester dried fiber sizings (#3 and #4) were added to resin to simulate the composition of a region of the fiber-matrix interphase. The composition of the interphase varies as a function of distance from the fiber surface, however to estimate the mechanical properties of the interphase, tensile specimens were produced by dissolving 25 weight percent dried fiber sizing in resin. After dissolution of the fiber sizings, the resin was catalyzed and cured using the same curing schedule used with the composites. Tensile testing was accomplished in accordance with ASTM D638 using a United Testing System SFM-20 with laser extensometer and a test rate of 1 mm/min at 23°C. Type IV specimens were used with 25 mm gage length and 0.7 mm thickness.

Composite mechanical properties were tested on a United Testing System in accordance with ASTM standards for short beam shear (ASTM D2344) and 3-point bend testing (ASTM D790). Flexural specimens measured 25 mm x 75 mm x 3.2 mm and short beam shear specimens were 25 mm x 6.4 mm x 3.2 mm.

FRACTURE SPECIMEN EXAMINATION

Shear and flexural specimen failure modes were examined using scanning electron microscopy (SEM) and documented in representative photomicrographs. The shear

specimen fracture surfaces were exposed for microscopic observation by cutting the samples from the top to the midplane crack and lifting off the now unconstrained portion of the samples. The fracture surfaces of this portion of the samples were coated with a 20 nm layer of gold and examined using SEM. The flexure specimens were strained beyond the onset of failure in order to obtain crack propagation through the entire specimen thickness. This facilitated examination of the flexure fracture surfaces, which were also coated with a 20 nm layer of gold and examined using the SEM. Representative photomicrographs were obtained for each sample set to document the differences in the fracture surfaces and failure modes.

MATERIALS

MATRIX RESIN

Dow's Derakane 411-C50 vinyl ester resin was chosen as a representative matrix because it is formulated for RTM (low viscosity). Benzoyl peroxide and dimethylaniline were the catalyst and accelerator used (1.0% and 0.10% by weight, respectively).

E-GLASS FIBERS

Six sized E-glass fibers were selected because the glass fiber sizings provide a wide range of surface free energy and solubility in the matrix. These commercial-type fibers provided by PPG Company have sizings which contain film-formers, anti-static agents, silane coupling agents and other constituents typical of commercial sizings. The glass fiber types are referred to by the film-formers present in the sizing systems: water (#6) - has no organic material on the fiber surface; soluble epoxy (#5) - contains an epoxy soluble in the vinyl ester matrix; soluble polyester (#4) - contains a polyester soluble in the vinyl ester matrix; semi-soluble polyvinyl acetate (#3) - contains a

polyvinyl acetate (PVA) slightly soluble in the vinyl ester matrix; insoluble polyurethane (#2) - contains a polyurethane completely insoluble in the vinyl ester matrix; and a non-wettable, soluble sizing system (#1). This fiber (#1) was not supplied by PPG and was produced by coating the soluble polyester sized fiber (#4) with Mono Coat mold release agent (Chem Trend) and heating at 120°C for two hours to evaporate the solvent.

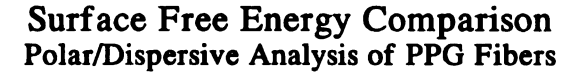
In addition, PPG Company supplied specially formulated liquid fiber sizings in emulsion form as representative of commercial semi-soluble polyvinyl acetate and soluble polyester sized fibers (#3 and #4). These sizings were dried in a manner similar to the commercial process used in the manufacture of glass fibers to produce materials comparable to the sizing present on the glass fiber surfaces. Small amounts of liquid sizing were heated to 110°C to remove the water from the emulsion and produce sizing films.

RESULTS AND DISCUSSION

FIBER SURFACE FREE ENERGIES

Fiber surface free energies were determined from micro-Wilhelmy measurements on the six glass fiber types with four probe liquids of known polar and dispersive components⁶³ (water, ethylene glycol, formamide and methylene iodide). Figure 23 shows the results of polar/dispersive analysis of equilibrium contact angle data, and the fibers are numbered in order of increasing total surface free energy. The error bars show the error associated with the total surface free energy. The sized glass fibers provide a range of total surface free energies from 28 to 59 mJ/m².

The total surface free energy of the sized glass fibers is an indicator of thermodynamic wetting. The resin (surface free energy of 32.2 mJ/m²) would be



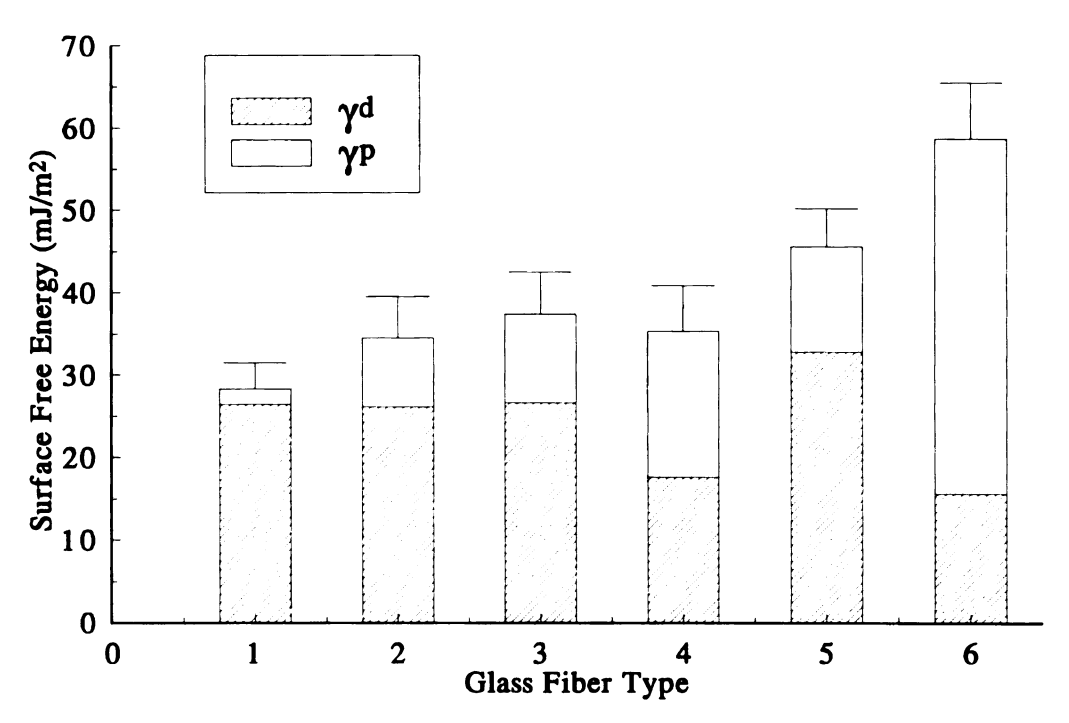


Figure 23. Surface Free Energy Comparison of PPG Sized Glass Fibers Calculated from Polar/Dispersive Analysis.

expected to initially "wet" water-sized glass fibers the best (smallest contact angle) because they have the highest total surface free energy (58.7 mJ/m²). The water-sized fiber has a hydroxylated surface from the application of water to the fiber immediately after it was manufactured. The hydroxylated surface is very polar and consequently this fiber has by far the highest polar component of surface free energy among the fibers $(43.1 \pm 4.3 \text{ mJ/m²})$, and the highest total surface free energy $(58.7 \pm 6.8 \text{ mJ/m²})$. The other fibers would be expected to have larger contact angles and hence poorer "wetting". The mold release sized fibers (#1) have a low polar component of surface free energy $(1.8 \pm 0.7 \text{ mJ/m²})$, and the lowest total surface free energy. The dispersive component

of surface free energy is constant for most of the fibers. Fibers #2, #3 and #4, polyurethane, polyvinyl acetate, and polyester sized fibers have very similar total surface free energies (approximately 35 ± 5 mJ/m²). The low value of dispersive surface free energy for fiber #4 (17.6 ± 2.8 mJ/m²) may be an artifact that is not be reflective of surface effects only because of the solubility of this sizing in the dispersive probe liquids. If the highly dispersive probe liquids dissolved the sizing during the contact angle measurements then the dispersive component of surface free energy would be lowered. The expected dispersive component should be similar to that of fibers #1, #2 and #3 (26 mJ/m²) which would increase the total surface free energy for fiber #4 to approximately 44 mJ/m². The soluble epoxy sizing (#5) has the highest total surface free energy of any of the fibers with commercial type sizings, and is expected to give the most favorable wetting conditions.

COMPOSITE PLAQUE APPEARANCE

The appearance of the composite plaques varied significantly depending on the fiber type used in the composite, but the vacuum assist and preform preheat processing cycles both produced composites of similar appearance for identical compositions. Unidirectional composite specimens were resin transfer molded with each of the six fiber types and the vinyl ester resin using vacuum assist and preform preheat processing cycles. Visual inspection of the composites revealed smooth surfaces on both sides of the composite plaques and no evident voids in any of the composites regardless of processing cycle. The first set of three composites, produced with mold release, polyurethane and polyvinyl acetate sized fibers (#1, #2 and #3), are opaque. The fiber tows are observable as discrete white cylinders surrounded by yellow matrix in the

composites made with the mold release sized fibers (#1). In the composites produced with polyurethane and polyvinyl acetate sized fibers (#2 and #3) the fiber tows are not evident, but some fibers can be identified within the matrix.

In contrast the second set of three composites, produced with polyester, epoxy and water sized fibers (#4, #5 and #6), are remarkably transparent. This indicates that the void contents are low because a substantial number of voids in the composites would interfere with the transmission of light through the composites. The transparent appearance of these composites is due in part to the matching of the refractive indicies of the glass and the matrix. The solubility of the fiber sizings is also important in obtaining transparency for the polyester and epoxy sized fibers (#4 and #5). The high solubility of these sizings cause them to dissolve into the matrix within the molding cycle which allows good glass fiber-matrix contact and consequently light transmission.

VOID VOLUME FRACTIONS

Void volume fractions were analyzed in the composites produced with each fiber type and both processing cycles. Table 7.1 shows that the void contents are exceptionally low for these fill rates and processing conditions. The composite properties are not expected to be effected by such low void fractions. The first set of three composites, produced with mold release, polyurethane and polyvinyl acetate sized fibers (#1, #2 and #3), has a slightly higher void fraction than the second three composites, produced with polyester, epoxy and water sized fibers (#4, #5 and #6). However, the difference between these two data sets is minimal. The resin flowrate and packing pressure superseded surface influences which would be expected to cause void formation. The composites produced with the mold release sized fibers (#1) were expected to contain

a much higher void fraction because the contact angle between the matrix and the fibers was greater than 90°, whereas the contact angles between the matrix and the other fibers was much less.

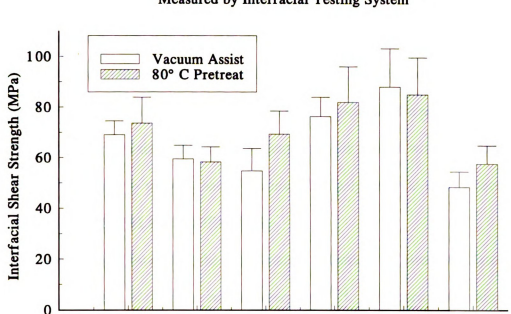
Table 7.1. Volume Fraction Voids for Composites Processed with Vacuum Assist (V.A.) and Heat Pretreat (H.P.).

Glass Fiber Sizing	V_v V.A. (%)	V_v H.P. (%)
1. Mold Release	0.102 ± 0.065	0.045 ± 0.054
2. Insoluble Polyurethane	0.28 ± 0.04	0.39 ± 0.11
3. Semi-Soluble PVA	0.61 ± 0.27	0.37 ± 0.14
4. Soluble Polyester	0.013 ± 0.019	0.005 ± 0.010
5. Soluble Epoxy	0.108 ± 0.031	0.31 ± 0.15
6. Water	0.031 ± 0.014	0.002 ± 0.004

FIBER-MATRIX ADHESION

The fiber-matrix adhesion data obtained from ITS measurements on unidirectional composite specimens fabricated with each of the six fibers and the vinyl ester resin are shown in Figure 24. The adhesion results are similar for the vacuum assist and the preheat processing cycles. There is a strong correlation between the fiber-matrix adhesion and the fiber total surface free energy. Fiber-matrix adhesion tends to be higher for the fibers with higher fiber total surface free energy. The formation of an interphase between the soluble sized fibers (#4 and #5) and the resin can be important in increasing adhesion in these systems. Chemical bond formation between the matrix and the soluble sizings as well as dissolution of the sizings by the resin further the development of an interphase with the soluble sized fibers (#4 and #5).

The mold release sized fibers (#1) have higher interfacial shear strength than expected (70 MPa), because the soluble sizing underneath the mold release was dissolved



Interfacial Shear Strength Comparison Measured by Interfacial Testing System

Figure 24. Interfacial Shear Strength Comparison Between Derakane/Unidirectional Glass Fiber Composites for Vacuum Assist and Heat Pretreat Processing Cycles Measured by Interfacial Testing System.

Glass Fiber Type

5

6

2

0

1

by the resin, carrying the low surface energy material away from the fiber interphase and allowing fiber-matrix adhesion similar to the soluble polyester sized fibers (#4) to be attained. This was verified by coating water sized fibers (#6) with the mold release coating and processing them with preheating into a composite of 50% fiber volume fraction. The resulting fiber-matrix adhesion determined by ITS was 29.4 ± 9.0 MPa, which is attributable to the low surface energy produced on the glass surface by the application of the mold release. The void fraction for this composite was also very low

 $(0.07 \pm 0.1\%)$, verifying that the rheological factors have superseded the surface effects in the heat pretreat composite processing cycle.

The water-sized fibers (#6) would be expected to have the highest fiber-matrix adhesion based on a thermodynamic argument alone, but has been attributed to an artifact in the sample preparation process. The fiber-matrix interface was not protected by a silane coupling agent and was damaged by exposure to water in the polishing procedure. This decreased the adhesion from the value expected for a fiber with this high level of total surface free energy to near that of the insoluble polyurethane sized fibers (#2).

INTERPHASE TENSILE PROPERTIES

It has been shown that the fiber-matrix adhesion is directly related to the mechanical properties of the fiber-matrix interphase^{64, 65}. The pertinent quantities may be estimated by studying the bulk tensile properties of a mixture of fiber sizing and resin. Table 7.2 shows that vinyl ester resin with 25 weight percent polyester sizing (#4) has properties identical to the resin with no sizing added to it. The tensile strength and modulus in this case show that the interphase properties and hence fiber-matrix adhesion in the composite material will be equivalent to those of the resin as the composition of the interphase changes as a function of distance from the fiber surface.

In contrast the tensile properties of specimens with 25 weight percent polyvinyl acetate sizing are much lower than the resin properties. The strength is diminished by a factor of 3, and the modulus is reduced by a factor of 3.5, which may be the result of the sizing interfering with the resin reaction chemistry. The fiber-matrix adhesion is dependent on the square root of the interphase shear modulus, thus the fiber-matrix adhesion in composites produced with polyvinyl acetate sized fibers (#3) would be

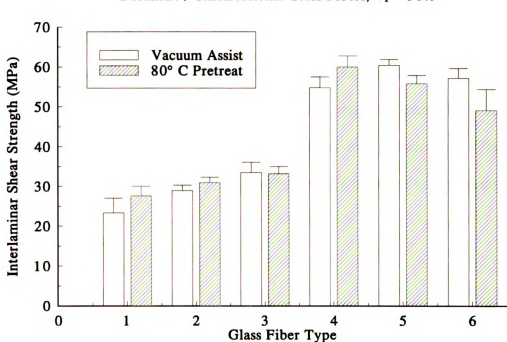
expected to be 1.9 times less than the fiber-matrix adhesion in composites produced with polyester sized fibers (#4) if the interphase was composed of 25 weight percent sizing or water sized fibers (#6). The interfacial shear strength results show a smaller difference in fiber-matrix adhesion which suggests that the interphase sizing concentration is less than 25 weight percent.

Table 7.2. Tensile Properties of Derakane 411-C50 and Mixtures of Derakane and 25 Weight Percent Polyvinyl Acetate (#3) and Polyester Sizing (#4).

<u>Sample</u>	Strength (MPa)	Modulus (GPa)
Derakane	61 ± 3	2.7 ± 0.2
Derakane + 25 wt% PVA	22 ± 4	0.8 ± 0.2
Derakane + 25 wt% PE	61 ± 6	2.8 ± 0.1

COMPOSITE SHEAR STRENGTH

Short beam shear strength of composites (ASTM D2344) was measured to determine the effect of the sizings and their interaction with the matrix on composite shear strength. Figure 25 shows that the vacuum assist and the preheat processing cycles produced comparable levels of shear strength with each of the fiber types. The correlation between the shear strength and the fiber-matrix adhesion is evident upon examination of Figure 25 and comparison with Figure 24. The shear strength is dependent on the fiber-matrix adhesion. The magnitudes of the short beam shear results are less than the ITS results, which is to be expected because any flaws in composites lower the short beam shear results. The shear failure mode is dominated by fiber-matrix interfacial failure for most of the composites (as will be discussed later).



Short Beam Shear Strength Comparison Derakane / Unidirectional Glass Fibers, $V_f = 50\%$

Figure 25. Short Beam Shear Strength Comparison Between Derakane/Unidirectional Glass Fiber Composites with 50% Fiber Volume Fraction for Vacuum Assist and Heat Pretreat Processing Cycles.

The water-sized fibers (#6) would be expected to have the highest shear strength of all the fiber types based on a thermodynamic argument alone. However, the water sized fibers (#6) have water adsorbed on the fiber surface, which may interfere with chemical bond formation between the fiber surface and the resin. The soluble polyester and epoxy sizings (#4 and #5) dissolve into the matrix and are removed from the fiber-matrix interface allowing the silane covered glass surface to interact and/or react with the matrix. The first set of three composites produced with mold release, polyurethane and polyvinyl acetate sized fibers (#1, #2 and #3) have similar low values of shear

strength. The lower values of fiber-matrix adhesion have a more pronounced effect on the shear results compared with the interfacial shear strength data. The lower shear strength is the result of inadequate fiber-matrix interaction. The polyvinyl acetate sizing (#3) lowered the modulus of the matrix in the interphase which hindered the transfer of stress to the fiber. The insoluble polyurethane sizing (#2) remained at the fiber-matrix interface and did not form an interphase. Consequently the matrix was kept from reaching the silane coated glass surface and low shear strength resulted. Finally, the mold release sizing (#1) migrated from the fiber-matrix interface and generated planes

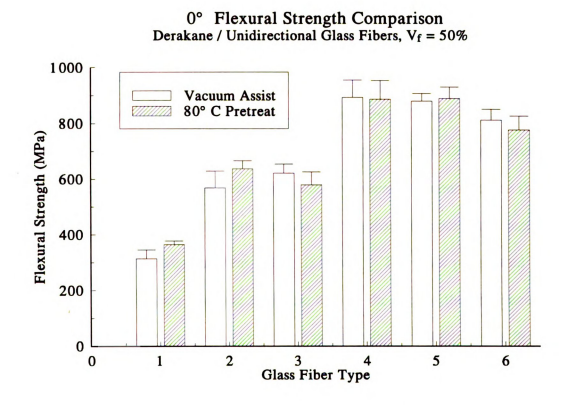


Figure 26. Longitudinal Flexural Strength Comparison for Derakane/Unidirectional Glass Fibers with 50% Fiber Volume Fraction for Vacuum Assist and Heat Pretreat Processing Cycles.

of low shear strength in the composite which will be fully discussed in conjunction with the composite shear fracture surface.

LONGITUDINAL COMPOSITE FLEXURAL STRENGTH

The longitudinal flexural strength of composites were measured using a three-point bend test (ASTM D790). All the composites have approximately the same longitudinal flexural modulus, 39.2 ± 4.5 GPa, because the composite flexural modulus is completely dominated by the fibers. Since the volume fraction of the fibers was kept constant at 50%, a constant value for the flexural modulus is expected. Figure 26, however, shows that while the longitudinal flexural strength data are independent of processing conditions, the flexural strength is quite sensitive to the choice of sizing. The data follow the same trend as the fiber-matrix adhesion results, emphasizing the previously documented^{66, 67} interrelationship between composite material properties and fiber-matrix adhesion.

The second set of three composites, manufactured with the polyester, epoxy and water sized fibers (#4, #5 and #6), have similar high values of flexural strength and failed on the tensile side of the three-point bend specimens. In contrast, the first set of three composites, produced with mold release, polyurethane and polyvinyl acetate sized fiber (#1, #2 and #3), failed in shear (Mode II failure). The crack propagated from the midpoint of the specimen near the midplane toward the end of the specimens. This change in failure mode is expected to increase the magnitude of difference in the flexural strength values between the first and second sets of composites.

The high flexural strengths of the soluble sizing fibers (#4 and #5) are attributed to the development of a fiber-matrix interphase within the time constraints of the molding

cycle. The fiber sizings have dissolved into the matrix and allowed the matrix to interact and/or react with the silane coupling agent covered glass fiber surface. The strong fiber-matrix interactions result in high levels of fiber-matrix adhesion which in turn yields high flexural strength.

The semi-soluble polyvinyl acetate sized fiber composite (#3) has low flexural strength because of the low fiber-matrix adhesion. As discussed previously, the interphase which develops as the sizing dissolves into the matrix has a modulus four times less than the matrix modulus. This weak interphase hinders the transfer of stress from the matrix to the fibers resulting in low fiber-matrix adhesion and consequently low flexural strength.

The low flexural strength of the insoluble polyurethane sized fiber composite (#2) is due to the poor fiber-matrix adhesion which results when a fiber-matrix interphase does not develop. The insoluble sizing does not dissolve in the matrix and hinders the matrix from interacting with the silane-covered glass fiber surface.

The water sized fibers (#6) would be expected to produce a composite with a higher of flexural strength than the polyester or epoxy sized fiber composites (#4 or #5), but the tensile strength of the water sized fibers (#6) is less than that of the fibers which have protective commercial sizings. The lack of any protective organic sizing on the surface of the water sized fibers (#6) reduces their tensile strength. During preform preparation the fibers incur surface damage as the fibers rub against one another. The scratched glass fibers have lower tensile strength compared with equivalent fibers which were sized with a protective organic sizing immediately after being produced⁶⁸.

The mold release sized fibers (#1) have a much lower flexural strength than would be expected from the fiber-matrix adhesion results. The mold release itself may have had a negative effect on the resin curing reaction and produced an interphase of different composition.

SHEAR FRACTURE SURFACES

Shear fracture surfaces for all the specimens have large regions exhibiting a uniform failure mode. Although all of the short beam shear specimens failed in shear (Mode II failure) near the midplane of the samples, representative photomicrographs were obtained to document the differences in the fracture surfaces, which vary widely with the fiber sizing type. The first set of three composites, made with mold release, polyurethane, and polyvinyl acetate sized fibers (#1, #2, and #3) have similar low levels of shear strength (approximately 30 MPa). The second set of three composites, made with epoxy, polyester, and water sized fibers (#4, #5, and #6) have much higher values of shear strength (approximately 55 MPa) compared to the first set of three composites.

These variations in shear strength are due to differences in the fiber sizings and their interaction with the matrix that cause significant changes in the fracture surfaces of the specimens. The first set of three composites with the low values of shear strength have smoother appearing fracture surfaces and less tortuous failure paths compared to the composites with higher shear strengths. While there are some hackles (triangular regions of matrix resulting from the shear failure path) in the first set of three composites, the second set has more and larger hackles. The larger and more numerous hackles are evidence of the higher degree of fiber-matrix adhesion causing a more tortuous failure path. The failure path is the result of the coalescence of tensile microcracks in the

matrix which occur oriented 45° toward or away from the direction of macroscopic crack propagation^{69, 70}. The coalescence of oriented microcracks results in a failure path through the matrix which has the tendency to produce hackles.

The failure surfaces in the shear specimens with mold release sized fibers (#1) were different from those of the other samples. These fibers are the soluble polyester sized fibers (#4) with a coating of mold release over the sizing. The composites exhibited high fiber-matrix adhesion comparable to the composites made with polyester sized fibers (#4) (80 MPa) but low shear and flexure strengths. This seemingly paradoxical data is the result of the mold release being removed from the fiber surface as the soluble sizing was dissolved into the matrix. The composites failed in shear within the matrix at the weak planes caused by migration of the mold release, leaving a sheath of matrix surrounding the fibers. The mold release caused weak planes by lowering the matrix cohesive strength in planes parallel to the fibers as shown in Figure 27. The fibers are covered with matrix leaving a comparatively smooth shear fracture surface with no fiber surface exposed. All the other shear fracture surfaces have much more fiber surface exposed.

Figure 28 and Figure 29 show that failure occurs at the fiber-matrix interface in the shear specimens made from polyurethane sized fibers (#2) and polyvinyl acetate sized fibers (#3). Fiber-matrix adhesion is comparatively low in these composites (approximately 60 MPa), and this caused relatively few hackles on the failure surfaces. The fiber surfaces have almost no matrix adhering to them. The shear failure propagates through the composite primarily near the fiber-matrix interface as this is the route of lowest fracture energy due to low fiber-matrix adhesion.

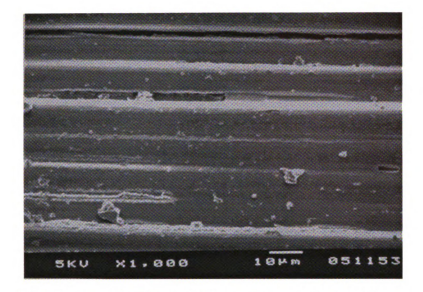


Figure 27. Shear Fracture Surface of Mold Release Sized Fiber (#1) Composite.

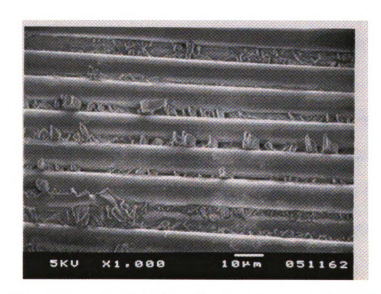


Figure 28. Shear Fracture Surface of Insoluble Polyurethane Sized Fiber (#2) Composite.

In specimens made from insoluble polyurethane sized fibers (#2) the matrix failed in a manner which generated small hackles limited to a 3 micron region of matrix between fibers (91). The hackles are not well adhered to the fibers as evidenced by the lack of matrix on the fibers near the hackles. By contrast the matrix surrounding the polyvinyl acetate sized fibers (#3) does not contain hackles (Figure 29). The lack of hackle formation is due to the lower strength and modulus of the interphase formed by the dissolution of the semi-soluble polyvinyl acetate sizing. This results in an interphase with a very high local concentration of sizing in it. As has been shown with the measurements on the neat matrix specimens blended with large amounts of sizings, the matrix modulus is decreased by a factor of 4 when 25 weight percent of polyvinyl acetate sizing is dissolved in it. This decrease in the matrix modulus accounts for the absence of hackles in these composites.

Composites having the highest fiber-matrix adhesion have shear fracture surfaces with tortuous failure paths, shown by the large number of hackles on the failure surfaces. The hackles are the result of the failure path varying from predominately fiber-matrix interfacial failure to a combination of cohesive matrix failure and fiber-matrix interfacial failure.

Composites made from soluble vinyl ester sized fibers (#4) have shear fracture surfaces with a very high density of hackles. Figure 30 shows the regular hackle pattern which dominates the fracture surface. This micrograph is composed of impressions left by the fibers after shear failure, not the fibers themselves. A well developed interphase has been formed by the sizing completely dissolving into the matrix, and no deleterious effects on the mechanical properties of the matrix have occurred. It has been shown

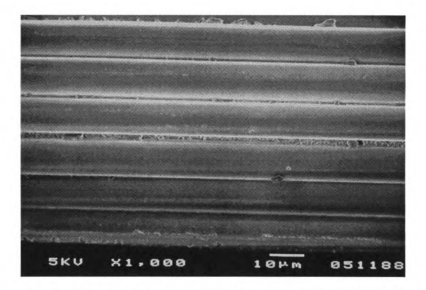


Figure 29. Shear Fracture Surface of Semi-Soluble Polyvinyl Acetate Sized Fiber (#3) Composite.

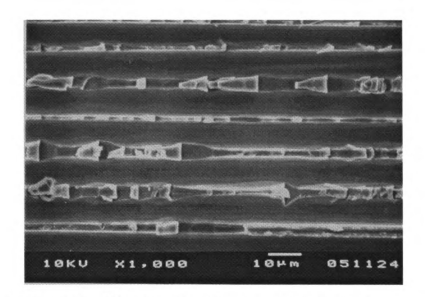


Figure 30. Shear Fracture Surface of Soluble Polyester Sized Fiber (#4) Composite.

previously that the matrix modulus is not affected when 25 weight percent of polyester sizing is dissolved in it. The higher level of fiber-matrix adhesion causes the failure plane to be further into the matrix since there is no compositional variability in the interphase mechanical properties, however the strong interphase tends to push the failure plane to the fiber-matrix interface. The resulting fracture surface has many hackles with a largest dimension on the order of the fiber diameter (15 microns). Fiber-matrix interfacial failure dominates, however the hackles are the result of the failure path varying from predominately fiber-matrix interfacial failure to a combined failure mode with both cohesive matrix failure and fiber-matrix interfacial failure. The hackles shown in Figure 30 are very narrow when fiber-matrix interfacial failure dominates, and a minimal amount of matrix is in the failure path. The hackles widen and penetrate further into the matrix revealing the combined failure mode which includes more matrix and less fiber-matrix interface in the failure path.

Soluble epoxy sized fibers (#5) also produced composites which have shear fracture surfaces with mixed failure modes evidenced by the presence of hackles. Figure 31 shows that the hackles are small and not regular compared to the hackles of Figure 30, but again a tortuous failure path is evident. The failure mode varies in the amount of cohesive matrix failure which occurred. Fiber-matrix adhesion is high in these composites (85 MPa) and the fibers would be expected to have a substantial fraction of their surfaces covered by matrix, and Figure 31 shows that this is the case, although the amount of fiber surface coverage varies from fiber to fiber.

The shear fracture surface of composites made from water sized fibers (#6) are similar to that of composites made from soluble polyester sized fibers (#4). Figure 32

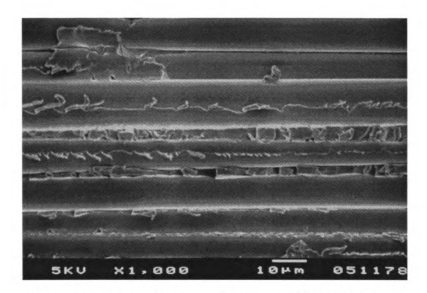


Figure 31. Shear Fracture Surface of Soluble Epoxy Sized Fiber (#5) Composite.

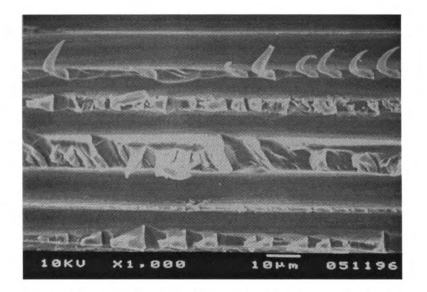


Figure 32. Shear Fracture Surface of Water Sized Fiber (#6) Composite.

shows the large hackles on their shear fracture surfaces with some regular hackles of the type seen in Figure 30. Figure 32 also shows that the maximum dimension of the hackles is on the order of the fiber diameter (15 microns) which is similar to the hackles of Figure 30. In fact the fracture surfaces of these two composites should be similar because the soluble polyester filmformer completely dissolves from the fiber surface into the matrix creating a well developed interphase with mechanical properties indistinguishable from the neat resin.

FLEXURE SPECIMENS

Flexure specimens exhibited different failure modes dependant upon the level of fiber-matrix adhesion. The second set of three composites, manufactured with the polyester, epoxy and water sized fibers (#4, #5 and #6), failed on the tensile side of the three-point bend specimens. In contrast, the first set of three composites, produced with mold release, polyurethane and polyvinyl acetate sized fiber (#1, #2 and #3), failed in shear. The crack propagated from the midpoint of the specimen near the midplane toward the end of the specimens. The flexure specimens were strained beyond the onset of failure in order to allow crack propagation through the entire specimen thickness. This facilitated examination of the flexure fracture surfaces. The fracture surfaces were coated with a 200 nm layer of gold and examined using the SEM. Representative photomicrographs were obtained for each composite to document the differences in the fracture surfaces and failure modes.

The results of these flexural tests can be divided in the same manner as the short beam shear specimens. The first set of three composites, made with mold release, polyurethane, and polyvinyl acetate sized fibers (#1, #2, and #3) have low flexural

strength, less than 600 MPa. The second set of three composites, made with epoxy, polyester, and water sized fibers (#4, #5, and #6) have high flexural strength, approximately 900 MPa. These variations in flexural strength may be attributed to differences in failure mode and fiber-matrix adhesion, which in turn are dependent upon the fiber sizings and the fiber-matrix interactions.

The composites produced with polyurethane and polyvinyl acetate sized fibers (#2 and #3) had small regions of tensile failure (i.e. the fibers fractured and pulled-out of their matrix sockets), but one set of samples, from the composite produced with mold release sized fibers (#1), had no tensile failure. These specimens failed in shear and not in tension because of the planes of exceptionally low shear strength provided by the mold release, as observed in Figure 27, the shear fracture surface. Consequently, no photomicrographs were obtained for composites made with mold release sized fibers (#1).

The composites produced with polyurethane sized fibers (#2) had a small region of tensile failure. As seen in Figure 33, the tensile failure zone is approximately the first 50 microns from the bottom of the specimen. The failure mode then undergoes a transition to shear failure further into the sample. Figure 33 shows that the tensile failure mode involves fiber pull-out from the matrix indicating low fiber-matrix adhesion. As previously discussed, the fiber-matrix adhesion has been shown to be lower (60 MPa) for this composite compared to the other composites because of the incompatibility of the polyurethane fiber sizing with the vinyl ester matrix.

The tensile failure region of the composites produced with semi-soluble polyvinyl acetate sized fibers (#3) also shows that fiber-matrix adhesion is low. Figure 34 reveals gaps between fiber and matrix, indicative of low fiber-matrix adhesion. The fracture



Figure 33. Tensile Fracture Surface of Insoluble Polyurethane Sized Fiber (#2) Composite.



Figure 34. Tensile Fracture Surface of Semi-Soluble Polyvinyl Acetate Sized Fiber (#3) Composite.

surface has numerous strands of matrix present which were removed from fiber surfaces during failure. The low modulus of the interphase matrix (previously shown to be a factor of four less than the matrix) would contribute to this appearance of the fracture surface. Figure 34 also shows some fibers which have failed in shear, indicated by the failure path through the fibers orientation 45 degrees from the fiber axis.

The second set of three flexure specimens have similar fracture surfaces as would be expected from their similar flexural strength values (approximately 900 MPa). The fiber pull-out lengths tend to be short compared with the first three flexure specimens, indicative of high fiber-matrix adhesion. A significant amount of matrix still is visible, adhering to the pulled-out fibers in contrast to the bare appearance of the previous set of composites. In contrast to the composites made from the polyvinyl acetate sized fibers (#3), the matrix material adhered to the fibers shows little or no gap between the fibers and matrix, also indicative of high fiber-matrix adhesion.

Comparison of Figure 35 and Figure 36 show that the fracture surfaces from composites produced with soluble polyester sized fibers (#4) and soluble epoxy sized fibers (#5) are almost indistinguishable. Both fracture surfaces contain fibers with short pull-out lengths, indicating high fiber-matrix adhesion, and the pulled-out fibers have significant amounts of matrix adhering to them, another indication of good adhesion. In both fracture surfaces the fibers toward the middle of a fiber tow tend to have longer pull-out lengths, perhaps indicating irregular stress transfer to the middle of the fiber tow because of less than optimal dissolution of the sizing.

In composite specimens made from water sized fibers (#6), the fracture surface is more uniform than the fracture surfaces of previously discussed samples because the

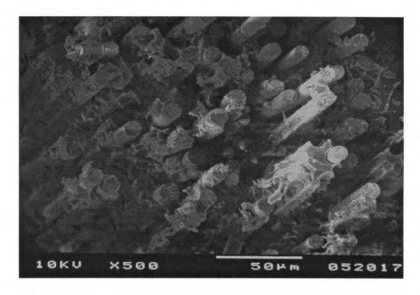


Figure 35. Tensile Fracture Surface of Soluble Polyester Sized Fiber (#4) Composite.

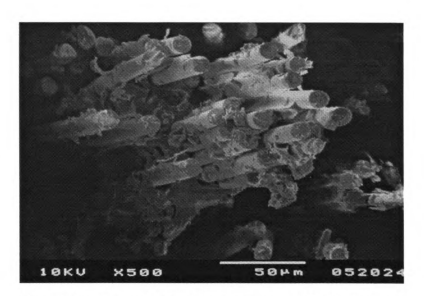


Figure 36. Tensile Fracture Surface of Soluble Epoxy Sized Fiber (#5) Composite.

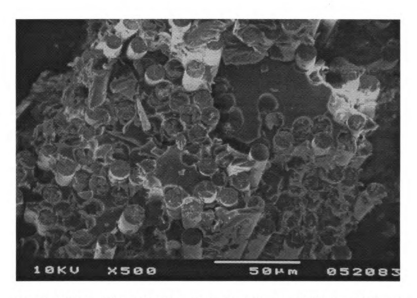


Figure 37. Tensile Fracture Surface of Water Sized Fiber (#6) Composite.

The fiber pull-out lengths are less than for the other fiber sizing types, as Figure 37 indicates. The fiber pull-out lengths are on the order of a fiber diameter, 15 microns, which suggests that the fiber-matrix adhesion is highest for this fiber sizing type. As previously discussed, the flexural strength of this composite is slightly lower than for the polyester or epoxy sized fiber composites (#4 or #5) because of the lower tensile strength of the water sized fibers (#6) compared with the other fiber types.

CONCLUSIONS

This research involved quantification of the parameters controlling the initial interactions between a variety of glass fiber sizings and reacting matrix resin in a liquid composite molding environment.

The surface free energy of sized glass fibers provides predictive information about the level of fiber-matrix interaction which occurs in liquid composite molding. A favorable thermodynamic driving force is necessary for obtaining a well developed interphase, which will result in good fiber-matrix adhesion and consequently higher composite mechanical properties compared with a system having an unfavorable thermodynamic driving force.

Composites produced with fibers having soluble sizings develop an interphase which leads to high composite mechanical properties as long as the sizing does not lower the mechanical properties of the interphase below those of the matrix resin. An interphase does not develop in composites produced with fibers having insoluble or nonwettable sizings, yielding low composite mechanical properties.

The shear failure mode is dominated by fiber-matrix interfacial failure more in composites having lower fiber-matrix adhesion and less in composites with greater fiber-matrix adhesion.

8. PROCESS MODELING

INTRODUCTION

Liquid Composite Molding is a process for producing large area advanced composites having high strength and high modulus while maintaining high speed and low cost compared to other advanced composite processing techniques⁷¹. For modeling purposes the process has been regarded to consist of two steps: mold filling and resin curing. Extensive research has been directed at the mold filling step of the process with a focus on using Darcy's law and the Carman-Kozeny equation to describe resin flow through the fiber preform^{72, 73, 74, 75, 76, 77, 78, 79}. Many researchers have also described the curing of the resin once the mold is filled^{72, 80, 81, 82}, but little research has been carried out on the interactions between the sizing normally present on glass fibers and the reacting liquid matrix⁸³. These interactions are of utmost importance in developing good fiber-matrix adhesion which results in optimum composite mechanical properties⁸⁴.

Favorable surface thermodynamics between the glass fiber sizing and reacting liquid matrix are important in optimizing the liquid composite molding of advanced composites. A minimization of the total surface free energy for the system provides the driving force for the formation of solid-liquid interfaces, ideally causing all the volatiles to be displaced from a mold by resin without leaving voids. Intimate fiber-matrix contact requires wetting of the fibers by the matrix, and is a prerequisite to the development of

strong adhesion across the fiber-matrix interface⁸⁵. Favorable surface thermodynamics are necessary for fiber-matrix interphase formation, which depends on dissolution of the fiber sizing into the matrix to create a region of matrix with gradually changing physical and chemical properties⁸⁶. The changes in surface free energy and viscosity that the reacting matrix undergoes as well as its interaction with the fiber sizing during impregnation can affect the "wetting" of the preform in different ways at different stages of mold filling, consequently affecting the mechanical properties of the composite⁸⁷.

This investigation of interphase formation in liquid composite molding has been accomplished using a series of sized glass fibers with commercial-type sizings having a wide range of surface free energies and solubilities in the vinyl ester matrix. A variety of composite processing cycles were developed for producing composites of low void fraction and good surface quality. Two room temperature processing cycles were used (one with vacuum assist and one with preform preheat) and three elevated mold temperature processing cycles with vacuum assist were used (40, 60 and 80°C). The effects of the different sizings on interphase formation were quantified by measuring the fiber-matrix adhesion in the composites as well as the composite shear and flexural properties⁸⁸.

This research has led to the formulation of a modified model of the liquid composite molding process which incorporates the fiber sizing solubility and surface properties of the fiber and the reactive polymer matrix and is in terms of the operating parameters of mold temperature and molding time. The sizing surface free energy and solubility in the matrix strongly affect the fiber-matrix interphase formation and consequently the fiber-matrix adhesion and composite mechanical properties.

BACKGROUND

The concept of a processability window or moldability diagram to describe the mold filling and curing steps in liquid composite molding has been advanced by Gonzalez-Romero and Macosko^{72, 89, 90}. The processability window is a valuable technique for conveying the chemical and physical processing constraints in the liquid composite molding process in terms of operating parameters. Figure 38 shows the moldability diagram for the mold filling step of the liquid composite molding process with the process variables defined as resin temperature (or mold wall temperature) and mold filling time. The resin temperature is approximately equal to the mold wall temperature because the fiber preform reaches thermal equilibrium with the mold wall

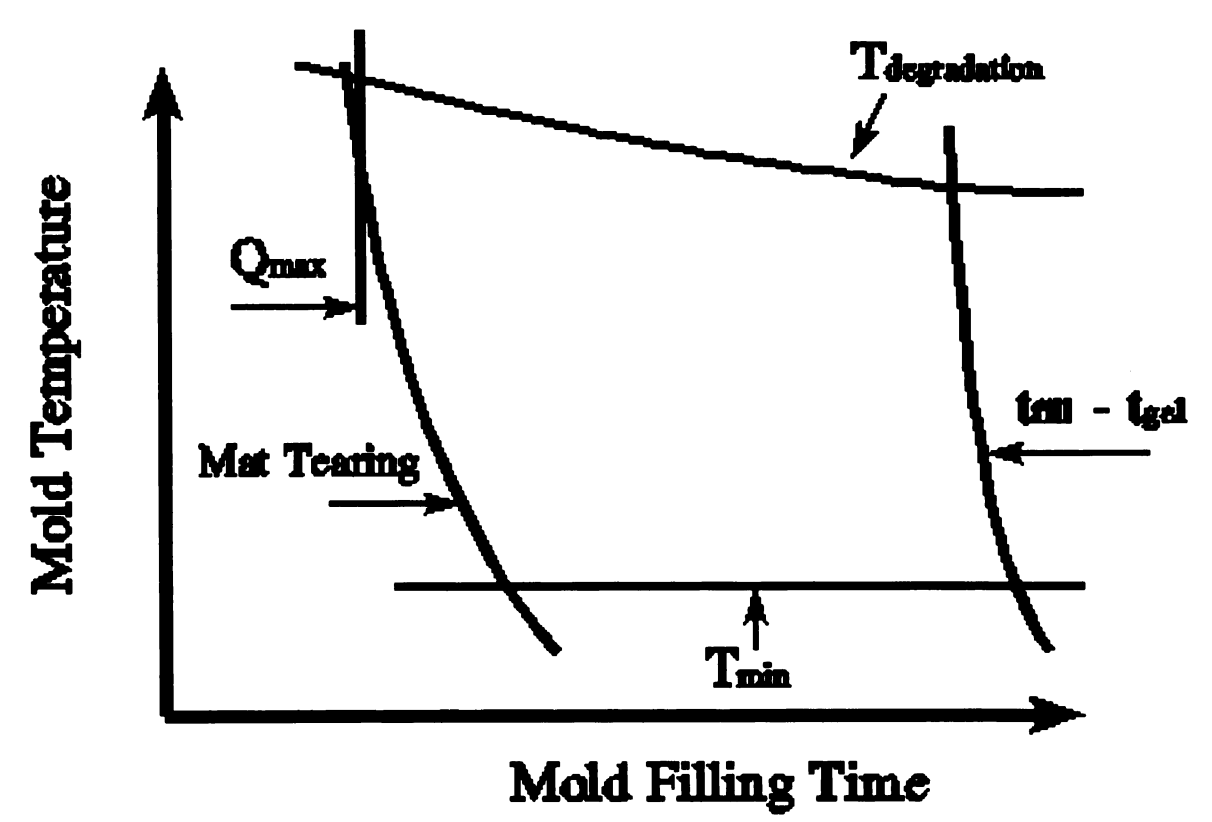


Figure 38. Moldability Diagram for the Filling Step of the Liquid Composite Molding Process. (Gonzalez-Romero and Macosko)

in typical molding cycles. As the reacting liquid resin penetrates the fiber preform the large contact area between the fibers and the resin aids heat transfer to the resin, quickly heating the resin to near the mold wall temperature.

The left boundary of the processability window is defined by two lines. The maximum flowrate attainable by the equipment (Q_{max}) defines one line and preform tearing or washing defines the other. Equipment constraints will typically be less of a problem than difficulties with the fiber preform. Depending on the type of preform, washing (movement of the preform in the mold) or tearing may be a more severe problem.

The right boundary of the moldability diagram is the maximum time for mold filling, which is equal to the difference between the time for mold filling (t_{fill}) and the gel time (t_{gel}) of the resin matrix. As the difference between these two times becomes less, the processability window shrinks.

The top boundary of the diagram is defined by the degradation temperature $(T_{degradation})$ of the matrix resin. The degradation temperature depends on the mold filling time, and it is lower for longer mold filling times. Finally, the minimum temperature (T_{min}) for processing may be defined by the initiator decomposition temperature or resin viscosity constraints. The processability window enclosed by these lines defines the mold filling parameters that will result in a liquid composite molded composite.

In addition, Gonzalez-Romero and Macosko developed the moldability diagram in Figure 39 for the curing step in liquid composite molding which shows the temperature and mold time constraints on the process. The left boundary is the time required to achieve acceptable "green strength" in the composite, which decreases as the resin

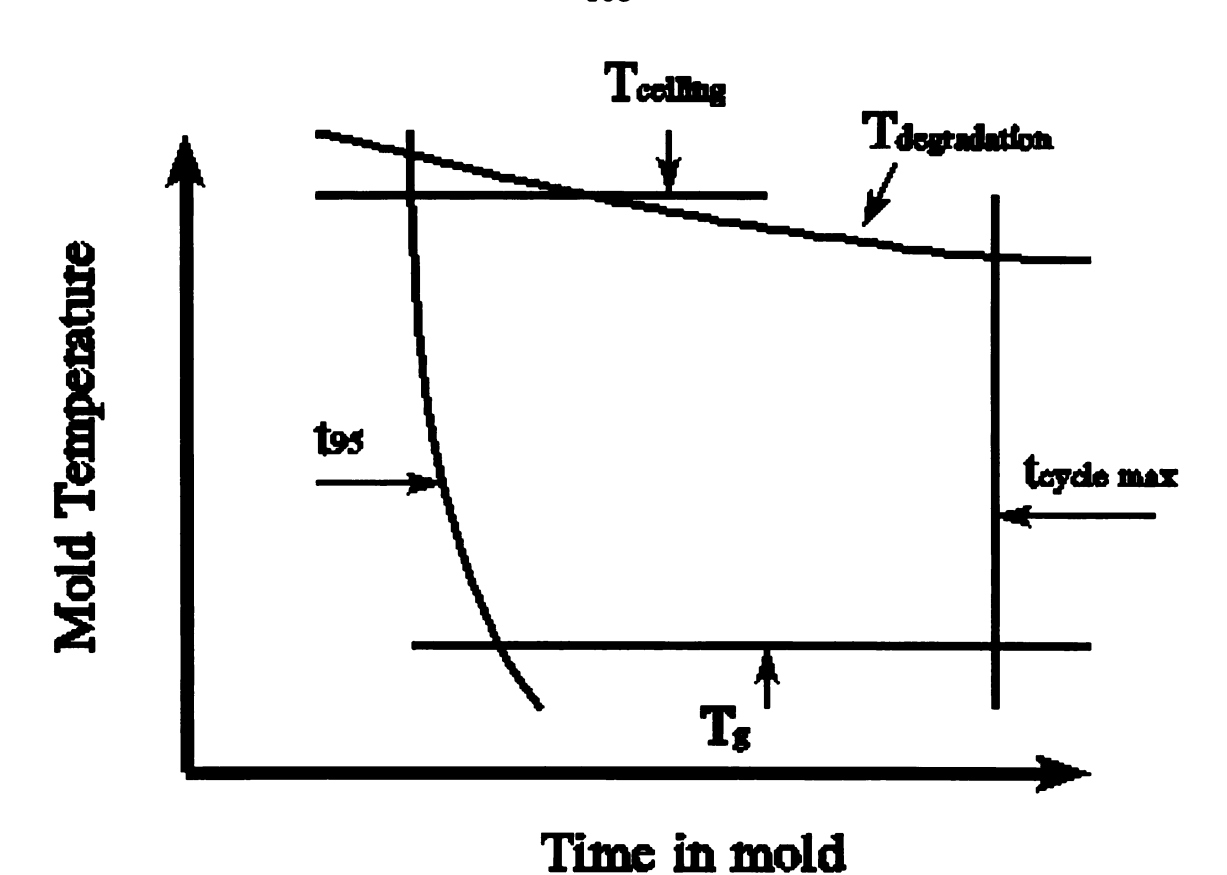


Figure 39. Moldability Diagram for the Curing Step of the Liquid Composite Molding Process. (Gonzalez-Romero and Macosko)

temperature is increased. Acceptable "green strength" has been reached when the composite has sufficient dimensional stability to be removed from the mold. With some resin systems, the acceptable "green strength" point coincides with an extent of cure of 95%, hence the left boundary is referred to as the time for 95% extent of reaction (t₉₅). If additional curing is required it may be accomplished in an oven which is a much less expensive alternative to curing the composite in the mold.

The right boundary of the processability window is the maximum cycle time $(t_{cycle\ max})$ due to economic constraints. The capital expense of the equipment and tooling used in liquid composite molding mandates a maximum cycle time to meet production requirements.

The top boundary of the moldability diagram consists of a ceiling temperature (T_{ceiling}) and a degradation temperature $(T_{\text{degradation}})$. The ceiling temperature may be defined by equipment constraints or it may be the depolymerization temperature of the resin. The degradation temperature line represents the maximum temperature the resin can be exposed to and depends on the time in the mold. It is lower for longer times in the mold.

The bottom boundary of the diagram is defined by the desired glass transition temperature (T_g) of the resin matrix. In order to attain the desired glass transition the resin cure temperature must exceed this temperature or vitrification will impede the polymerization reaction and a lower glass transition temperature will result, giving lower mechanical properties than desired⁹¹. The limits of the processing diagram were defined based on the mechanical properties of the final composite material. This model neglects the time dependent interaction of the fiber sizing with the reacting matrix and is the subject of this study.

EXPERIMENTAL PROCEDURE

Many of the experimental techniques which have been used to obtain the data necessary to the formulation of the model of the liquid composite molding process have been discussed in previous chapters. Chapter 3 includes the discussion of the Micro-Wilhelmy technique for determining single fiber contact angles, the discussion of the Interfacial Testing System for determining the fiber-matrix interfacial shear strength in composite materials and mechanical testing of composites. Although composite processing cycles were discussed in chapter 3, additional processing cycles were

introduced to aid in the formulation of the liquid composite molding process and their description follows.

COMPOSITE PROCESSING CYCLES

Resin transfer molding processing cycles were developed for producing composite plaques with 50% E-glass fiber volume fraction. In addition to the two processing cycles discussed earlier, using vacuum assist or preform preheat, three other processing cycles which incorporate vacuum assist were used. Figure 39 shows the five processing cycles graphically. The elevated temperature processing cycles were similar to the vacuum assist processing cycle except that 10 minutes before the room temperature resin was injected into the mold, its temperature (and consequently the preform temperature) was raised to 40, 60 or 80°C. After two hours at 40 or 60°C, a two hour postcure at 80°C was added, whereas the 80°C process was complete after two hours. These three processes included a slow cooling rate to room temperature. These elevated mold temperatures are designed to provide less time for interphase formation in the resin transfer molding processing cycle. From dynamic scanning calorimetry data the gel time has been calculated for these mold temperatures. Table 8.1 shows how the gel time changes as a function of temperature from 33.7 minutes to a mere 1.3 minutes with the range of moldtemperature used in these experiments. These ranges of gel times provide insight into how the interphase at different stages of development affects the fiber-matrix adhesion and mechanical properties.

RESULTS AND DISCUSSION

The results from the evaluation of the fiber surface free energies and properties of composites manufactured with a variety of processing cycles have led to the

formulation of a modified model of the liquid composite molding process which incorporates the solubility of the fiber sizing in the matrix resin and the surface free energies of the sized fiber and matrix resin.

FIBER SURFACE FREE ENERGY

The fiber surface properties have been previously discussed in chapter 5. The fibers have a wide range of total surface free energies varying from 28 to 59 mJ/m², which will aid in discerning the effects of the surface free energy driving force on composites processed with liquid composite molding.

FIBER-MATRIX ADHESION

The fiber-matrix adhesion results obtained from ITS measurements on unidirectional composite specimens fabricated with each of the six fibers and the vinyl ester resin have shown the dependence of high adhesion on complete dissolution of the sizing at two processing conditions (as discussed in chapter 5). Additional data on fiber-matrix adhesion in composites produced using soluble polyester sized fibers (#4) and a series of elevated mold temperatures is shown in Figure 40 and included in Table 8.1. The increasing mold temperatures accelerated the polymerization reaction, shortening the gel time of the resin but decreasing the time for swelling and dissolution of the fiber sizing (interphase formation). The fiber-matrix interfacial shear strength as measured by the ITS decreased 32% as the mold temperature was increased from 23°C to 80°C.

Table 8.1. The Effect of the Mold Temperature on the Time for Interphase Formation (t_{xy}) Which is Equal to the Gelation Time (t_{y}) , Interfacial Shear Strength (IFSS), Short Beam Shear Strength (SBSS), and Flexural Strength (FS).

T _{mold} (°C)	t _{LF} (min)	IFSS (MPa)	SBSS (MPa)	FS (MPa)
23	33.7	92.2 ± 5.0	58.5 ± 2.1	948 ± 52
40	12.2	75.2 ± 6.7	57.9 ± 2.8	918 ± 67
60	3.1	72.4 ± 9.0	50.2 ± 3.9	812 ± 41
80	1.3	62.7 ± 11.7	48.3 ± 2.6	765 ± 83

Interfacial Shear Strength vs. Temperature Derakane/Glass Fiber, Measured Using ITS

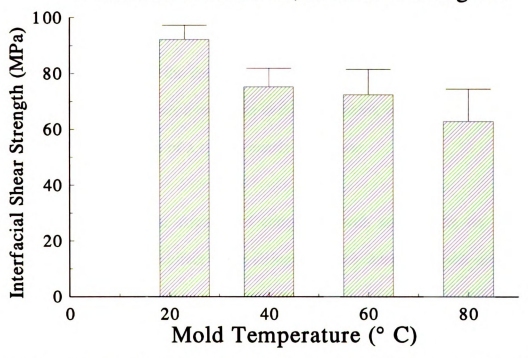


Figure 40. Interfacial Shear Strength of Derakane/Glass Fiber (with Soluble Polyester Sizing) Composites Processed with Vacuum Assist vs. Mold Temperature.

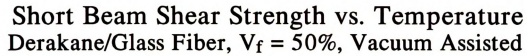
An alternative explanation for this observation could be that the mechanical properties of the reacting matrix itself change with processing temperature. The effect

of the mold temperature on the modulus of the matrix was evaluated through neat resin tensile testing. Two neat resin plaques were produced at mold temperatures of 23°C and 80°C, using the same mold and processing conditions used to produce composites. The neat resin plaque produced with a mold temperature of 23°C was cured at room temperature for twelve hours and then postcured at 80°C for two hours while the plaque produced with a mold temperature of 80°C remained in the mold for two hours at 80°C. Tensile specimens were cut from the plaques and tested in accordance with ASTM D638.

The plaque produced at 23°C had a modulus of 2.71 ± 0.09 MPa compared with 2.54 ± 0.16 MPa for the plaque produced at 80°C. The difference is statistically significant according to Student's t-test at the 97.5% confidence level. However, the reduction of 6.5% in matrix modulus only accounts for a 3.2% decrease in the fibermatrix adhesion based on the dependence on matrix modulus⁹². Thus the increase in mold temperature also causes a reduction in the fiber-matrix adhesion which is probably the result of the formation of a sizing -matrix interphase.

SHEAR STRENGTH

The short beam shear strength of composites with each of the six fibers was measured to determine the effect of the sizings and their interaction with the matrix on composite shear strength and was discussed in chapter 7. Figure 41 and Table 8.1 show that the composite shear strength measured by the short beam shear test decreases 17% as the mold temperature is increased from 23°C to 80°C. No difference is evident between the shear strength at the lower two temperatures, however at the two higher temperatures the shear strength is significantly reduced. These results are in qualitative agreement with the fiber-matrix adhesion results and further confirm the dependence of



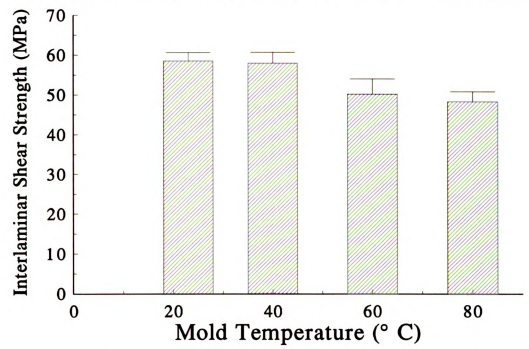


Figure 41. Short Beam Shear Strength of Derakane/Glass Fiber (with Soluble Polyester Sizing) Composites with 50% $\rm V_t$ Processed with Vacuum Assist vs. Mold Temperature.

composite shear strength on fiber-matrix adhesion.

LONGITUDINAL FLEXURAL STRENGTH

The longitudinal flexural strength of composites with each of the six fibers were measured using a three-point bend test (ASTM D790). The flexural strength decreases 19% as the time for interphase formation decreases from 33.7 to 1.3 minutes as shown in Figure 42 and Table 8.1. The trend of the data is very similar to that of the shear strength data, with the data from the lower two temperatures indistinguishable, and a significant decrease in the flexural strength at the two higher temperatures. This decrease is again attributed to the decrease in fiber-matrix adhesion, and not changes in

Flexural Strength vs. Temperature Derakane/Glass Fiber, $V_f = 50\%$, Vacuum Assisted

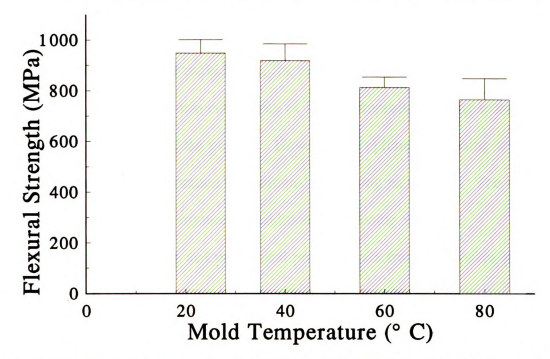


Figure 42. Flexural Strength of Derakane/Glass Fiber (with Soluble Polyester Sizing) Composites with 50% V, Processed with Vacuum Assist vs. Mold Temperature.

the resin matrix since the matrix modulus is only slightly changed by the different processing cycles, as shown by the neat resin tensile testing.

LIQUID COMPOSITE MOLDING MODEL

The model developed by Gonzalez-Romero and Macosko for the mold filling process is sufficient to define the boundaries of the process. The large variation in the surface free energy of the sized glass fibers, discussed in chapter 5, was expected to have an effect on the mold filling process and consequently the void fraction in the composites. The void content in the entire series of composites was consistently very low, less than 1% by volume. The choice of resin flowrate and high packing pressure overcame the

surface energy which would be expected to allow void formation in this study. Future work will be conducted to determine if the fiber and resin surface properties need to be included in a model of the mold filling process in liquid composite molding which includes void formation.

As with the model for mold filling, the model developed by Gonzalez-Romero and Macosko to describe the resin curing step of liquid composite molding is sufficient for defining the boundaries of the process. However, an optimal processing window may be defined through incorporation of additional processing parameters. The model does provide a framework to introduce the additional processing variables.

Fiber-matrix adhesion and mechanical property data from composites produced in this study with various sized glass fibers at various processing conditions have provided additional information to modify the liquid composite molding process model by incorporation of the interfacial properties of the glass fiber sizings and reacting liquid resin. Specifically the resin and sized glass fiber surface free energy and the dissolution time of the glass fiber sizing are key parameters to be added to the model to define an optimum processing window.

The sizing dissolution time and surface energy effects have been incorporated into the processability diagram to define a region of optimum composite processing. Figure 43 shows the processability window for the curing step of liquid composite molding including the optimum processing window with the principle axes being the mold wall temperature (or the resin temperature) and the time in the mold. For clarity the optimum processing window is shown larger than it is for most systems. Based on results from this study, the additional axes which must be included in the model are the

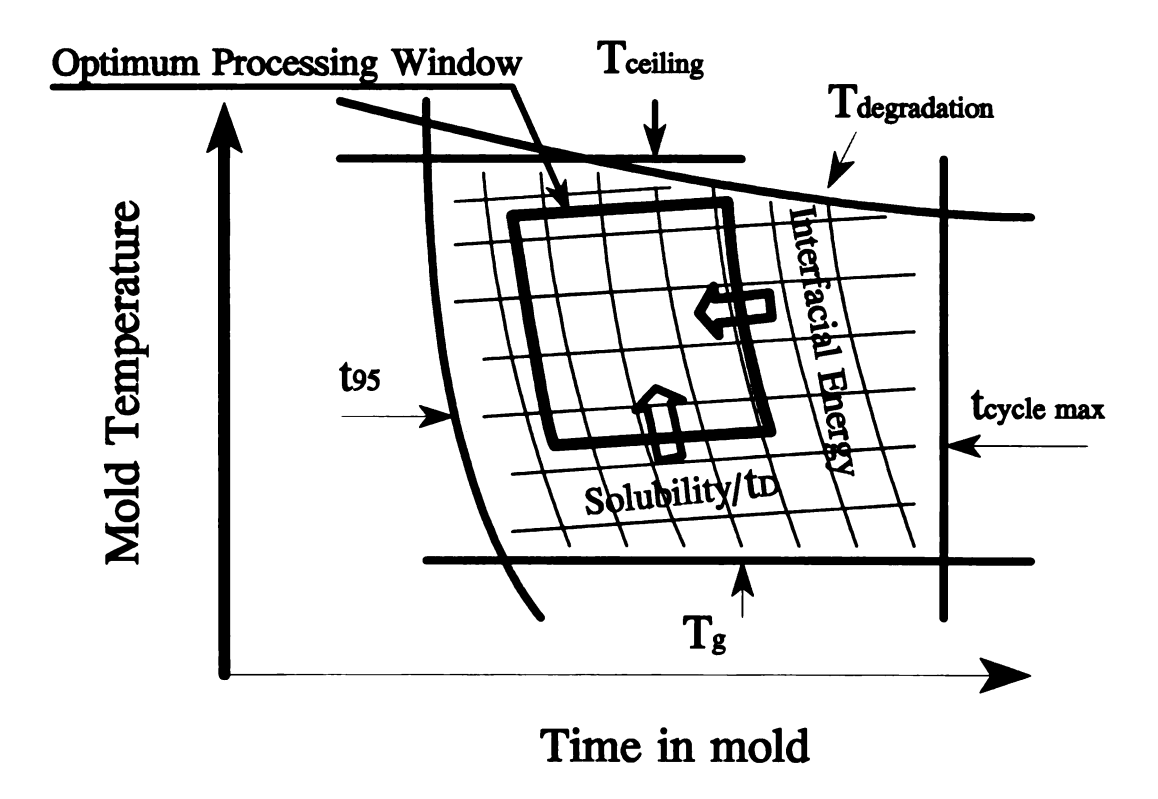


Figure 43. Moldability Diagram for the Curing Step of the Liquid Composite Molding Process Incorporating the Effects of the Sizing Solubility and Surface Free Energy.

interfacial energy driving force (the difference between the surface free energy of the sized glass fibers and the resin) and dissolution time for the glass fiber sizing in the resin. Figure 43 shows lines defining regions of constant sizing dissolution time, with the dissolution time decreasing with increasing temperature. The dissolution time will be approximated as a characteristic time for diffusion (t_D) divided by the solubility of the sizing in the resin. The characteristic time for diffusion is defined as a characteristic length squared, divided by the diffusion coefficient⁹³. The length may be estimated from the weight percent of sizing applied to the fibers, and the diffusion coefficient may be measured using the microdielectric technique discussed in chapter 6. The inverse of the

dissolution time is shown in Figure 43, increasing with increasing temperature. The sizing dissolution time required to obtain optimum composite mechanical properties decreases as the resin temperature increases because the resin gel time decreases. The shorter gel time allows less time for interphase formation, and the interphase must be well developed to obtain optimum composite mechanical properties. The lower bound to the optimum processing window is the longest sizing dissolution time which will result in complete dissolution of the fiber sizing from the glass fiber surface within the molding time. A sizing which is 100% soluble in the matrix resin and has a short characteristic diffusion time provides the upper bound to the process model.

CONTRACTOR CANADA SERVICE

Liquid composite molding within the region associated with complete dissolution of the sizing will result in a composite with optimum properties. However, composites processed in the region outside the associated sizing dissolution time limits will have less than optimal properties. Specifically, the properties will be decreased in proportion to the amount above the appropriate dissolution time line. The higher temperature shortens the time for interphase formation and the development of fiber-matrix adhesion and results in composites with lower mechanical properties. As the processing temperature exceeds the temperature recommended by the model the fiber-matrix adhesion will decrease in the manner shown in Figure 40. Likewise, the composite shear strength and flexural strength decreases are expected to follow the trends shown in Figure 41 and Figure 42.

The interfacial energy driving force is represented by the lines perpendicular to the sizing dissolution time lines in Figure 43. The interfacial energy lines increase as the molding time decreases. The lowest interfacial energy is the result of no difference

between the surface free energy of the fiber sizing and reacting liquid matrix. At the highest interfacial energy line the difference in surface free energies is maximized. The larger the thermodynamic driving force between sizing and matrix, the better wetting will take place at shorter times. Processing at longer molding times than the time associated with the surface energy line results in composites with optimally developed interphases and optimum fiber-matrix adhesion and composite mechanical properties. Processing at shorter molding times than designated by the interfacial energy driving force line results in composites with underdeveloped interphases and the associated lower fiber-matrix adhesion and lower composite mechanical properties.

AL DIT ALL STORES

Inherent in this model is the assumption that the fiber sizing will, when combined with matrix resin, produce a material having mechanical properties comparable to the properties of the matrix resin. Thus, the sizing must not have a negative impact on the polymerization reaction which would have a deleterious effect on the mechanical properties of the matrix resin. Future work will continue to quantify the relationships identified here in order to develop an analytical process model.

CONCLUSIONS

This research involved identification of the parameters controlling the interactions between a glass fiber sizing and reacting matrix resin in a liquid composite molding environment.

The surface free energy of sized glass fibers provides a basis for optimizing the level of fiber-matrix interaction which occurs in liquid composite molding. A favorable thermodynamic driving force is necessary for obtaining thermodynamic wetting and a well developed interphase. It has been shown that this condition will result in good

fiber-matrix adhesion and consequently higher composite mechanical properties compared with a system having an unfavorable thermodynamic driving force.

Composites produced with fibers having sizings soluble in the matrix develop an interphase which leads to optimum composite mechanical properties. A beneficial interphase does not develop in composites produced with fibers having insoluble or nonwettable sizings, yielding low composite mechanical properties.

The observations made on the effect of the sizing solubility and surface free energy driving force have been incorporated into a model of the liquid composite molding process which uses a processing window (or moldability diagram) to convey the optimum processing conditions and processing constraints on the curing step of the liquid composite molding process.

CONCLUSIONS

The surface free energy of sized glass fibers provides predictive information about the level of fiber-matrix adhesion which occurs in liquid composite molding. A favorable thermodynamic driving force is necessary for obtaining a well developed interphase, which will result in good fiber-matrix adhesion and consequently good composite mechanical properties.

Single fiber contact angle measurements are not sufficient by themselves to predict the velocity of resin flow into a sized fiber bundle due to capillary forces. Wicking experiments provide more information about the environment encountered in liquid composite molding. They provide the permeability of the packed fiber bed in addition to contact angle data.

Rheological factors such as resin flow rate and packing pressure are able to overcome the surface influences which would be expected to cause voids in composites produced with liquid composite molding.

Microdielectric analysis is a powerful technique for monitoring the swelling of polymer films by liquids and the dissolution of polymer films into liquids. Diffusion coefficients describing the aforementioned processes may be obtained through microdielectric monitoring.

Composites produced with fibers having soluble sizings develop an interphase which leads to high composite mechanical properties as long as the sizing does not lower the mechanical properties of the interphase below those of the matrix resin. An interphase does not develop in composites produced with fibers having insoluble or nonwettable sizings, yielding low composite mechanical properties.

The shear failure mode is dominated by fiber-matrix interfacial failure more in composites having lower fiber-matrix adhesion and less in composites with greater fiber-matrix adhesion.

A model of the curing step of the liquid composite molding process has been developed which uses the processing window (or moldability diagram) to convey the optimum processing conditions and processing constraints. The model incorporates the solubility of the fiber sizing in the matrix resin and the surface free energies of the sized fiber and the matrix resin.

REFERENCES

- 1. Macosco, C.W., "RIM, fundamentals of reaction injection molding", Carl Hanser Verlag, Munich, (1989) pp 181.
- 2. Macosco, C.W., ibid, pp 209-217.
- 3. Drzal, L.T., et al, "A single filament technique for determining interfacial shear strength and failure mode in composite materials," Paper 20-C, 35th Annual Technical Conference, Reinforced Plastics/Composites Institute (1980).
 - 4. Sharpe, L.H., and H. Schonhorn, "Contact angle, wettability and adhesion," R.F. Gould ed., ACS, Washington, D.C., (1964).
 - 5. Wilhelmy, J., Ann. Physik., 119, (1863) pp 177.
 - 6. Miller, B., "The wetting of fibers," Surface Characteristics of Fibers and Textiles, M.J. Schick ed., Vol. II, Marcel Dekker, Inc., New York, (1977).
 - 7. Mozzo, G., and R. Chadburd, Society of the Plastic Industry, Inc., 23rd Annual Tech. Conf. Section 9-C (1968) pp 1-8.
 - 8. Neumann, A.W., and W. Tanner, Vth International Conference on Surface Activity, Barcelona 1968, Vol.2, Ediciones Unidas, Barcelona (1969) pp 727-734.
 - 9. Lee, W.J., et al., "Characterizing high performance composite processability with dynamic fiber wettability measurements," Polymer Composites, Feb., (1988) Vol. 9, No. 1, pp 36-41.
 - 10. Tagawa, M., et al., "Contact angle hysteresis in carbon fibers studied by wetting force measurements," Colloid and Polymer Science, 267, (1989) pp 702-706.
 - 11. Wesson, S.P., and A. Tarantino, "Wetting characteristics of E-glass textile filaments," Journal of Non-Crystalline Solids, 38&39, (1980) pp 619-624.
 - 12. Penn, L.S., and E.R. Bowler, "A new approach to surface energy characterization for adhesive performance prediction," Surface and Interface Analysis, Vol. 3, No. 4, (1981) pp 161-164.
 - 13. Bystry, F.A., and L.S. Penn, "Preparation of brittle thermoset specimens for surface characterization by contact angles," Surface and Interface analysis, Vol. 5, No. 3, (1983) pp 98-100.
 - 14. Escoubes, M., et al., "Interactions that can appear at the fiber/matrix interface during polyepoxide/carbon fiber composite making," Journal of Colloid and Interface Science, Vol. 124, No. 1, July, (1988) pp 375-378.

- 15. Li, S.K., R.P. Smith, and A.W. Neumann, "Wilhelmy technique and solidifaction front technique to study the wettability of fibres," Journal of Adhesion, Vol. 17, (1984) pp 105-122.
- 16. Chang, H.W., et al., "Wettability of reinforcing fibers," Polymer Science and Technology, 27 Molecular Characterization of Composite Interfaces, eds. Hatsuo Ishida and Ganesh Kumar, (1985) pp 413-21.
- 17. Hammer, G.E., and L.T. Drzal, "Graphite Fiber Surface Analysis by X-ray photoelectron spectroscopy and polar/dispersive free energy analysis," Applications of Surface Science, 4, (1980) pp 340-355.
- 18. Cain, J.B., et al., "Dynamic contact angles on smooth and rough surfaces," Journal of Colloid and Interfaces Science, Vol. 94, No. 1, July (1983) pp 123-130.
- 19. Adamson, A.W., *Physical Chemistry of Surfaces*, 5th Edition, Wiley Interscience (1990).
- 20. Bascom, W.D., et al., Journal of Adhesion, 34 (1991) pp 79-98.
- 21. Drown, E., Journal of Adhesion Science and Technology, 5, No. 10, (1991) pp 856-881.
- 22. Fowkes, F.M., Journal of Physical Chemistry, 66 (1962) pp 382.
- 23. Kaelble, D.H., et al., Journal of Adhesion, 6 (1974) pp 23-48.
- 24. Bashforth, F., and J.C. Adams, "An Attempt to Test the Theories of Capillary Action", University Press, Cambridge, England, (1883).
- 25. Hammer, G.E. and L.T. Drzal, Applications of Surface Science, 4 (1980) pp 340-355.
- 26. Chwastiak, S., "A wicking method for measuring wetting properties of carbon yarns," Journal of Colloid and Interface Science, Vol. 42, No. 2, February (1973) pp 298-309.
- 27. Waterbury, M.C. and L.T. Drzal, Journal of Reinforced Plastics and Composites, 8, November (1989) pp 627-636.
- 28. Odian, G., *Principles of Polymerization*, 3rd ed., John Wiley & Sons, Inc., New York, N.Y., (1991) pp 198-208.
- 29. Odian, pp 510.
- 30. Odian, pp 237-243.

- 31. Plueddemann, E.P., Silane Coupling Agents, Plenum Press, New York, N.Y. (1982).
- 32. Plueddemann, E.P., Silane Coupling Agents, Plenum Press, New York, N.Y. (1982), Ch. 5.
- 33. Plueddemann, E.P., Silane Coupling Agents, Plenum Press, New York, N.Y. (1982), pp 20.
- 34. Hammer, G.E., and L.T. Drzal, Applications of Surface Science, 4, (1980) pp 340-355.
- 35. Trevino, L., et al., *Polymer Composites*, 12, No. 1, February (1991) pp 20-29.
- 36. Larson, B.K. and L.T. Drzal, submitted to Polymer Composites.
- 37. Drumm, C.A. and J.C. Ulicny, Polymer Composites, Vol. 10. No. 1, 44 (1989).
- 38. Drown, E., H. Al Moussawi and L.T. Drzal, Journal of Adhesion Science and Technology, 5, No. 10, (1991) pp 865.
- 39. Day, D.R., "Dielectric Properties of Polymeric Materials", Micromet Instruments Inc., Cambridge, MA, (1988).
- 40. Crank, J., The Mathematics of Diffusion, 2nd Ed., Oxford, Claredon Press, (1975) pp 4.
- 41. Crank, p.29.
- 42. Denton, D., D.R. Day, Priori, Senturia, Anolick and Schnieder, *Journal of Electronic Materials*, 14, (1985) pp 119.
- 43. Day, D.R., D.D. Shepard and K.J. Craven, *International SAMPE Symposium*, 34, (1989), pp 2411.
- 44. Day, D.R., private communication, May 12, 1993.
- 45. Crank, p.13.
- 46. Gonzalez-Romero, V.M., and C.W. Macosko, *Polymer Engineering and Science*, 30, No. 3 (1990) pp 142 146.
- 47. Young, R.K., et.al., SAMPE Quarterly, April (1991) pp 16-22.
- 48. Cai, Z. and A.L. Berdichevsky, *Polymer Composites*, 14, No. 4, Aug. (1993) pp 314-323.

- 49. Gibson, A.G., Composites Manufacturing, No. 2 (1992) pp 113-118.
- 50. Skartsis, L., et al., SAMPE Journal, 28, No. 5, Sept./Oct. (1992) pp 19-24.
- 51. Chan, A.W. and R.J. Morgan, SAMPE Quarterly, April (1992) pp 48-52.
- 52. Young, W.B., et al., *Polymer Composites*, 12, No. 6, December (1991) pp 391-403.
- 53. Trevino, L., et al., *Polymer Composites*, **12**, No. 1, February (1991) pp 20-29.
- 54. Kim, D.H., and S.C Kim, *Polymer Engineering and Science*, 29, No. 7 (1989) pp 456-462.
- 55. Chan, A.W. and S. Hwang, *Polymer Engineering and Science*, 32, No. 5, Mid-March (1992) pp 310-318.
- 56. Salem, A.J., et al., SAMPE Journal, 27, No. 1, Jan./Feb. (1991) pp 17-22.
- 57. Damani, S.G., and L.J. Lee, *Polymer Composites*, **11**, No. 3, June (1990) pp 174-183.
- 58. Sharpe, L.H., and H. Schonhorn, "Contact Angle, Wettability and Adhesion," R.F. Gould ed., ACS, Washington, D.C., (1964).
- 59. Drzal, L.T., et al., Paper 20-C, 35th Annual Technical Conference, Reinforced Plastics/Composites Institute (1980).
- 60. Li, S.K., et al., Journal of Adhesion, 17, (1984) pp 105-122.
- 61. Waterbury, M.C. and L.T. Drzal, *Journal of Reinforced Plastics and Composites*, 8, November (1989) pp 627-636.
- 62. Herrera-Franco, P.J., and L.T. Drzal, Composites, 23, No. 6, January (1992) pp 2-27
- 63. Hammer, G.E., and L.T. Drzal, *Applications of Surface Science*, 4, (1980) pp 340-355.
- 64. Drown, E.K., et al., Journal of Adhesion Science and Technology, 5, No. 10 (1991) pp 865-881.
- 65. Al-Moussawi, H., et al., *Polymer Composites*, 14, No. 3, June (1993) pp 195-200.
- 66. Madhukar, M.S., and L.T. Drzal, *Journal of Composite Materials*, 25, August (1991) pp 932-957.

- 67. Madhukar, M.S., and L.T. Drzal, *Journal of Composite Materials*, 25, August (1991) pp 958-991.
- 68. Drown, E., unpublished research.
- 69. Engineered Materials Handbook, Vol. 1 Composites, ASM International, Metals Park, OH (1987) pp 786-793.
- 70. Fractography and Failure Mechanisms of Polymers and Composites, A. C. Roulin-Moloney ed., Elsevier Science Publishers, New York, N.Y., (1988) pp 364-377.
- 71. Opportunities for Innovation: Polymer Composites, Stuart H. Munson-McGee ed., NIST GCR 90-577-1, U.S. Department of Commerce, National Institute of Standards and Technology, Gaithersburg, MD, August (1990) pp 59-110.
- 72. Gonzalez-Romero, V.M., and C.W. Macosko, *Polymer Engineering and Science*, **30**, No. 3 (1990) pp 142 146.
- 73. Young, R.K., et.al., SAMPE Quarterly, April (1991) pp 16-22.
- 74. Cai, Z. and A.L. Berdichevsky, *Polymer Composites*, 14, No. 4, Aug. (1993) pp 314-323.
- 75. Gibson, A.G., Composites Manufacturing, No. 2 (1992) pp 113-118.
- 76. Skartsis, L., et al., SAMPE Journal, 28, No. 5, Sept./Oct. (1992) pp 19-24.
- 77. Chan, A.W. and R.J. Morgan, SAMPE QUARTERLY, April (1992) pp 48-52.
- 78. Young, W.B., et al., *Polymer Composites*, 12, No. 6, December (1991) pp 391-403.
- 79. Trevino, L., et al., Polymer Composites, 12, No. 1, February (1991) pp 20-29.
- 80. Kim, D.H., and S.C. Kim, *Polymer Engineering and Science*, 29, No. 7, Mid-April (1989) pp 456-462.
- 81. Chan, A.W. and S. Hwang, *Polymer Engineering and Science*, 32, No. 5, Mid-March (1992) pp 310-318.
- 82. Salem, A.J., et al., SAMPE Journal, 27, No. 1, Jan./Feb. (1991) pp 17-22.
- 83. Damani, S.G., and L.J. Lee, *Polymer Composites*, 11, No. 3, June (1990) pp 174-183.
- 84. Drown, E., et al., Journal of Adhesion Science and Technology, 5, No. 10, (1991) pp 856-881.

- 85. Sharpe, L.H., and H. Schonhorn, "Contact Angle, Wettability and Adhesion," R.F. Gould ed., ACS, Washington, D.C., (1964).
- 86. Al-Moussawi, H., et al., Polymer Composites, 14, No. 3, June (1993) pp 195-200.
- 87. Drzal, L.T., et al., Paper 20-C, 35th Annual Technical Conference, Reinforced Plastics/Composites Institute (1980).
- 88. Larson B.K. and L.T. Drzal, submitted to Polymer Composites.
- 89. Gonzalez-Romero, V.M. and C.W. Macosko, Society of Plastics Engineers Technical Papers, 31 (1985) pp 1292-1294.
- 90. Macosko, C.W., RIM, Fundamentals of Reaction Injection Molding, Oxford University Press, New York, N.Y., (1989) pp 209-238.
- 91. Kim, D.H. and S.C. Kim, *Polymer Engineering and Science*, 29, No. 7, Mid-April (1989) pp 456-462.
- 92. Rao, V. and L.T. Drzal, *Polymer Composites*, 12, (1991) pp 48-56.
- 93. Newman, A.B., Transactions of the American Institute of Chemical Engineers, 27, No. 203, (1931) pp 310.

